# Linkages between continental hydrology, vegetation and biomass burning in East Java since the Last Glacial

Dissertation for the doctoral degree in
Natural Sciences (Dr. rer. nat.)
in the Faculty of Geosciences
University of Bremen

submitted by
**Yanming Ruan**

Bremen, Germany
August 2020

# - Gutachter -

Prof. Dr. Dierk Hebbeln

Dr. Antonio García-Alix

- Tag des Prüfungskolloquiums -

9 November 2020

# Abstract

The Maritime Continent is the vast region between the tropical Indian Ocean and Pacific Ocean, consisting of the Indo-Pacific warm pool and thousands of islands of various sizes. It is the primary region of strong atmospheric convection and widespread land-sea interaction on Earth. Today, the tropical rainforest ecosystem and millions of residents in this region are facing great threats such as droughts, floods and wildfires in the context of ongoing global warming and continuing greenhouse gas emission. The understanding of interactions between rainfall, vegetation and fire is essential but limited. Satellite-based monitoring of rainfall, vegetation and fire occurrence, which only exists in the past few decades, are too short to understand their long-term feedbacks with each other. An accurate reconstruction of the past changes in hydro-climate (rainfall), vegetation and fire in this region is therefore a prerequisite for understanding tropical ecosystems and for projections into the future.

With a focus on East Java, Indonesia, a monsoonal region of the Maritime Continent, this thesis applies multiple proxies to the same climate archive (a sediment core retrieved off the southern shore of East Java) in order to accurately reconstruct the regional vegetation, rainfall and fire regime (frequency and intensity of fires) over the past 22,000 years.

Leaf wax $\delta^{13}$C based on multiple *n*-alkane homologues (*n*-C29, *n*-C31 and *n*-C33) together with palynological data are used to reconstruct vegetation types, while leaf wax $\delta$D based on the multiple homologues is used to reconstruct the rainfall intensity during the wet season. The results show that different homologues predominantly reflect distinct ecosystems: *n*-C29 mainly reflects montane rainforest during the Last Glacial Maximum (LGM, around 21,000 years ago) and lowland rainforest during the Holocene (since 10,000 years ago), while *n*-C31 and *n*-C33 predominantly reflect lowland vegetation through the record. The results further suggest that in East Java, evergreen rainforest remained the dominant vegetation type in montane regions since the rainfall seasonality there remained relatively unaltered over the past 22,000 years. In contrast, the East Javanese lowlands were characterized by C4 grass expansion and an extended dry season but a wetter rainy season, thus stronger seasonality, during the LGM.

The past fire regime is reconstructed using micro-charcoal in combination with two molecular markers of burning, i.e. levoglucosan and polycyclic aromatic hydrocarbons. While the micro-charcoal accumulation rate reflects general fire occurrence in East Java, the ratio of levoglucosan vs. polycyclic aromatic hydrocarbons indicates fire intensity. The results show that both fire occurrence and intensity were high during the LGM but low during the Heinrich Stadial 1 (17,500-14,600 years ago), the Younger Dryas (12,900-11,600 years ago) and the early Holocene (10,000-3,000 years ago). A comparison of the fire history with the regional lowland vegetation and hydro-climate shows that both fire regime and vegetation were primarily controlled by rainfall seasonality. However, fire additionally stabilized the savannah (rainforest)-dominated ecosystem during the LGM (early Holocene) but caused transitions between the two vegetation types during the deglaciation (17,500-11,600 years ago) and the late Holocene (3,000 years ago till now).

The impact of human activities need to be considered in assessing the vegetation cover and fire history of East Java during the late Holocene. Therefore, the history of land use/land cover (vegetation cover, fluvial erosion and fire disturbance) in East Java over the past 5,000 years is reconstructed. To assess the climatic vs. human impact on it, regional rainfall reconstructions and archaeological records are evaluated respectively. The results show that the fluvial erosion co-varied with the regional annual rainfall amount throughout the record; the highest erosion between 2,800 and 1,800 years ago occurred with a gradual increase in both C4 vegetation and high intensity fire occurrence. The results suggest a primary hydro-climatic impact on the East Javanese fluvial system over the past 5,000 years. In the meanwhile, the prehistoric human society of East Java potentially caused deforestation by swidden cultivation using fire as a tool, which further enhanced soil erosion. Such a human impact became step-wise profound through the record reflected by the increasing occurrence of high intensity fires.

# Zusammenfassung

Der Maritime Kontinent bezeichnet das ausgedehnte Gebiet zwischen dem tropischen Indischen Ozean und dem Pazifischen Ozean in Südostasien, welches aus dem Indo-Pazifischen Warmwasserkörper sowie einer Vielzahl von Inseln verschiedenster Größe besteht. Global betrachtet ist diese Region von primärer Bedeutung für atmosphärische Konvektionsprozesse und Schauplatz weitreichender Kontinent-Ozean Wechselwirkungen. Heutzutage sind im Zuge der fortschreitenden Erderwärmung aufgrund anhaltender Treibhausgasemissionen sowohl das Ökosystem des Tropischen Regenwaldes, als auch Millionen von Einwohner dieser Region beständigen Bedrohungen wie Dürren, Überschwemmungen und Lauffeuern ausgesetzt. Daher ist ein tieferes Verständnis der Wechselwirkungen zwischen Niederschlägen, der Vegetationsdecke und Feuer essentiell, welches jedoch zu diesem Zeitpunkt noch begrenzt ist. Satellitengestützte Beobachtungen von Niederschlagsmengen, Vegetationsveränderungen und des Auftretens von Waldbränden reichen lediglich einige Jahrzehnte zurück, und sind somit zu kurz, um langfristige Rückkopplungen zwischen diesen Variablen zu verstehen. Die genaue Rekonstruktion vergangener Veränderungen der hydroklimatischen Bedingungen (Variation der Niederschlagsmengen), der Vegetation und der Häufigkeit von Bränden in dieser Region ist daher eine Voraussetzung für das Verständnis tropischer Ökosysteme, sowie für die Projektion zukünftiger Veränderungen in dieser Region.

Mit einem Schwerpunkt auf Ostjava (Indonesien), einer vom Monsun geprägten Region innerhalb des Maritimen Kontinents, wird in dieser Arbeit ein repräsentatives Klimaarchiv (ein vor der südlichen Küste Javas entnommener Sedimentkern) mit Hilfe verschiedener (Klima-)Proxies untersucht, um regionale Veränderung der Vegetationsverteilung, der Niederschlagsmenge und des Feuerregimes (Häufigkeit und Intensität von Bränden) während letzten 22.000 Jahre detailliert zu rekonstruieren.

Die stabile Kohlenstoffisotopie ($\delta^{13}$C) epikutikulärer Pflanzenwachse wurde, basierend auf der homologen Reihe langkettiger $n$-alkane ($n$-C29, $n$-C31 und $n$-C33), zusammen mit palynologischen Datensätzen zur Rekonstruktion vergangener Vegegationsveränderungen eingesetzt, während der Gehalt stabiler Wasserstoffisotope ($\delta$D) in diesen Pflanzenwachsen zur Rekonstruktion der Niederschlagsintensität während der Regenzeit bestimmt wurde. Die Ergebnisse zeigen, dass Variationen im Vorkommen

dieser Homologe das Vorherrschen bestimmter Ökosysteme wiederspiegeln: Während das Homolog *n*-C29 hauptsächlich ein Indikator für die Existenz montaner Regenwälder während des Letzteiszeitlichen Maximums (LGM, ungefähr vor 21.000 Jahren) und Tieflandregenwälder während des Holozäns (beginnend vor 10.000 Jahren) darstellt, deuten die Homologe *n*-C31 und *n*-C33 auf das überwiegende Vorkommen einer in der Tiefebene anzutreffenden Vegetation während des rekonstruierten Zeitraums hin. Die Ergebnisse legen ferner nahe, dass immergrüner Regenwald der vorherrschende Vegetationstyp in montanen Regionen Ostjavas blieb, da sich die saisonale Variabilität im Niederschlag während der letzten 22.000 Jahre weitestgehend unverändert verhielt. Im Gegensatz dazu war die ostjavanische Tiefebene während des LGM zum einen durch anhaltende Trockenzeiten und der damit einhergehenden Ausbreitung von C4-Gräsern, aber auch durch eine feuchtere Regenzeit, und somit einer insgesamt ausgeprägteren Saisonalität, beeinflusst.

Das vergangene Feuerregime wurde anhand von Mikroholzkohlepartikel zusammen in Kombination mit zwei für die Verbrennung von Biomasse diagnostischen molekularen Markern, Levoglukosan und polyzyklische aromatische Kohlenwasserstoffen, rekonstruiert. Während die Akkumulationsrate der Mikroholzkohlepartikel auf das Auftreten von Waldbränden in Ostjava generell hinweist, so deutet die Konzentration von Levoglukosan im Verhältnis zu der von polyzyklischen aromatischen Kohlenwasserstoffen auf die Intensität dieser Brände hin. Die Ergebnisse zeigen, dass sowohl das Auftreten von Waldbränden als auch deren Intensität hoch während des LGM, aber niedrig während des Heinrich-Stadials 1 (vor 17.500 - 14.600 Jahren), der Jüngeren Dryaszeit (vor 12.900 - 11.600 Jahren) und des frühen Holozäns (vor 10.000 - 3.000 Jahren) waren. Ein Vergleich der zeitlichen Entwicklung dieser Brände mit Veränderungen in der regionalen Verteilung der Vegetation in der Tiefebene und hydroklimatischer Rahmenbedingungen zeigt, dass sowohl das Feuerregime, als auch die Vegetationsmuster hauptsächlich durch die Saisonalität der Niederschläge bestimmt werden. Allerdings zeigt sich, dass Brände das Savannen- (Regenwald-) dominierte Ökosystem während des LGM (frühes Holozän) zusätzlich stabilisierten, jedoch aber auch Übergänge zwischen diesen beiden Vegetationstypen während der letzten Deglaziation (vor 17.500 - 11.600 Jahren) und des späten Holozäns (vor 3.000 Jahren bis heute) ausgelöst haben.

Die Auswirkungen menschlicher Aktivitäten müssen bei der Beurteilung der Vegetation- und Feuerhistorie Ostjavas während des späten Holozäns mit berücksichtigt werden. Daher wurden zusätzlich Veränderung der Landnutzung/Landbedeckung Ostjavas (Vegetationsmuster, fluviale Erosionsprozesse und Feuerstörungen) über einen Zeitraum von 5.000 Jahren rekonstruiert. Zur Beurteilung der klimatischen Auswirkungen gegenüber menschlicher Einflussfaktoren hinsichtlich regionaler Veränderungen wurden sowohl Niederschlagsrekonstruktionen als auch archäologische Befunde ausgewertet. Die Ergebnisse zeigen, dass während des gesamten rekonstruierten Zeitraums fluviale Erosionsprozesse mit der regionalen jährlichen Niederschlagsmenge einhergingen; die höchsten Erosionsraten traten vor 2.800 - 1.800 Jahren im Zusammenhang mit einer allmählichen Zunahme sowohl der C4-Vegetation, als auch dem Auftreten hochintensiver Brände, auf. Diese Befunde deuten auf einen primär hydroklimatischen Einfluss auf das ostjavanische Flusssystem während der letzten 5.000 Jahre

hin. Währenddessen zeichneten sich prähistorische menschliche Gemeinschaften durch das Betreiben von Wanderfeldbau unter Verwendung von Brandrodungstechniken möglicherweise verantwortlich für die Abholzung von Teilen des Regenwaldes Ostjavas, wodurch sich die Bodenerosion weiter verstärkte. Die Auswirkungen eines solchen menschlichen Eingriffs wurden während des rekonstruierten Zeitraums schrittweise tiefgreifender, was sich im zunehmenden Auftreten hochintensiver Brände widerspiegelt.

## Versicherung an Eides Statt / *Affirmation in lieu of an oath*

**gem. § 5 Abs. 5 der Promotionsordnung vom 18.06.2018 /**
***according to § 5 (5) of the Doctoral Degree Rules and Regulations of 18 June, 2018***

Ich / I, _____
(Vorname / First *Name*, Name / *Name*, Anschrift / *Address*, ggf. Matr.-Nr. / *student ID no., if applicable)*

versichere an Eides Statt durch meine Unterschrift, dass ich die vorliegende Dissertation selbständig und ohne fremde Hilfe angefertigt und alle Stellen, die ich wörtlich dem Sinne nach aus Veröffentlichungen entnommen habe, als solche kenntlich gemacht habe, mich auch keiner anderen als der angegebenen Literatur oder sonstiger Hilfsmittel bedient habe und die zu Prüfungszwecken beigelegte elektronische Version (PDF) der Dissertation mit der abgegebenen gedruckten Version identisch ist. / *With my signature I affirm in lieu of an oath that I prepared the submitted dissertation independently and without illicit assistance from third parties, that I appropriately referenced any text or content from other sources, that I used only literature and resources listed in the dissertation, and that the electronic (PDF) and printed versions of the dissertation are identical.*

Ich versichere an Eides Statt, dass ich die vorgenannten Angaben nach bestem Wissen und Gewissen gemacht habe und dass die Angaben der Wahrheit entsprechen und ich nichts verschwiegen habe*. / I affirm in lieu of an oath that the information provided herein to the best of my knowledge is true and complete.*

Die Strafbarkeit einer falschen eidesstattlichen Versicherung ist mir bekannt, namentlich die Strafandrohung gemäß § 156 StGB bis zu drei Jahren Freiheitsstrafe oder Geldstrafe bei vorsätzlicher Begehung der Tat bzw. gemäß § 161 Abs. 1 StGB bis zu einem Jahr Freiheitsstrafe oder Geldstrafe bei fahrlässiger Begehung. / *I am aware that a false affidavit is a criminal offence which is punishable by law in accordance with § 156 of the German Criminal Code (StGB) with up to three years imprisonment or a fine in case of intention, or in accordance with § 161 (1) of the German Criminal Code with up to one year imprisonment or a fine in case of negligence.*

_____ _____
Ort / *Place*, Datum / *Date* Unterschrift / *Signature*

# Acknowledgements

I would like to thank my promotor Dierk Hebbeln and my two supervisors, Enno Schefuß and Mahyar Mohtadi, for making this exciting PhD project possible. With their great help my PhD proposal got funded by the Chinese Scholarship Council, which is sincerely acknowledged. I am grateful for having Dierk as my promotor, who is always glad to offer help and share experience. I thank Enno for his consistent support starting from our first E-mail communication. His careful supervision guided me through every step of the PhD project. Many thanks go to Mahyar, the man of knowledge and ideas; I benefited enormously from all the discussions we had. I am also lucky to have Lydie Dupont in my thesis committee, who offered great support to all my manuscripts and my thesis.

I enjoyed working in Enno's lab a lot with the company of Lottie, Christoph, Adhitya, Vera, Julia, Mia, Pushpak, Abdullah etc. Special thanks go to Ralph Kreutz for all the laboratory support. It was also always pleasant to meet and communicate with many enthusiastic guest scientists: Dailson, Andrea, Mathia, Jaqueline, Rodrigo, Niclas etc. I also enjoyed being a part of the Marine Sedimentology group and would like to thank each member of it. The yearly Christmas dinners and the occasionally coffee breaks (both live and virtual ones) make me feel at home. I thank my office mates Christoph, Xueqin, Friederike, Vera, Adhitya and Julia for the nice working/leisure atmosphere. Stefan Schouten and Ellen Hopmans are thanked for hosting my wonderful research stay in NIOZ. I especially enjoyed the morning coffee with the MMB members there. Denise Dorhout, Monique Verweij and Ellen are acknowledged for laboratory support. I acknowledge the enthusiastic working environment created by all the colleagues and fellows from MARUM and GLOMAR. GLOMAR is additionally acknowledged for offering courses/seminars and supporting my research stay in NIOZ and participation in the IMOG 2019.

I appreciate the contribution from all the co-authors of the manuscripts. Special thanks go to Sander van der Kaars for his great support of the palynological dataset, and to Edward Hyer for his expertise with satellite data. I thank Jeffrey Reid for introducing Edward to me.

I thank Antonio García-Alix for being the external reviewer of my dissertation and for his positive comments. Elda Miramontes García, Tilo von Dobeneck, Igor Obrecht, Yue Leng, Vera and Pushpak are thanked for attending my defense as examining committee members.

I am grateful for the four years of life in Bremen, which gave me the opportunities to meet so many dear friends: Hadar, Ádám, Guoxing, Günther, Jing, Wanzhang, Junli, Shuhui, Ting-Wei, Cenling, Bingbing, Min, Alex, Sandy, Marine, Mathia, José and many more. Special thanks go to Lukas Mühlena for his great help in translating the abstract of the thesis. I want to thank all the friends from the table tennis club Tus Vahr. It was a lot of fun to train, compete and hang out with them.

In the end I would like to thank my dear family for their love, trust and continuous support.

# Contents

# Chapter 1

# Introduction

## 1.1 Significance of the Maritime Continent

The Maritime Continent is a term used by meteorologists, climatologists, and oceanographers to describe the vast region between the tropical Indian Ocean and Pacific Ocean (Fig 1.1). The **maritime** part is where the Indo-Pacific warm pool is located, which is characterized by annual mean sea surface temperatures over 28°C [Fig 1.1; World Ocean Atlas 2013; Locarnini et al., 2013]. As a result, strong atmospheric convective activities make the warm pool the largest and most important area of deep atmospheric convection on Earth, where high convective clouds can reach altitudes up to 15 km and generate a large amount of latent heat in the process of convection [De Deckker, 2016]. The warm pool is located in the upper branches of both large-scale zonal atmospheric overturning cells above the equatorial Indian Ocean and Pacific Ocean (the Walker circulations); it is therefore sensitive to the states of both tropical oceans [Cai et al., 2019]. The **continent** part includes the archipelagos of Indonesia, Borneo, New Guinea, the Philippine Islands, the Malay Peninsula etc. (Fig 1.1). The extensive interaction between ocean and land makes this region even more special in the climate system [Yang et al., 2019, and references therein].

Rainfall is one of the most important climate parameters in the Maritime Continent, because it affects the fates of the vast tropical rainforest ecosystem as well as millions of people living there. The large-scale modern rainfall distribution in the Maritime Continent is influenced by three major climate systems: the Asian–Australian monsoon [e.g. Webster et al., 1998] associated with the seasonally latitudinal migration of the Intertropical Convergence Zone (ITCZ) and two inter-annual coupled atmosphere-ocean oscillations: El Niño and Southern Oscillation (ENSO) in the Pacific Ocean and the Indian Ocean Dipole (IOD) in the Indian Ocean [e.g. Timmermann et al., 2018; Rasmusson and Wallace, 1983; Saji et al., 1999]. On a smaller spatial scale, high-resolution satellite observations and climate model results show that precipitation over the Maritime Continent is more concentrated over islands than surrounding seas, a feature associated with the complex topography and land-ocean interaction of this region [Qian, 2008; Rauniyar and Walsh, 2013].

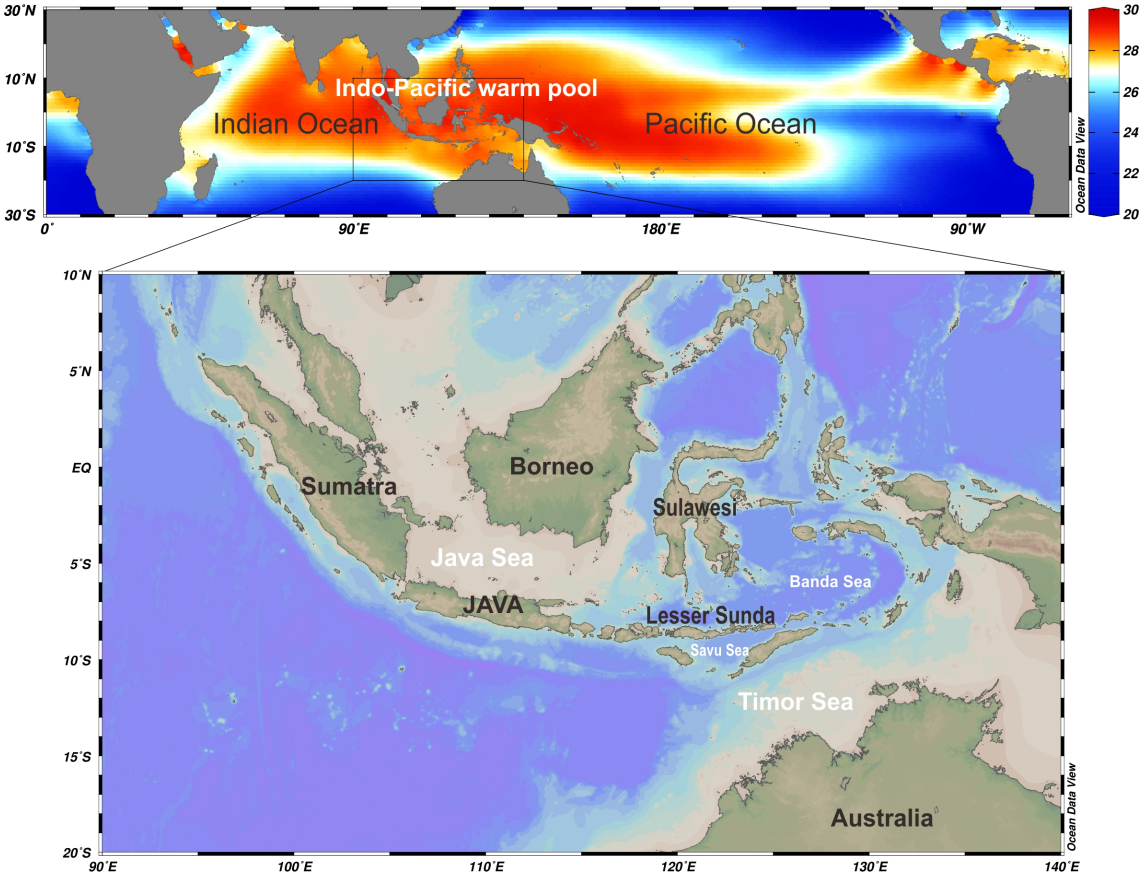


**Figure 1.1:** The upper part shows the annual sea surface temperature distribution of the tropical oceans [World Ocean Atlas 2013; Locarnini et al., 2013]. The Indo-Pacific Warm Pool, characterized by high sea surface temperatures, is located in the upper branches of two Walker Circulation cells in both the equatorial Pacific Ocean and the equatorial Indian Ocean. The lower part shows the geography of the Maritime Continent.

Although the Maritime Continent is generally characterized by heavy annual rainfall amounts, fire is a severe problem in this region. Large-scale emissions generated by Indonesian fires can significantly reduce visibility due to the continuous burning of peat soils for as long as four months [Field et al., 2009]. During the El Niño event in 1997-98 as an extreme, fires damaged over 8 million hectares on Borneo and Sumatra, putting 70 million people in risk of haze; the economic lost reached over 9 billion US dollars [Lohman et al., 2007; Bowman et al., 2009].

Predicting fires, however, is hindered by the complex interplay of fire, climate and vegetation [Archibald et al., 2013; Murphy and Bowman, 2012]. Fire frequency and fire intensity are two important fire regime characteristics in describing fire patterns [Bond and Keeley, 2005; Gill, 1975]. While fires in tropical moist broadleaf forests are predominantly of low intensity (burning temperature) and low to intermediate frequency, tropical grassland fires are more frequent and tend to reach higher intensity (burning temperature) [Archibald et al., 2013]. Modern observation in the Maritime Continent discovers more frequent fires in years with extended dry seasons [van der Werf et al., 2008]. Fire experiments in savannah ecosystems observe high fire intensity when the moisture content of fuel is low [Govender et al., 2006].

Therefore, climate and vegetation are two important factors in understanding how fire interacts with environmental changes, although only about half of the existing studies on fire feedbacks tackle both factors [Archibald et al., 2018].

In the context of ongoing global warming and continuing anthropogenic greenhouse gas emission, the understanding of interaction between climate, vegetation and fire is essential but limited. Satellite-based monitoring of rainfall, change in vegetation as well as fire occurrence/intensity which only exist in the past few decades are too short to understand their long-term feedbacks with each other. Therefore, an accurate reconstruction of the past changes in hydro-climate (rainfall), vegetation and fire regime in this region is a prerequisite for understanding the tropical climate system and for projections into the future. Such results can also be used to validate outcomes from climate models and fire ecology models to assess past climates across a range of different background climate states.

With a focus on East Java, located in the monsoonal region of the Maritime Continent, this thesis applies multi-proxies to the same climate archive in order to accurately reconstruct the past regional rainfall, vegetation and fire regime from the Last Glacial to the present. The goal is to better understand the long-term hydro-climate system of the region as well as the feedbacks between hydro-climate, vegetation and fire. Further goals of the thesis are to re-evaluate debated scenarios on the hydro-climatic evolution in the Maritime Continent, and to improve our understanding of proxies for rainfall and fire regime. Specific research objectives are listed in Section 1.5.

## 1.2 Modern environmental setting of the study area

The rainfall of Java is influenced by the seasonally reversing Australian-Indonesian monsoon associated with the latitudinal migration of the Intertropical Convergence Zone (ITCZ) (Fig. 1.2), featured with one rainy season and one dry season. High rainfall amounts occur during the northwestly (Australian-Indonesian summer monsoon, AISM) season from December to March, when the ITCZ is situated above the Maritime Continent between 0° and 15°S; dry conditions accompany the southeastly (Australian-Indonesian winter monsoon, AIWM) season from June to September, when the ITCZ migrates towards the north with a mean position near 12°N (Fig. 1.2).

The state of the two tropical oceans exert important impacts on the climate of Indonesia through inter-annual and decadal coupled atmosphere-ocean oscillations such as El Niño and Southern Oscillation (ENSO) and the Indian Ocean Dipole (IOD) related with the Walker circulations. During El Niño events, the upwelling of cold subsurface waters in the estern Pacific cold tongue is reduced, which leads to surface warming in the central/eastern Pacific Ocean; the positive sea surface temperature anomaly shifts atmospheric convection from the warm pool to the central equatorial Pacific, causing a reduction in equatorial trade winds which in turn further reduces the zonal sea surface temperature gradient and intensifies surface warming

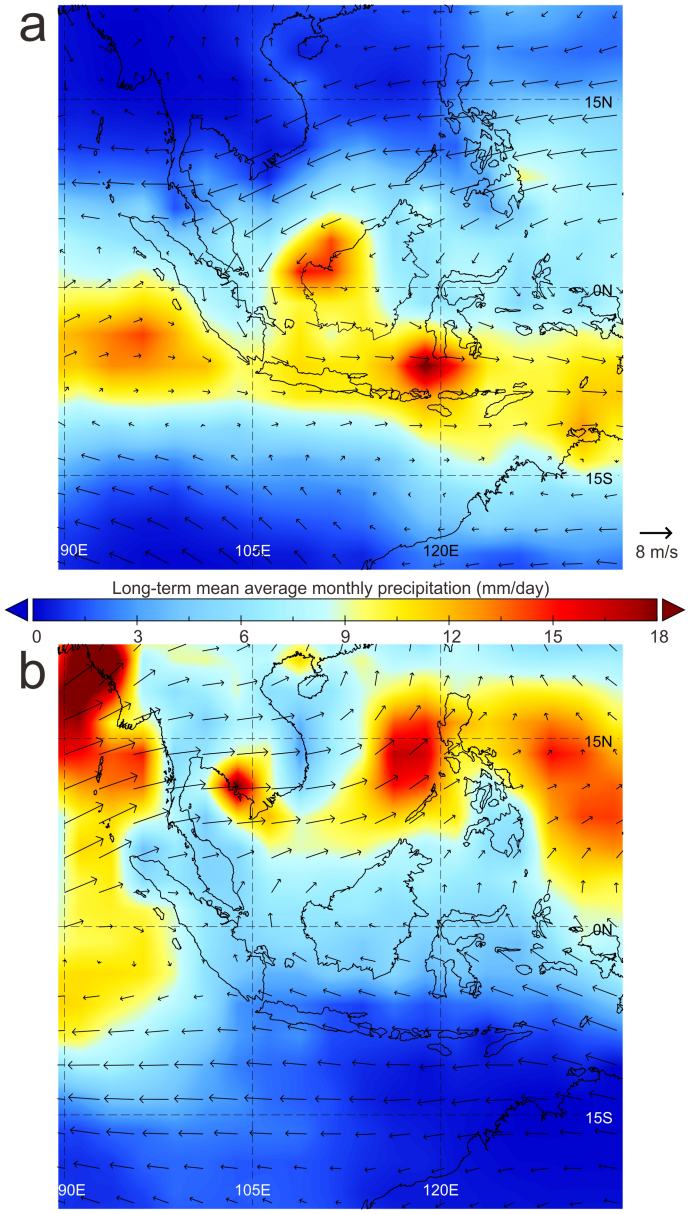


**Figure 1.2:** Large scale modern wind pattern and precipitation distribution in January (a) and July (b) of the Maritime Continent. Shading: long-term monthly mean precipitation (mm/day) from 1981 to 2010 by CPC Merged Analysis of Precipitation (CMAP; 2.5° latitude x 2.5° longitude resolution) [Xie et al., 1997]. Arrows: long-term monthly mean vector winds (m/s) at 850 mb from 1981 to 2010 by NCEP/NCAR Reanalysis 1 project [Kalnay et al., 1996].

in the central/eastern Pacific Ocean (the positive Bjerknes feedback) [Timmermann et al., 2018]. The average (composite) progression of El Niño involves two consecutive years, with the initiation in April to its peak in December and a transition to La Niña in August of the subsequent year [Timmermann et al., 2018]. El Niño events are generally larger in amplitude but shorter in duration than La Niña events, which can persist for up to several years. In addition to this common ENSO evolution, individual El Niño events differ considerably from each other and show complexity in terms of spatial pattern, amplitude and temporal development [Timmermann et al., 2018]. IOD is seasonally phase-locked by the wind reversals corresponding with the

AIWM season [Cai et al., 2013; Saji et al., 1999]. For positive IOD events, anomalous southeasterly winds around June initiate enhanced upwelling along the Javan and Sumatran coasts, which cools the atmosphere aloft and feedbacks positively on convection and the atmospheric circulation inducing stronger south-easterlies. The positive Bjerknes feedback sustains and strengthens the positive IOD anomalies (sea surface warming and increased atmospheric convection in the western Indian Ocean vs. cooling and decreased convection in the eastern tropical Indian Ocean) until the reversal of the monsoonal winds in October cause the events to peak and then rapidly demise in December [Saji et al., 1999; Abram et al., 2020]. A range of perspectives about ENSO-IOD relationships extend from the IOD being an independent climate mode [Saji et al., 1999] that can induce super El Niño events in the Pacific Ocean [Hameed et al., 2018], to the IOD being solely the manifestation of ENSO variability in the Indian Ocean combined with stochastic noise [Stuecker et al., 2017]. Recent developments of research have seen a shift towards the viewpoint of a more integrated tropical climate system, the variability of which involves interactions between all three tropical ocean basins, including two-way interactions between the IOD and ENSO [Cai et al., 2019; Abram et al., 2020]. During El Niño events, higher than normal atmosphere pressure occurs in the Australia-Asia region, which causes widespread drought across many parts of Australia and Indonesia [Chiang, 2009]. Similarly, positive IOD events are characterized by netative rainfall anomalies over western Indonesia [Saji et al., 1999].

The rainfall seasonality in the study area is additionally influenced by montane elevation. There are four mountain ranges in East Java (Kelud-Arjuna-Welirang, Tengger-Semeru, Lamongan-Argapura and Raung-Merapi-Ijen) and one in the centre of Bali (Barukau-Batur-Agung), with peaks around 3000 m (Fig. 1.3). With increasing altitude, the length of the dry season generally decreases. Lowland regions below 500 m generally have a dry season length (monthly rainfall <100 mm) up to >5 months; while montane regions above 1000 m generally have a dry season shorter than 3 months [Whitten et al., 1996] (Fig. 1.3).

The distribution of natural vegetation types of the study region depends on the distribution of rainfall together with elevation. Briefly, raingreen forests [forests with one or more deciduous species; Box, 1995; Roderick et al., 1999] are the dominant natural lowland vegetation types in East Java, while evergreen highland rainforests occur with altitudes above 1000 m [van der Kaars et al., 2010]. Six major natural vegetation types are mapped by Whitten et al. [1996] based on elevation, annual rainfall amount and dry month length (Fig. 1.4). Both evergreen rainforests and semi-evergreen rainforests (with a few deciduous trees) are distributed in areas with high annual rainfall (over 2,000 mm), but the former experience less than two dry months while the latter experience two to four dry months. Moist deciduous forests (where at least half of the trees are deciduous) occur with an annual rainfall amount between 1,500 and 4,000 mm and four to six dry months. Dry deciduous forests (where almost all the trees are deciduous) are distributed in coastal areas with less than 1,500 mm of annual rainfall and more than six dry months. The former four vegetation types all grow below 1,200 m, while aseasonal and seasonal montane forests occur on mountainous areas higher than 1,000 m [Whitten et al., 1996].

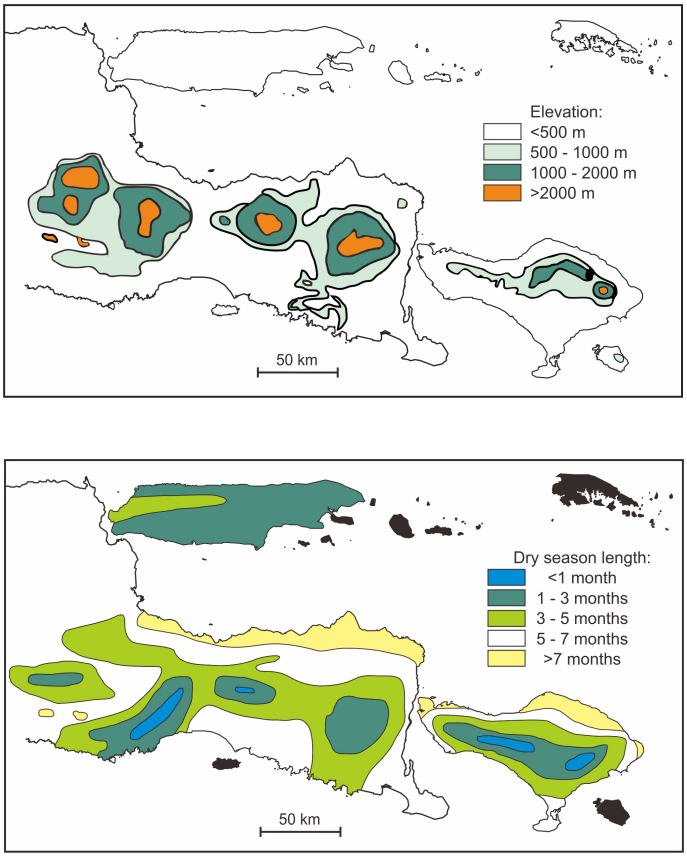


**Figure 1.3:** Regional elevation (upper graph) and lengths of dry months with monthly rainfall <100 mm (lower graph) of East Java. Data are not shown in regions in black color in the lower graph. Modified from Whitten et al. [1996].

Since Java is one of the most densely populated areas of the world today, most of the natural vegetation has been replaced by rice fields, grasslands, urban areas etc. [Stibig et al., 2002]. More than 90% of pristine natural vegetation of Java is lost, with the remaining rainforests restricted to isolated montane patches [Collins et al., 1991]. Major exploitation of the rainforest for timber, particularly in Java, began in the 1960s and is continuing today [Collins et al., 1991]. Fire occurrence also interferes with the vegetation distribution, resulting in montane grasslands in Java [Collins et al., 1991].

Fires in Java display a distinct seasonal pattern although a large part of the fires are human-induced in modern times, with high fire occurrence during the dry (AIWM) season and low fire occurrence during the wet (AISM) season; a sufficient amount of dry fuel for ignition is the prerequisite for fires [Reid et al., 2012]. Over longer time periods, severe burning events from 1960 to 2006 occurred during periods of anomalously low seasonal precipitation [Field et al., 2009]. Dendrochronological and observational studies reveal a correspondence between fire occurrence and ENSO events [Bowman et al., 2009]. During extreme drought events, fire usage tends to evade control more often [Page et al., 2002]. There is a marked increase in fire occurrences in Indonesia under relatively dry conditions during El Niño phases [Reid et al., 2012], with the 1997-98 as an extreme [Lohman et al., 2007]. The most

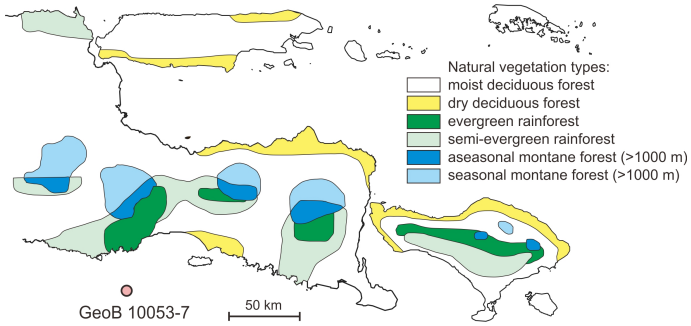


**Figure 1.4:** Natural distribution of six major vegetation types of East Java and Bali. Modified from Whitten et al. [1996].

extensive fires are potentially associated with the co-occurrence of a positive IOD event and an El Niño event, when reduced Walker circulations of both the Pacific and the Indian Ocean resulted in severe drought conditions in Indonesia (e.g. 1972, 1982-83 and 1997-98)[Saji and Yamagata, 2003; Field et al., 2009; Field and Shen, 2008].

## 1.3 Past hydro-climate since the last glacial

The hydro-climate variations in the Maritime Continent during the late Quaternary remain poorly constrained, with diverse remote and local forcings proposed over different time scales. Over orbital time scales, stalagmite oxygen isotopic records from northern Borneo, indicated to be the isotopic compositions of rainfall, suggest a dominant precessional forcing with weak glacial-interglacial changes [Carolin et al., 2013]. In Sulawesi, runoff and vegetation records, in contrast, show little influence of precessional forcing but are coupled with sea level changes; high-latitude remote forcing (global temperature, green-house gases and ice sheets) via the latitudinal migration of the mean ITCZ position is proposed to be more significant [Russell et al., 2014]. On millennial time scales, another influence on the hydro-climatic variability of Indonesia comes from high-latitude North Atlantic forcing during the last deglaciation [Mohtadi et al., 2014, 2011].

High-resolution coral data dating back to the last millennium show a strong coupling of the magnitudes of inter-annual variability between the IOD and ENSO: time intervals of reduced (strengthened) IOD variance co-occurred with intervals of reduced (strengthened) ENSO variance [Abram et al., 2020]. However, such a coupling appears to have not persisted in very different climate states such as the Mid-Holocene and the Last Glacial Maximum (LGM) [Abram et al., 2020]. Although single ENSO or IOD events are often not resolved in the time resolution of marine sediments, the associated mean state of the tropical Pacific or Indian Ocean is proposed to exert a substantial impact on the rainfall in the Maritime Continent during the Holocene [Niedermeyer et al., 2014; Kwiatkowski et al., 2015; Denniston et al., 2013] and during the LGM [Mohtadi et al., 2017]. However, rainfall reconstruction based on a high-resolution sediment core offshore Sumba (one of the Lesser Sunda Islands) displays no correlatin to ENSO variablity but statistically significant correlation with

the sunspot number during the past 6,000 years, implying a solar activity control on monsoonal rainfall at multi-decadal and longer timescales [Steinke et al., 2014].

The stable hydrogen isotope compositions ($\delta$D) of sedimentary higher-plant derived leaf wax lipids (see Section 2.2 for details) have shown great potential in reconstructing past rainfall changes in the Maritime Continent [Konecky et al., 2016; Mohtadi et al., 2017; Niedermeyer et al., 2014; Tierney et al., 2012; Wicaksono et al., 2017]. Long chain leaf wax lipids, as components of terrestrial organic matter, are transported by rivers or wind before deposition in sedimentary archives, where they can serve as measures of the continental vegetation that biosynthesized them [e.g. Eglinton and Eglinton, 2008]. The leaf wax $\delta$D serves as a recorder of the $\delta$D values of the precipitation [Sachse et al., 2012, and references therein], which primarily reflect rainfall intensity via the 'amount effect' in the tropics [more negative precipitation $\delta$D values suggest higher rainfall amounts; Dansgaard, 1964; Rozanski et al., 2013] (see Section 2.2 for details). When applying the amount effect concept to the climate archives, past changes in rainfall amounts are reconstructed by leaf wax $\delta$D from marine sediment cores in the western part of the Maritime Continent, shedding light on past changes in the Indian Ocean Walker circulation during the Holocene [Niedermeyer et al., 2014] and the LGM [Mohtadi et al., 2017]. In Sulawesi, however, two scenarios other than the amount effect are proposed in the interpretation of the sedimentary leaf wax $\delta$D records, which complicates the reconstruction of the climate of the Maritime Continent during the LGM. (1) Konecky et al. [2016] propose that an intensified atmospheric circulation over the Maritime Continent drove the isotopic depletion of rainfall despite widespread aridity during the LGM ('dry convection' scenario). (2) A change in moisture sources is inferred to cause shifts in rainfall $\delta$D values, with the northerly monsoon winds carrying D-depleted air masses; a stronger northerly monsoon during the LGM tended to cause the more negative $\delta$D values recorded by leaf wax lipids ('moisture source change' scenario) [Konecky et al., 2016; Wicaksono et al., 2017].

## 1.4 Past interaction of fire, vegetation and climate

Several studies have considered rainfall amount as the most important driver of the past vegetation variability [Visser et al., 2004; van der Kaars and Dam, 1995, 1997; van der Kaars et al., 2001]. However, the distribution of stable carbon isotopes of leaf wax lipids (see Section 2.2 for details) suggests that the rainfall seasonality (dry season water stress) instead of the rainfall amount controlled the vegetation changes within the Maritime Continent [Dubois et al., 2014]. By applying this proxy to sediment cores, a savannah expansion during the Last Glacial was recorded off Sumba [Dubois et al., 2014], in southern and central Sulawesi [Wicaksono et al., 2017; Russell et al., 2014] and in southern Borneo [Wurster et al., 2019]. However, during the same period, close canopy forest remained according to the results from Sumatra [Niedermeyer et al., 2014], northeastern Borneo [Dubois et al., 2014] and Lake Matano (central Sulawesi) [Wicaksono et al., 2015].

In contrast to the discussion about the hydro-climatic impact on vegetation, little attention has been given to the role of fire in shaping the ecotone from savannah- to rainforest-dominated ecosystems. According to modern ecological studies, fires characterized of high frequent and/or intensity effectively limit tree cover and maintained an open canopy savannah vegetation [Bond and Midgley, 2000; Hoffmann et al., 2012a]. As a positive feedback, the presence of a grassy ground layer significantly increases the flammability of the ecosystem, allowing frequent and high intensity fires to occur [Stott, 2000; Bond, 2008; Hoffmann et al., 2012a]. In contrast, rainforest ecosystems are relatively fire free; the dense canopy of tropical rainforest suppresses fires by reducing grass fuel loads and maintaining a humid and low-wind micro-climate [Hoffmann et al., 2012b]. Multi-proxy paleo-studies integrating fire, climate and vegetation [eg. Shanahan et al., 2016; Dupont and Schefuß, 2018] are limited in the Maritime Continent. Changes in fire regime, i.e. frequency and intensity of fires, are often not resolved in paleo-records [Archibald et al., 2018; Han et al., 2016].

Humans have long been transforming natural vegetation for agriculture and settlement purposes, using fire as a tool [Ellis et al., 2013, and references therein]. Prehistoric human activities generally evolved from the less intensive forms like foraging, hunting and gathering to more intensive forms such as agriculture, pastoralism and even urbanization [Stephens et al., 2019]. Humans affect fire occurrence in either a positive or a negative way, by increasing ignition or supressing/eliminating fires [Whitlock et al., 2010]. The extent and intensity of prehistoric human impact on land cover is, however, difficult to quantify. Integrating paleoclimatology based on multiple proxies with archaeological results is a potential way to study long-term land-climate-human interactions on a regional scale [Ellis et al., 2013]. Modern humans are believed to have been present in East Java since at least the LGM, based on findings of human skull fragments of ***Homo sapiens*** dated back to 37-29 ka [Storm et al., 2013]. The Neolithic period, which is generally dated between 4,000 to 2,000 years ago, is characterized of intensified human activities such as pottery fragments and adze manufacturing flakes [Morwood et al., 2008; Simanjuntak and Asikin, 2004]. The Neolithic period co-occurred with the expansion of Austronesian population and cultivation practices [Bellwood, 2007]. Before the Neolithic period, hunting and gathering seemed to be the major form of local human activities [Simanjuntak and Asikin, 2004].

## 1.5 Scientific questions and hypotheses

This thesis applies a multi-proxy methodology (see Chapter 2) to a sediment core collected off the southern shore of East Java dating back to 22,000 years before present, in order to address the following scientific questions:

a Did a savannah vegetation expansion occur in East Java during the Last Glacial? Did the vegetation in lowland and highland ecosystems evolve differently?

b Did the 'amount effect' remain the dominant control on the rainfall $\delta$D values

in East Java during the LGM? How did the past rainfall (seasonality) in such a monsoonal region of the Maritime Continent evolve and respond to various forcings since the LGM?

c How did the fire regime, i.e. frequency and intensity of fires, change in East Java since the Last Glacial? How did fire interact with vegetation and climate?

d How did prehistoric human activities influence land cover and fluvial erosion in East Java over the past 5,000 years?

Based on the scientific questions, the following hypotheses are going to be tested:

1. Vegetation in lowland and highland ecosystems of East Java evolved differently since the LGM. While a savannah expansion at the cost of the rainforest occurred in the lowlands during the LGM, rainforest remained the dominant vegetation in the highlands during that period.
2. The sedimentary leaf wax $\delta$D record captures the wet season rainfall intensity in East Java since the LGM via the 'amount effect'. The LGM-Holocene contrast in rainfall seasonality is small in the highlands but significant in the lowlands.
3. Past fire regime changes can be reconstructed based on micro-charcoal and two molecular markers of burning (levoglucosan and polycyclic aromatic hydrocarbons). Both the frequency and intensity of fires were higher during the LGM than the Holocene.
4. East Javanese vegetation has been constantly shaped by both climate and fire since the Last Glacial, while the prehistoric human impact on land cover became increasingly significant over the past 5,000 years.

## 1.6 Thesis outline and own contributions

This thesis is written in a cumulative form. In Chapter 2 the material and methods used are introduced. Chapter 3 to 5 consist of three individual manuscripts, which address the scientific questions raised above. The manuscripts are either published in, submitted to or in preparation for international peer-reviewed scientific journals. A short outline of my own and the co-authors' contributions is given below for each manuscript:

Chapter 3 (Manuscript 1):

**Differential hydro-climatic evolution of East Javanese ecosystems over the past 22,000 years**

*by Yanming Ruan, Mahyar Mohtadi, Sander van der Kaars, Lydie M. Dupont, Dierk Hebbeln, Enno Schefuß*

Published in *Quaternary Science Reviews* 218 (2019): 49-60

This study addresses **Scientific question a and b**. Detailed changes in past regional vegetation are reconstructed using leaf wax $\delta^{13}$C of three *n*-alkane homologues (*n*-

C29, *n*-C31 and *n*-C33) together with pollen data. The $\delta$D record based on the *n*-alkane homologues allows for the reconstruction of the hydro-climate evolution in East Java. Debated scenarios on the LGM hydro-climate in the Maritime Continent are evaluated.

Y. Ruan: Methodology, Validation, Investigation, Writing – Original Draft. M. Mohtadi: Conceptualization, Writing – Review and Editing, Supervision. S. van der Kaars: Methodology, Validation. L.M. Dupont: Validation, Writing – Review and Editing, Supervision. D. Hebbeln: Writing – Review and Editing, Supervision. E. Schefuß: Conceptualization, Methodology, Validation, Writing – Review and Editing, Supervision.

Chapter 4 (Manuscript 2):

**Interaction of fire, vegetation and climate in tropical ecosystems: a multi-proxy study over the past 22,000 years**

*by Yanming Ruan, Mahyar Mohtadi, Lydie M. Dupont, Dierk Hebbeln, Sander van der Kaars, Ellen C. Hopmans, Stefan Schouten, Edward J. Hyer, Enno Schefuß*

Submitted to *Global Biogeochemical Cycles*

To address **Scientific question c**, past changes in fire regime are reconstructed based on micro-charcoal and two molecular markers of burning, i.e. levoglucosan and polycyclic aromatic hydrocarbons. They are further compared with vegetation and rainfall reconstructed from the same climate archive to study their long-term interactions.

Y. Ruan: Conceptualization, Methodology, Validation, Investigation, Writing - Original Draft. M. Mohtadi: Conceptualization, Writing - Review and Editing, Supervision. L.M. Dupont: Validation, Writing – Review and Editing, Supervision. D. Hebbeln: Writing - Review and Editing, Supervision. S. van der Kaars: Methodology, Validation, Writing - Review and Editing. E.C. Hopmans: Methodology, Validation, Writing – Review and Editing. S. Schouten: Validation, Writing – Review and Editing. E.J. Hyer: Methodology, Validation. E. Schefuß: Conceptualization, Methodology, Validation, Writing – Review and Editing, Supervision.

Chapter 5 (Manuscript 3):

**Interplay of climate, fire and human activities on land cover and fluvial erosion in East Java over the past 5,000 years**

*by Yanming Ruan, Mahyar Mohtadi, Lydie M. Dupont, Dierk Hebbeln, Sander van der Kaars, Matthias Prange, Ellen C. Hopmans, Stefan Schouten, Enno Schefuß*

In preparation

This study addresses **Scientific question d**. Past changes in rainfall and land use/land cover (vegetation cover, fluvial erosion and fire disturbance) of East Java are integrated with existing archaeological results to study the linkages between prehistoric human, land over and climate.

Y. Ruan: Conceptualization, Methodology, Validation, Investigation, Writing - Original Draft. M. Mohtadi: Conceptualization, Writing - Review and Editing, Supervision. L.M. Dupont: Validation, Writing – Review and Editing, Supervision. D. Hebbeln: Writing - Review and Editing, Supervision. S. van der Kaars: Methodology, Validation, Writing - Review and Editing. M. Prange: Methodology, Validation, Writing - Review and Editing. E.C. Hopmans: Methodology, Validation, Writing – Review and Editing. S. Schouten: Validation, Writing – Review and Editing. E. Schefuß: Conceptualization, Methodology, Validation, Writing – Review and Editing, Supervision.

A detailed description of my own contributions is given below:

I prepared the sampling requests for the GeoB core repository at MARUM and took samples from the sediment core. I conducted the lipid extraction, separation and cleaning steps of all the samples. For leaf wax *n*-alkanes and their hydrogen and carbon isotope compositions, I conducted the GC-FID and then GC-IRMS analyses with the laboratory support of Ralph Kreutz. I developed and conducted the methodology for polycyclic aromatic hydrocarbon quantification using GC-MS with the help of Ralph Kreutz. For levoglucosan analysis, I did extra cleaning steps before the measurements. Analysis using the UHPLC-TOF was conducted with the help of Denise Dorhout, Monique Verweij and Ellen Hopmans. The ideas for each manuscript came from the discussions with the thesis committee (Lydie Dupont, Dierk Hebbeln, Mahyar Mohtadi and Enno Schefuß). All three manuscripts were written by myself with contributions from all the co-authors.

# Chapter 2

# Methodology

## 2.1 Marine sediment core as paleo-climatic archive

During the R/V Sonne cruise SO-184, gravity core GeoB 10053-7 (8°41'S, 112°52'E; 1375 m water depth; core length: 750 cm) was collected off south Java [Hebbeln and cruise participants, 2006]. This sedimentary archive spans the past 22,000 years with a solid age model based on 19 AMS $^{14}$C dates [Mohtadi et al., 2011]. Prior to this thesis, changes in AIWM induced upwelling were reconstructed using planktonic foraminiferal $\delta^{18}$O and faunal composition, while element composition and grain-size distribution were used to infer AISM variabilities [Mohtadi et al., 2011].

## 2.2 Leaf wax lipids and isotopes

Important tools employed in this thesis are leaf wax biomarkers. They are long-chain lipid molecules constituting the hydrophobic wax coatings of plant leaves [Eglinton and Hamilton, 1967]. These lipids are transported by wind or rivers before deposition in sedimentary archives, where they can serve as excellent measures of the continental vegetation that biosynthesized them [Eglinton and Eglinton, 2008]. These straight-chain non-polar compounds lacking functional groups are relatively stable biomarkers over geologic time-scales due to their water insolubility, negligible volatility, chemical inertness and resistance to biodegradation [Eglinton and Eglinton, 2008]. These alkyl lipids are also highly isotopically conservative; for example, the leaf wax $\delta$D information from the time of biochemical synthesis is preserved even in early stages of maturation [Schimmelmann et al., 2006]. Thus, the compound-specific stable isotope compositions of carbon and hydrogen of long chain leaf wax lipids provide information about terrestrial vegetation type and hydro-climate, respectively [Eglinton and Eglinton, 2008, and references therein].

### 2.2.1 Paleo-vegetation reconstruction based on multi-homologue leaf wax $\delta^{13}C$

The carbon isotope compositions of leaf wax biomarkers provide insights into carbon cycling, paleo-vegetation and paleo-climate. Atmospheric $CO_2$ is the original carbon source used by plants; the $\delta^{13}C$ values of the past atmospheric $CO_2$ constrain the leaf wax $\delta^{13}C$ from the geological past [Diefendorf and Freimuth, 2017, and references therein]. From atmospheric $CO_2$ to plant carbon, fractionation occurs because plants prefer to use $^{12}CO_2$ than $^{13}CO_2$; thus plant carbon has lower $\delta^{13}C$ values than the atmospheric $CO_2$. Different photosynthetic pathways utilized by different plant species result in different sizes of fractionation: plants using C3 carbon fixation pathway (Calvin-Benson) have the largest net photosynthetic fractionation, while plants using C4 carbon fixation pathway (Hatch-Slack) have the smallest net photosynthetic fractionation; plants using Crassulacean Acid Metabolism (CAM), a third metabolic pathway, have intermediate fractionation [O'Leary, 1988]. Other factors such as plant physiology, climate and ecology may also have considerable influence on net photosynthetic fractionation [Diefendorf and Freimuth, 2017, and references therein]. After that, further fractionation related with biosynthesis occurs from leaf carbon to leaf wax lipids [e.g. Chikaraishi et al., 2004].

In this thesis, the sedimentary leaf wax $\delta^{13}C$ is majorly used as a paleo-vegetation proxy to reflect the contribution by C3 versus C4 vegetation [Diefendorf and Freimuth, 2017]. In tropical regions, the C4 photosynthetic pathway typically occurs in warm-season grasses and sedges, while the C3 pathway is mostly utilized by trees and shrubs [Ehleringer et al., 1997; Eglinton and Eglinton, 2008]. According to the tropical plant compilation (Fig. 2.1, references in the table caption), the C4 photosynthetic pathway results in less net isotopic fractionation and thus higher leaf wax $\delta^{13}C$ values than the C3 pathway (Fig. 2.1, upper part). The mean $\delta^{13}C$ values for the C3/C4 vegetation end-members are within errors similar among the *n*-alkane **homologues** (straight-chain alkanes with the formula C*n*-H*2n+2* but different numbers of carbon and hydrogen atoms) (Fig. 2.1, higher part). Therefore, changes in leaf wax $\delta^{13}C$ values can be a good indicator of the relative abundance of forests vs. grasslands through time [Diefendorf and Freimuth, 2017]. Plants using Crassulacean Acid Metabolism (CAM) pathway may grow on ground or as epiphytes in forests [Lüttge, 2004]. However, as a stress survival strategy, the CAM pathway does not become dominant in most parts of the world [Lüttge, 2004]. The productivity of CAM plants and their contribution to sedimentary leaf waxes are thus low relative to C3 and C4 plants for most natural ecosystems [Diefendorf and Freimuth, 2017].

Moreover, analyses based on multi-homologue leaf wax lipids provide more information than using one single leaf wax compound. Among the leaf wax *n*-alkane homologues for example, isotope studies generally use *n*-C29 (abbreviation for *n*-C29 alkane, similarly for *n*-C31 and *n*-C33) and/or *n*-C31, because these two homologues are ubiquitous and usually have the highest abundance in both plants and sedimentary archives [Garcin et al., 2014]; isotope studies also often focus on one homologue if a strong correlation between changes in isotope values of several homologues is observed [e.g. Wicaksono et al., 2015]. However, this single compound

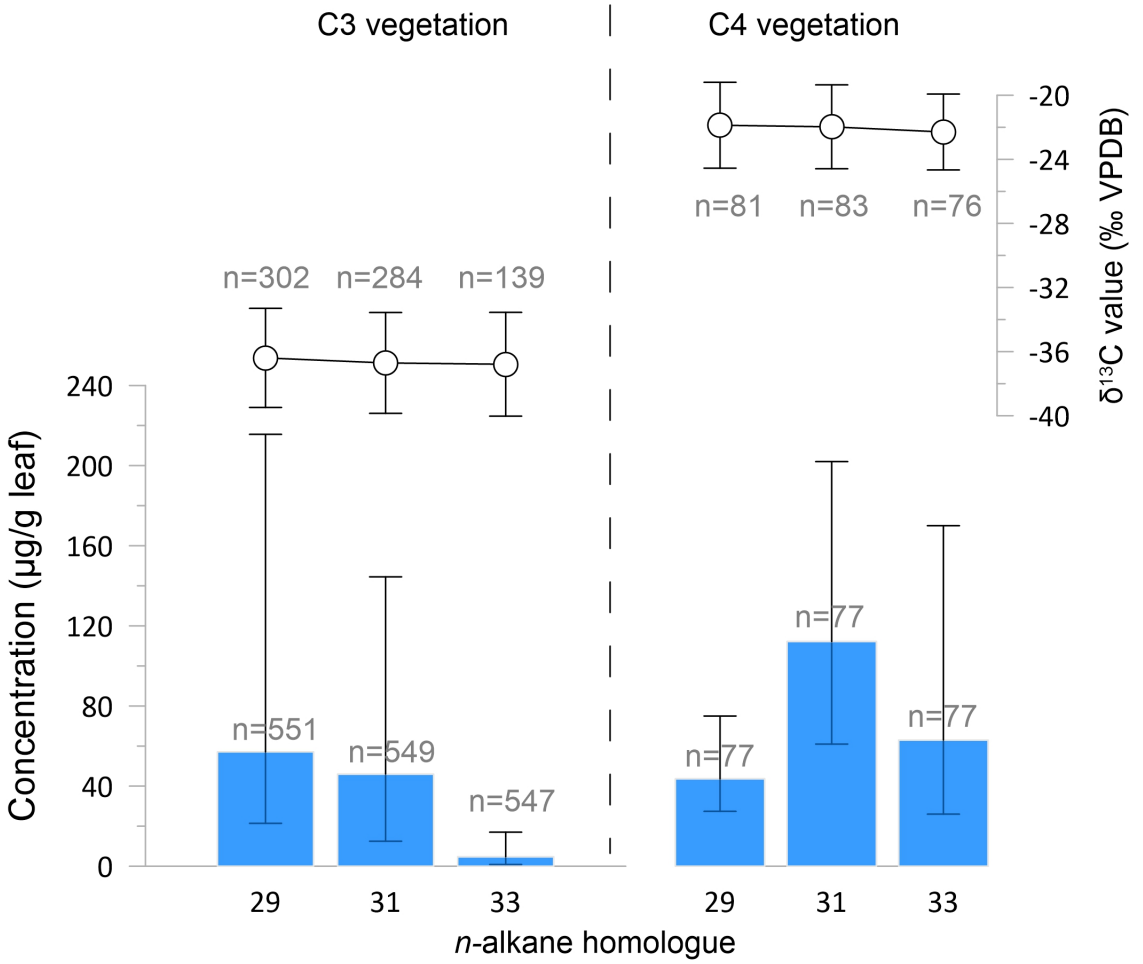


**Figure 2.1:** End-member information of the *n*-C29, *n*-C31 and *n*-C33 alkane homologues for C3 (left panel) and C4 plants (right panel) in the tropics. The upper part shows the $\delta^{13}C$ values (Mean $\pm$ 1$\sigma$ of the homologues in ‰ against Vienna PeeDee Belemnite (VPDB). The lower part shows the concentration (µg/g leaf) of the homologues: bar heights represent 50% quartiles, while the lower and upper error bars represent 25% and 75% quartiles, respectively. Data are based on global compilations from Sachse et al. [2012] and Diefendorf and Freimuth [2017] plus the data from tropical South America [Wu et al., 2017]. Only the data from tropical locations (between 30°N/30°S) are considered [Badewien et al., 2015; Bezabih et al., 2011; Bi et al., 2005; Bush and McInerney, 2015; Chikaraishi and Naraoka, 2003; Duan and He, 2011; Garcin et al., 2014; Krull et al., 2006; Liu and Yang, 2008; Mortazavi et al., 2012; Rommerskirchen et al., 2006; Vogts et al., 2009; Wu et al., 2017].

approach tends to overlook the additional information provided by comparing the isotopic compositions of multiple homologues. For C3 rainforest plants, commonly the major *n*-alkane compound is *n*-C29, with high relative abundances of *n*-C31 but low relative abundances of *n*-C33 [Garcin et al., 2014; Vogts et al., 2009; Wu et al., 2017]. On the other hand, the average *n*-alkane concentration profile of tropical C4 graminoids shows lower abundances of *n*-C29 but higher abundances of *n*-C33, with *n*-C31 being the major compound [Bush and McInerney, 2013; Rommerskirchen et al., 2006; Vogts et al., 2009; Wang et al., 2013]. Such a pattern in the concentrations of the *n*-alkane homologues is distinct in the tropical plant compilation (Fig. 2.1, lower part) despite the large ranges of variation due to the compilation of data

from various ecosystems. Studies have proposed to use *n*-C29 as an indicator for C3 vegetation and *n*-C33 as a C4 plant biomarker [Diefendorf and Freimuth, 2017; Garcin et al., 2014]. In this thesis, isotope analyses based on multi-homologue leaf wax *n*-alkanes are employed, which are further compared with the palynology data from the same core to achieve a detailed vegetation reconstruction.

### 2.2.2 Leaf wax $\delta$D as recorder of precipitation $\delta$D

Studies of both living plants and lake-surface sediments show a strong linear correlation between leaf wax *n*-alkane $\delta$D values and source water (precipitation) $\delta$D values along climatic gradients, implying that precipitation $\delta$D is the primary control of leaf wax $\delta$D [e.g. Sachse et al., 2012; Garcin et al., 2012; Herrmann et al., 2017].

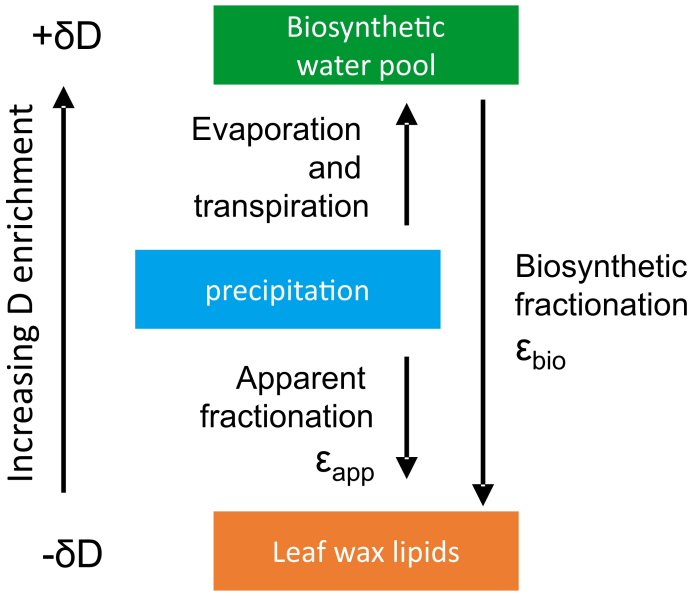


**Figure 2.2:** Conceptual diagram explaining the hydrogen isotope fractionations from precipitation to leaf wax lipids. Modified from Sachse et al. [2012]; Vogts et al. [2016].

From a more detailed perspective, hydrogen atoms introduced into plant biomass via photosynthesis are derived from leaf water; soil water is another water pool that connects leaf water with the original precipitation [Sachse et al., 2012, and references therein]. The apparent fractionation ($\varepsilon_{app}$) describes the total isotopic fractionation between precipitation and the leaf wax lipids. The $\varepsilon_{app}$ is the net effect of (1) possible evaporation of soil water especially in arid climates causing D enrichment relative to precipitation; and leaf water transpiration causing D enrichment relative to soil water; (2) the biosynthetic fractionation ($\varepsilon_{bio}$) related to different leaf wax synthesis pathways [Sachse et al., 2012, and references therein] (Fig. 2.2).

In the tropical plant compilation (Table 2.1, references in the table caption), the apparent fractionation between each of the three *n*-alkane homologues and mean annual precipitation ($\varepsilon_{alk/MAP}$) displays similar values within errors regardless of C3 and C4 photosynthetic carbon fixation pathways [Konecky et al., 2016]. The differences in $\varepsilon_{alk/MAP}$ between C3 and C4 vegetation types are always smaller than the

standard deviations of each, which tend to introduce large uncertainties if a vegetation correction is applied [Konecky et al., 2016; Collins et al., 2013; Sachse et al., 2012]. A study based on a marine sediment transect off south-western Africa finds relatively constant apparent hydrogen fractionation factors along a prominent C3 to C4 vegetation shift, suggesting that the plant type transition (possibly related with changes in $\varepsilon_{\text{bio}}$) might counteract the effects of aridity (soil/leaf-water enrichment) in tropical regions [Vogts et al., 2016]. These findings support the straightforward use of leaf wax $\delta$D as the recorder of precipitation $\delta$D.

Much of the $\delta$D variability of precipitation can be explained by condensation-evaporation processes [Gat, 1996; Craig, 1961]. When seawater evaporates, the corresponding vapor becomes depleted in D relative to the seawater because $^{1}H_{2}^{16}O$ has a higher vapor pressure and evaporates faster than $^{1}HD^{16}O$; when the water vapor condenses and leaves the air mass in the form of precipitation, the corresponding rain becomes enriched in D relative to the vapor while the remaining vapor is depleted in D. Several environmental factors are identified to control the the spatial and temporal distribution of precipitation $\delta$D [Dansgaard, 1964]:

1. During the transport of water vapor from the coast into the continental interior, the preferential loss of D on the way leads to increasingly lower precipitation $\delta$D values further inland (Continental effect).

2. A similar effect is observed with increasing altitude: highlands receive precipitation characterized by more negative $\delta$D values than the surrounding lowlands (Altitude effect).

3. Across regions with strong temperature variability (particularly outside the tropics), a positive correlation is observed between precipitation $\delta$D values and surface air temperatures (Temperature effect).

4. In tropical regions characterized by limited temperature variation but strong rainfall seasonality, stronger depletion in D of the rain occurs with higher precipitation rates (Amount effect).

Apart from these factors, the isotope composition of seawater in the vapor source region also plays an important role [Gat, 1996].

## 2.3 Multiple fire proxies

The combustion continuum model describes a continuum of materials produced with increasing burning temperature, ranging from slightly charred, degradable biomass to highly condensed, refractory soot [Hedges et al., 2000]. Charcoal, commonly used as a proxy to indicate past fire activity in climate archives, is a carbonaceous material produced by incomplete combustion of biomass with temperatures between 280 °C and 500 °C [Whitlock and Larsen, 2001]. Micro-charcoal abundance in marine sediments reflects general fire occurrence on a regional scale, representing fire frequency, intensity and extent [Power et al., 2008; Daniau et al., 2010, 2019; Beaufort et al., 2003].

| | $\varepsilon$C29/MAP (‰) (Mean ± 1$\sigma$) | $\varepsilon$C31/MAP (‰) (Mean ± 1$\sigma$) | $\varepsilon$C33/MAP (‰) (Mean ± 1$\sigma$) |
|---|---|---|---|
| C3 plants | -129 ± 23 n = 168 | -123 ± 40 n = 154 | -130 ± 23 n = 26 |
| C4 plants | -131 ± 32 n = 18 | -136 ± 28 n = 21 | -128 ± 19 n = 7 |

**Table 2.1:** Apparent hydrogen isotope fractionation between *n*-alkane homologues and mean annual precipitation (Supplementary Table S2 from Ruan et al., 2019). Average values and standard deviations are obtained from a global compilation from Sachse et al. [2012] plus the data from tropical South America [Feakins et al., 2016]. Only the data from tropical locations (between 30°N/30°S) are considered [Bi et al., 2005; Chikaraishi and Naraoka, 2003; Feakins et al., 2016; Krull et al., 2006; Liu and Yang, 2008]

Monosaccharide anhydrate compound levoglucosan (1,6-anhydro-$\beta$-D-glucopyranose), a product of cellulose combustion, is a tracer for biomass burning due to its high emission factor and specific pyrogenic sources [Simoneit et al., 1999; Schkolnik and Rudich, 2006; Bhattarai et al., 2019; Suciu et al., 2019]. It is only formed at low burning temperatures (150-350 °C) and thus reflects low intensity fires [Kuo et al., 2008].

Polycyclic aromatic hydrocarbons (PAHs) are also produced by biomass burning, but at a wider range of higher burning temperatures (200-700 °C) compared to levoglucosan [Lu et al., 2009; Keiluweit et al., 2012]. They are less source specific than levoglucosan, which complicates their use for fire reconstruction. Apart from pyrogenic origin (pyrogenic PAHs), other origins include petroleum (petrogenic PAHs) and diagenesis of biogenic precursors [Lima et al., 2005, and references therein]. Petrogenic PAHs enter the environment directly through either human-induced oil spill or natural oil seepage [Lima et al., 2005, and references therein]. Biogenic PAHs occur as a localized source, and only types of PAHs not analyzed in this thesis are generated, such as perylene, phenanthrene homologues etc. [Wakeham et al., 1980]. There are, however, ways to distinguish petrogenic and pyrogenic sources of PAHs and to further identify the sources of combustion (biomass or fossil fuels), with PAH diagnostic ratios as an example [Tobiszewski and Namieśnik, 2012]. Diagnostic ratios mostly involve pairs of PAHs which share the same molecular weight, similar physical and chemical properties, and undergo comparable environmental fates [Tobiszewski and Namieśnik, 2012]. Pyrogenic input is inferred from an increase in the proportion of the less stable isomer relative to the more stable isomer compared to petrogenic input [Yunker et al., 2002].

Since levoglucsan and pyrogenic PAHs occupy two different ranges in the combustion continuum (Fig. 2.3), they may provide more detailed information about the source fire regime once they originate from the same source. According to an in-situ fire emission study, more particle-associated PAHs are produced during the flaming phase of combustion (with higher burning intensity) than during the smoul-

dering phase of combustion (with lower burning intenstiy), while higher emission of levoglucosan occurs during the smouldering phase than during the flaming phase [Wang et al., 2007]. Combining sedimentary charcoal record with combustion-derived molecular markers, such as levoglucosan and/or polycyclic aromatic hydrocarbons (PAHs), is a promising way of reconstructing past fire intensity [Sikes et al., 2013; Schüpbach et al., 2015; Shanahan et al., 2016; Battistel et al., 2017; Miller et al., 2017; Argiriadis et al., 2018; Dietze et al., 2019; Schreuder et al., 2019]. Such an important fire regime characteristic is yet often not resolved in paleo-records [Archibald et al., 2018; Han et al., 2016].

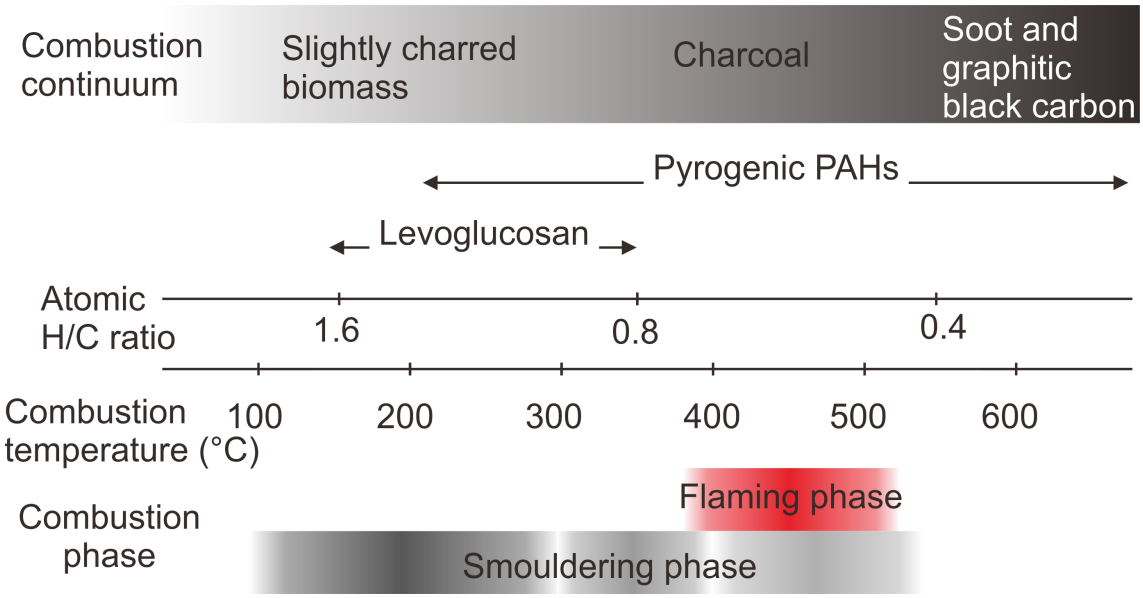


**Figure 2.3:** Combustion continuum figure modified from Kuo et al. [2008] and Hsieh et al. [2018]. The respective ranges of levoglucosan and polycyclic aromatic hydrocarbons in the continuum are shown. The flaming phase of fires are charecterized by higher burning temperatures (thus higher intensity) than the smouldering phase [Hsieh et al., 2018].

# Chapter 3

# Differential hydro-climatic evolution of East Javanese ecosystems over the past 22,000 years

Yanming Ruan[a], Mahyar Mohtadi[a], Sander van der Kaars[b,c,d], Lydie M. Dupont[a], Dierk Hebbeln[a], Enno Schefuß[a]

a MARUM – Center for Marine Environmental Sciences, University of Bremen, D-28359 Brmen, Germany
b School of Earth, Atmosphere and Environment, Monash University, Clayton, VIC 3800, Australia
c Cluster Earth and Climate, Faculty of Earth and Life Sciences, Vrije Universiteit, 1081 HV Amsterdam, Netherlands
d Department of Palynology and Climate Dynamics, Albrecht-von-Haller Institute for Plant Sciences, University of Göttingen, 37073 Göttingen, Germany

Published in *Quaternary Science Reviews* 218 (2019): 49-60

**Abstract:** The Maritime Continent, home to widespread tropical rainforest and millions of people, is the primary region of deep atmospheric convection on the Earth. However, debate exists whether the isotopologues of water reflect rainfall amount during the Last Glacial Maximum (LGM), resulting in different interpretations of the LGM climate of the Maritime Continent. Here we present paired leaf wax $\delta^{13}$C and $\delta$D records together with pollen data from a sediment core retrieved off East Java dating back to 22,000 years before present. We use three *n*-alkane homologues (*n*-C29, *n*-C31 and *n*-C33) in order to reconstruct past changes in vegetation types and seasonal rainfall. Our results suggest that in East Java, evergreen rainforest remained the dominant vegetation type in montane regions since the seasonality there remained relatively unaltered over the entire period. In contrast, the East Javanese lowlands were characterised by C4 grass expansion and an extended dry season but a wetter rainy season, thus stronger seasonality, during the LGM.

**Keywords:** Last Glacial Maximum; Paleoclimatology; Maritime Continent; ecosystem; leaf wax isotopes; leaf wax homologues

## 3.1 Introduction

The Maritime Continent is the largest and most important area of deep atmospheric convection on the Earth. An accurate reconstruction of the past hydro-climatic changes in this region is a prerequisite for understanding its role in the Earth system and for projections into the future, especially as the rainfall patterns in Indonesia affect the fates of the vast tropical rainforest and the lives of millions of people. The analyses of stable hydrogen isotope compositions ($\delta$D) in tandem with the stable carbon isotope compositions ($\delta^{13}$C) of sedimentary higher-plant derived leaf wax lipids have shown great potential in this regard [Konecky et al., 2016; Mohtadi et al., 2017; Niedermeyer et al., 2014; Russell et al., 2014; Tierney et al., 2012; Wicaksono et al., 2017]. Long chain leaf wax lipids, as components of terrestrial organic matter, are transported by rivers or wind before deposition in sedimentary archives, where they can serve as measures of the continental vegetation that biosynthesized them [e.g. Eglinton and Eglinton, 2008]. The leaf wax $\delta$D serves as a recorder of the $\delta$D values of the precipitation [Sachse et al., 2012, and references therein], which should primarily reflect rainfall intensity via the 'amount effect' in the tropics [more negative precipitation $\delta$D values suggest higher rainfall amounts; Dansgaard, 1964; Rozanski et al., 2013]. The leaf wax $\delta^{13}$C reflects the regional vegetation composition in terms of C3 and C4 plants [Diefendorf and Freimuth, 2017, and references therein], which is further linked to rainfall seasonality in the Maritime Continent [Dubois et al., 2014].

In the western part of the Maritime Continent (bordering the eastern tropical Indian Ocean), past changes in rainfall amounts are reconstructed by leaf wax $\delta$D from marine sediment cores; the leaf wax $\delta$D records shed light on past changes in the Indian Ocean Walker circulation during the Holocene [Niedermeyer et al., 2014] and the Last Glacial Maximum (LGM) [Mohtadi et al., 2017]. In Sulawesi, however, factors other than the amount effect are inferred in the interpretation of the sedimentary leaf wax $\delta$D records. During the LGM, more positive leaf wax $\delta^{13}$C values are inter-

preted as an expansion of C4 vegetation and thus drier climatic conditions, which seem to contradict the more negative leaf wax $\delta$D values from Lake Towuti and Mandar Bay during that period [Konecky et al., 2016; Russell et al., 2014; Wicaksono et al., 2017]. Two scenarios are proposed to explain this phenomenon. Konecky et al. [2016] propose that an intensified atmospheric circulation over the Maritime Continent drove the isotopic depletion of rainfall despite widespread aridity during the LGM ('dry convection' scenario). A change of moisture sources is also inferred to cause shifts in rainfall $\delta$D values, with the northerly monsoon winds carrying D-depleted air masses; thus a stronger northerly monsoon during the LGM tended to cause the more negative $\delta$D values recorded by leaf wax lipids ('moisture source change' scenario) [Konecky et al., 2016; Wicaksono et al., 2017].

Most published leaf wax isotope records in the Maritime Continent are based on one single compound [Konecky et al., 2016; Mohtadi et al., 2017; Niedermeyer et al., 2014; Russell et al., 2014; Tierney et al., 2012; Wicaksono et al., 2015, 2017]. Among the leaf wax *n*-alkane homologues (straight-chain alkanes with the formula CnH2n+2 but different numbers of carbon and hydrogen atoms), isotope studies generally use *n*-C29 (abbreviation for *n*-C29 alkane, similarly for *n*-C31 and *n*-C33) and/or *n*-C31 as these homologues are usually the most abundant and ubiquitous in both plants and sedimentary archives Garcin et al. [2014]; isotope studies also focus on one homologue if a strong correlation between changes in isotope values of several homologues is observed [e.g. Wicaksono et al., 2015]. However, this single compound approach tends to overlook the additional information provided by comparing the isotopic compositions of more homologues. For C3 rainforest plants, commonly the major *n*-alkane compound is *n*-C29, with high relative abundances of *n*-C31 but low relative abundances of *n*-C33 [Garcin et al., 2014; Vogts et al., 2009; Wu et al., 2017, Table S1]. On the other hand, the average *n*-alkane concentration profile of tropical C4 graminoids shows lower abundances of *n*-C29 but higher abundances of *n*-C33, with *n*-C31 being the major compound [Bush and McInerney, 2013; Rommerskirchen et al., 2006; Vogts et al., 2009; Wang et al., 2013, Table S1]. Studies have thus proposed to use *n*-C29 as an indicator for C3 vegetation and *n*-C33 as a C4 plant biomarker Diefendorf and Freimuth [2017]; Garcin et al. [2014]. For example, comparing $\delta^{13}$C compositions of the *n*-alkane homologues (*n*-C27 to *n*-C33) enables a more detailed reconstruction of past vegetation types in tropical South America [Fornace et al., 2016].

In this study, we present paired leaf wax $\delta^{13}$C and $\delta$D records of three *n*-alkane homologues (*n*-C29, *n*-C31 and *n*-C33) from a sediment core collected off the southern shore of East Java, within the Australian-Indonesian monsoon region of the Maritime Continent. We compare the carbon isotope compositions of the homologues with the pollen data from the same core to achieve a detailed vegetation reconstruction. The $\delta$D values of the homologues allow the evaluation of different scenarios regarding the seasonal hydro-climatic evolution of East Java from the LGM to the present.

## 3.2 Background

### 3.2.1 Modern climate

The precipitation pattern in East Java is connected to the seasonally reversing Australian-Indonesian monsoon linked with the latitudinal migration of the Intertropical Convergence Zone (ITCZ). The strong annual rainfall cycle is featured with one dry season and one rainy season. Higher rainfall amounts occur during the northwest monsoon (Australian-Indonesian summer monsoon, AISM) season, when the ITCZ is situated above the Maritime Continent between 0° and 15°S (Fig. 3.1a); drier conditions accompany the southeast monsoon (Australian-Indonesian winter monsoon, AIWM) season, when the ITCZ migrates towards the north with a mean position near 12°N (Fig. 3.1b). Two lowland stations in coastal East Java (Global Historical Climatology Network) - Pasirian (115m ASL) and Kencong (12m ASL) show that the mean monthly rainfall amount exceeds 200 mm/month from December to March. Low mean monthly precipitation amount lasts from June to September, with values below 100 mm/month for Pasirian and below 40 mm/month for Kencong [Peterson and Vose, 1997] (Fig. 3.2a). The state of the Pacific and the Indian Ocean exerts impacts on the climate of Java through inter-annual coupled atmosphere-ocean oscillations such as El Niño /Southern Oscillation [Chiang, 2009] and the Indian Ocean Dipole Mode [Saji et al., 1999].

The seasonal variation in precipitation is additionally influenced by montane elevations in the study area. There are four mountains in East Java (Kelud-Arjuna-Welirang, Tengger-Semeru, Lamongan-Argapura and Raung-Merapi-Ijen) and one in the centre of Bali (Barukau-Batur-Agung), with peaks around 3000 m (Fig. 3.1c). With increasing altitude, the length of the dry season generally decreases. Lowland areas below 500 m generally have a dry season length (monthly rainfall <100 mm) up to >5 months; while montane areas above 1000 m generally have a dry season shorter than 3 months (Fig. 3.1c, d) Whitten et al. [1996]. For example, the dry season length in Sumberasin (650m above sea level, 2 months) is shorter than in the two lowland stations (Fig. 3.2a). The pattern of reduced seasonality with higher elevations is also observed in other parts of the Maritime Continent, such as Sumatra [van der Kaars et al., 2010] and Sulawesi [Wicaksono et al., 2015].

### 3.2.2 Modern vegetation

The distribution of rainfall affects the distribution of vegetation types. Raingreen forests [forests with one or more deciduous species; Box, 1995; Roderick et al., 1999] are the dominant natural lowland vegetation types in East Java, while evergreen highland rainforests are restricted to altitudes above 1000 m [van der Kaars et al., 2010]. The distribution of the closed-canopy montane rainforest mimics the topography of the mountain ranges; patches of dry deciduous forests (where almost all the trees are deciduous) occur in coastal areas Whitten et al. [1996]. Major exploitation of the rainforest for timber began in the 1960s and is continuing today; more than 90% of pristine natural vegetation of Java is lost [Collins et al., 1991].

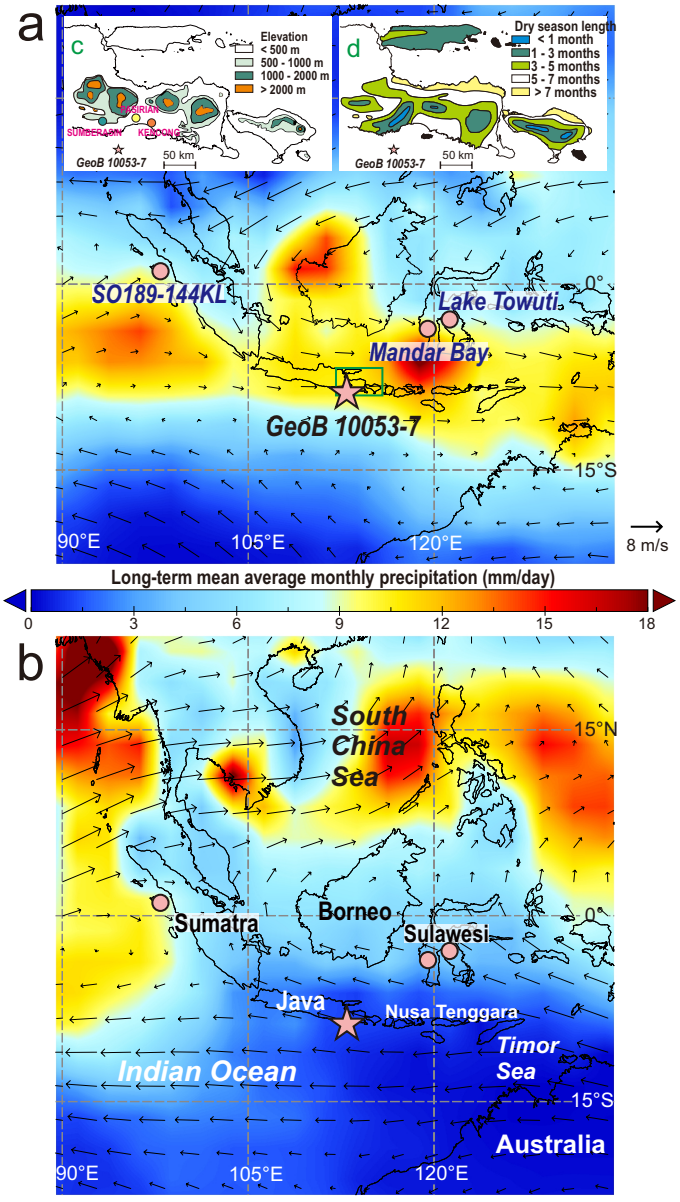


**Figure 3.1:** Modern wind pattern and precipitation distribution in January (a) and July (b) of the Maritime Continent. Shading, long-term monthly mean precipitation (mm/day) from 1981 to 2010 by CPC Merged Analysis of Precipitation (CMAP) [Xie et al., 1997]. Arrows, long-term monthly mean vector winds (m/s) at 850 mb from 1981 to 2010 by NCEP/NCAR Reanalysis 1 project [Kalnay et al., 1996]. Regional maps of elevation (c) and lengths of dry months with monthly rainfall <100 mm (d) of East Java - green rectangle in (a) are modified from Whitten et al. [1996]. Location of the sediment core GeoB10053-7 (Star) and other site locations discussed in the text (circles) are shown. Name of the proxy sites are shown in (a); geographic names are shown in (b); climate station names are shown in (c).

### 3.2.3 Controls on modern rainfall $\delta$D

The 'amount effect' describes the negative correlation between $\delta^{18}O/\delta D$ values of precipitation and rainfall amount on monthly timescales in tropical regions [Dansgaard, 1964; Rozanski et al., 2013]. This effect is the dominant control of the oxygen/hydrogen isotope compositions of modern rainfall in the monsoonal regions of the Maritime Continent [Belgaman et al., 2017; Konecky et al., 2013; Kurita et al., 2009; Suwarman et al., 2013]. A three-year observation by Belgaman et al. [2017] used the seasonal $\delta^{18}O$ variability in rain to divide the 33 stations in Indonesia into 4 clusters. Stations in East Java and Bali show the highest $\delta^{18}O$ values in the dry season (June – November) and the lowest values in the wet season (December – May), with a clear seasonal amount effect [Belgaman et al., 2017].

Different moisture sources associated with the reversing Australian-Indonesian monsoon are also inferred to contribute to the seasonal $\delta^{18}O/\delta D$ variability of precipitation in the Maritime Continent [Konecky et al., 2016; Suwarman et al., 2013]. Modelling studies show that distant moisture from the tropical eastern Indian Ocean to the west of Sumatra and from the north (South China Sea and western Pacific) is more subject to condensation during transport, producing more negative $\delta^{18}O$ values in stations from Java and Bali [Suwarman et al., 2013]. In contrast, moisture from the southern sources (Indian Ocean south of Java, Arafura Sea and Timor Sea) corresponding with the Australian-Indonesian winter monsoon tends to produce higher $\delta^{18}O$ values [Suwarman et al., 2013]. Thus, the alteration of moisture sources enhances the observed amount effect in the Australian-Indonesian monsoonal region.

We trace the modern moisture sources towards the core site by analysing rain-bearing back trajectories using NOAA's Hybrid Single Particle Lagrangian Integrated Trajectory (HYSPLIT4) model [Stein et al., 2015] with the NCEP/NCAR Reanalysis gridded dataset [Kalnay et al., 1996]. During December to March (austral summer) moisture originates from the west associated with AISM (Fig. 3.2b); during June to September (austral winter) moisture originates from the east associated with AIWM (Fig. 3.2c). During DJFM, 90% of the trajectories (red part in Fig. 3.2b) originate proximally from the Indian Ocean to the core site. A modelling study by Suwarman et al. [2013] shows that distant moisture from the Indian Ocean produces precipitation of more negative $\delta^{18}O/\delta D$ values; but its contribution is relatively minor (up to 1%, blue part in Fig. 3.2b). During JJAS, the tropical Indian Ocean off southern Java remains the major moisture source to our site (90%) (red part in Fig. 3.2c). Less than 10% of the trajectories originate from Timor Sea and Arafura Sea (green and blue parts in Fig. 3.2a), and this moisture source contributes even less than that due to the low amounts of rainfall during the dry season.

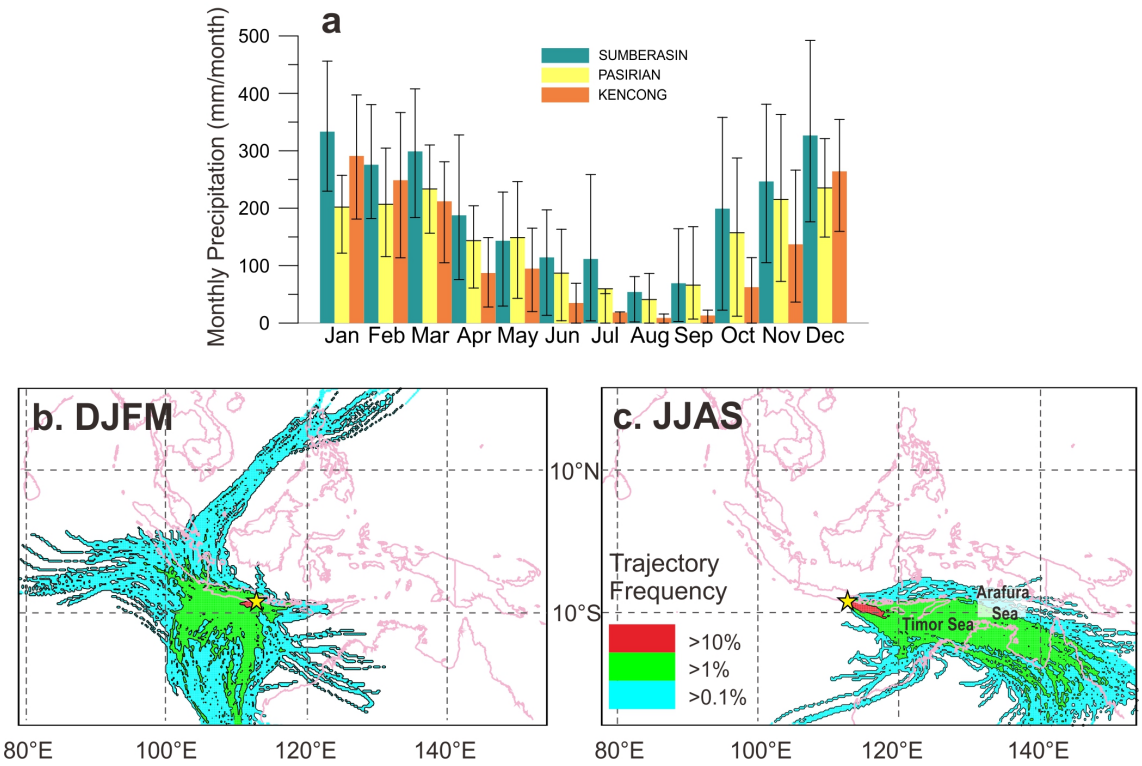


**Figure 3.2:** Monthly precipitation distribution and moisture trajectories of East Java. (a) Long-term monthly precipitation for three Global Historical Climatology Network (GHCN) stations near the core site in East Java [Peterson and Vose, 1997]: Sumberasin (650m ASL, 57yrs, 1915-1975), Pasirian (115m ASL, 26yrs, 1951-1976), Kencong (12m ASL, 34yrs, 1910-1975). Climate station locations are shown in Fig. 3.1c. The lower and upper error bars represent 17% and 83% percentiles, respectively. The moisture trajectory frequency is generated using the trajectory frequency analysis of 6-day back-trajectories over (b) December 2003 to March 2004 and (c) June to September in 2004. These two periods are chosen because no El Niño - Southern Oscillation and Indian Ocean Dipole-related anomalies occurred then. We used NOAA's Hybrid Single Particle Lagrangian Integrated Trajectory (HYSPLIT4) model [Stein et al., 2015] with the NCEP/NCAR Reanalysis gridded dataset [Kalnay et al., 1996]. The trajectory frequency is calculated as percentages of rain-bearing trajectories (>0 mm/day) to the location (8.5° S, 112.75° E) generated every 6 hours.

## 3.3 Leaf wax lipids and isotopes

### 3.3.1 Production and transport of leaf waxes

In tropical rainforests, plants grow year round and leaf production continues perennially [Moser et al., 2014]. The tropical forest (and leaf) production is higher in the wet season than in the dry season, associated with the seasonal rainfall changes [Moser et al., 2014; Rowland et al., 2014]. Thus, we assume a year-round production of leaf waxes, slightly rising during the wet season. This wet season bias is more significant in grasslands, where productivity is correlated with seasonal rainfall [Snyman and Fouché, 1993; Wiegand et al., 2004].

Riverine transport of leaf waxes is the major transport process from the continent to the ocean in wet areas. Leaf waxes are constantly eroded by rain either directly from plants or from the top-soils throughout the wet season and transported as

riverine suspended materials before deposited in marine sediments [Bird et al., 1995]. Riverine discharge in East Java is controlled by precipitation, which peaks in the rainy season in austral summer [Jennerjahn et al., 2004].

Leaf wax transport by aerosols may play a role during drier and windier periods. Leaf waxes can be ablated from the leaf surface directly by wind or emitted into the atmosphere by biomass burning. These leaf wax aerosols are prone to long distance transport, and can be deposited in marine sediments via both dry and wet deposition [Diefendorf and Freimuth, 2017].

### 3.3.2 Leaf wax $\delta^{13}$C as vegetation recorder

Different $^{13}$C fractionation due to the different metabolic pathways in C3 and C4 plants is encoded in their leaf wax $\delta^{13}$C values. The sedimentary leaf wax $\delta^{13}$C thus can serve as a proxy to reflect the contribution by C3 versus C4 vegetation [Diefendorf and Freimuth, 2017]. Plants using Crassulacean Acid Metabolism (CAM), a third metabolic pathway, may grow on ground or as epiphytes in forests [Lüttge, 2004]. But the CAM pathway is a stress survival strategy, which does not become dominant in most parts of the world [Lüttge, 2004]. The productivity of CAM plants and their contribution to sedimentary leaf waxes are low relative to C3 and C4 plants for the natural ecosystems in the Maritime Continent.

In tropical regions, the C4 photosynthetic pathway typically occurs in warm-season grasses and sedges, while the C3 pathway is utilized by trees and shrubs [Ehleringer et al., 1997; Eglinton and Eglinton, 2008]. According to the tropical plant compilation (Table S1, references in the table caption), the C4 photosynthetic pathway results in less isotopic fractionation and thus higher $\delta^{13}$C values than the C3 pathway. The mean $\delta^{13}$C values for the C3/C4 vegetation end-members are similar among the homologues (Table S1).

### 3.3.3 Leaf wax $\delta$D as recorder of precipitation $\delta$D

Studies of both living plants and lake-surface sediments show a strong linear correlation between leaf wax *n*-alkane $\delta$D values and source water (precipitation) $\delta$D values along climatic gradients, implying that precipitation $\delta$D is the primary control of leaf wax $\delta$D [Sachse et al., 2012, and references therein].

The apparent fractionation ($\varepsilon_{app}$) describes the total isotopic fractionation between precipitation and the leaf wax lipids. The $\varepsilon_{app}$ is thus the net effect of (1) the isotopic enrichment of soil water and leaf water in specific ecosystems, and (2) the biosynthetic fractionation ($\varepsilon_{bio}$) related to leaf wax synthesis. In the tropical plant compilation (Table S2, references in the table caption), the apparent fractionation between each of the three *n*-alkane homologues and mean annual precipitation ($\varepsilon_{alk/MAP}$) displays similar values within errors regardless of C3 and C4 photosynthetic carbon fixation pathways [Konecky et al., 2016]. The differences in $\varepsilon_{alk/MAP}$ between C3 and C4 vegetation types are always smaller than the standard deviations of each, which tend to introduce large uncertainties if a vegetation correction is applied [Konecky et al., 2016; Collins et al., 2013; Sachse et al., 2012]. A study of a marine sediment

transect off south-western Africa finds relatively constant apparent hydrogen fractionation factors along a prominent C3 to C4 vegetation shift, suggesting that the plant type transition (possibly related with changes in $\varepsilon_{bio}$) might counteract the effects of aridity (soil/leaf-water enrichment) in tropical regions [Vogts et al., 2016]. These findings support the straightforward use of leaf wax $\delta$D as the recorder of precipitation $\delta$D at our site.

## 3.4 Material and Methods

Sediment core GeoB 10053-7 (8° 40.59' S, 112° 52.35' E, 1375 m water depth, 750 cm core length) was retrieved south off Java during the SO-184 PABESIA expedition in 2005 [Hebbeln and cruise participants, 2006]. The age model is based on 19 accelerator mass spectrometry (AMS) 14C dates; the sediment core covers the past 22,000 years [Mohtadi et al., 2011].

A total of 72 sediment samples with dry weights between 9 and 24 g were collected for lipid analysis. The depths of the sediment samples were chosen according to the age model. In the upper 4.4 m of the core with higher sedimentation rates, we took samples every 10 to 20 cm (14.2 cm on average). Below 4.4 m till the base, the intervals of the sampling were 2 to 18 cm, with an average of 7.6 cm. The average time resolution of the record is ca. 300 years.

Lipid extractions were carried out using a DIONEX Accelerated Solvent Extractor (ASE 200) with a mixture of dichloromethane to methanol (9:1) at 1000 psi and 100°C (three cycles, 5 minutes each). An internal standard was added to each sample prior to extraction. After desulphurisation, water was removed using 2-cm $Na_2SO_4$ columns. Saponification was carried out with 0.1M KOH-solution, then neutral fractions were recovered by *n*-hexane. Silica gel columns (5-cm) were used to separate the neutral fractions: elution with *n*-hexane, dichloromethane and dichloromethane to methanol (1:1) yielded the apolar, ketone and polar fractions, respectively. The apolar fractions were additionally eluted with *n*-hexane over 5-cm $AgNO_3$-coated silica columns to remove unsaturated compounds.

We used a ThermoFisher Scientific Focus Gas Chromatography (GC) equipped with a DB-5MS capillary column (60 m, 0.32 mm, 0.1 µm) and a flame ionization detector to determine the concentrations of the *n*-alkanes. We identified the compounds according to the retention times of an external standard (a mixture of 12 *n*-alkanes, 10 ng/µl each), which was measured between every six samples. Quantification was performed by comparing peak areas of the target compounds to the external standard and to the internal standard squalane. The long-term precision of compound quantification is 5%, based on repetitive measurements of the external standard.

$\delta$D values of the *n*-alkanes were measured using a Thermo Trace GC (HP-5MS capillary column, 30 m, 0.25 mm, 1 µm) coupled via a pyrolysis reactor (1420 °C) to a Thermo Fisher MAT 253 isotope ratio mass spectrometer. A programmable-temperature vaporization injector was used to ensure no isotopic fractionation during injection. An external standard (a mixture of 12 *n*-alkanes of known isotope compositions) was measured between every six sample measurements to monitor the

machine performance. The long-term mean absolute deviation based on the external standard was 3‰. The analyses of the internal standard (squalene, $\delta$D = -180‰) in all samples revealed a precision of 2‰ and an accuracy of 3‰ (n = 125). The $H_3^+$ factor, which was determined on a daily basis, had a mean value of 5.17 (n = 13) and varied between 5.13 and 5.22 throughout measurements. Samples were analysed in duplicate, except for 14 samples that were analysed only once because of low compound abundances. The difference between the duplicates ranges from <1‰ to 6‰ with a mean value of 1‰ for each homologue (*n*-C29, *n*-C31 and *n*-C33) (Fig. S1). $\delta$D values were calibrated against the external $H_2$ reference gas, and are reported in ‰ against Vienna Standard Mean Ocean Water (VSMOW). We adjusted the $\delta$D of the *n*-alkanes for ice volume changes by using a seawater $\delta^{18}$O curve (Waelbroeck et al., 2002) and converting it to $\delta$D assuming an LGM D-enrichment of 8‰ (Fig. S1).

$\delta^{13}$C values of *n*-alkanes were measured using a Thermo Trace GC (Rxi-5MS capillary column, 30 m, 0.25 mm, 0.25 µm) coupled via a combustion interface (1000 °C) to a ThermoFinnigan MAT 252 isotope ratio mass spectrometer. A programmable-temperature vaporization injector was used to ensure no isotopic fractionation during injection. $\delta^{13}$C values were calibrated against the external $CO_2$ reference gas, and are reported in ‰ against Vienna PeeDee Belemnite (VPDB). The external standard was routinely measured similar to the $\delta$D analyses. The long-term mean absolute deviation based on the external standard was 0.3‰. The analyses of the internal standard (squalene, $\delta^{13}$C = -19.8‰) across the measurements corroborated a precision of 0.3‰ and an accuracy of <0.1‰ (n = 88). Samples were analysed in duplicate, except for 35 samples that were measured only once due to low compound abundances after $\delta$D analyses. The difference between the duplicates ranges from <0.1‰ to 0.5‰ with a mean value of 0.1‰ for each homologue (*n*-C29, *n*-C31 and *n*-C33) (Fig. S2).

For palynological analysis, 34 sediment samples were collected at depth intervals of 3 – 40 cm. Between 4.8 and 6.0 ml of sediment was suspended in approximately 40 ml of tetra-sodium-pyrophosphate (±10%) then sieved over 200 and 7 micrometre screens, followed by hydrochloric acid (10%) treatment, heavy liquid separation (sodium-polytungstate, SG 2.0, 20 min at 2,000 rpm, twice), acetolysis and sodium carbonate (20%) treatment. The resulting organic residues were mounted in glycerol and slides were sealed with paraffin wax. Prior to chemical treatment a known amount of Lycopodium marker spores was added to each sample in order to estimate palynomorph concentrations. Pollen percentage values (unless otherwise specified) were calculated on the dryland pollen sum, which was comprised of the total number of gymnosperm and angiosperm pollen grains counted per sample excluding pollen from mangrove taxa. Slides were counted along evenly spaced transects until a minimum count of 250 dryland pollen grains was reached, except for 5 samples in which pollen concentration was poor and the minimum dryland pollen count was 100. The average number of dryland pollen grains counted was 530 per sample. Confidence intervals (95%) of the pollen percentages/ratios were calculated following Maher [1972].

## 3.5 Results

The dominant *n*-alkane homologues in the core samples are *n*-C31 (230 ± 130 ng/g dry sediment), *n*-C29 (150 ± 85 ng/g dry sediment) and *n*-C33 (140 ± 85 ng/g dry sediment). The long chain *n*-alkane homologues show a distinct odd-over-even predominance, a feature of higher plant leaf waxes [Eglinton and Hamilton, 1967]. The predominance is quantified by the carbon preference index (CPI, Equation 3.5.1). Strong degradation of organic matter will result in lower CPI values [Bray and Evans, 1961], with a CPI value approximating 1 for petroleum as an extreme [Kolattukudy, 1967]. The overall high CPI values in our core, which range from 4.5 to 6.8 between 22 ka (thousand years before present) and 10 ka, and from 3.0 to 4.9 since 10 ka, indicate the dominance of relatively non-degraded plant-derived long chain *n*-alkanes.

$$CPI_{27\text{-}33} = \frac{1}{2} \times \frac{[n\text{-}27] + [n\text{-}29] + [n\text{-}31] + [n\text{-}33]}{[n\text{-}26] + [n\text{-}28] + [n\text{-}30] + [n\text{-}32]} + \frac{1}{2} \times \frac{[n\text{-}27] + [n\text{-}29] + [n\text{-}31] + [n\text{-}33]}{[n\text{-}28] + [n\text{-}30] + [n\text{-}32] + [n\text{-}34]} \tag{3.5.1}$$

The $\delta^{13}$C values of the three homologues (abbreviated to $\delta^{13}C_{n\text{-}29}$, $\delta^{13}C_{n\text{-}31}$ and $\delta^{13}C_{n\text{-}33}$) are most positive during the LGM and most depleted during the Holocene, with stepwise decreases during the deglaciation (Fig. 3.3a). The range of variation for the $\delta^{13}$C values over the record is 2.6‰ for *n*-C29, which is smaller than that of *n*-C31 (5.8‰) and *n*-C33 (7.3‰). During the LGM, the $\delta^{13}C_{n\text{-}29}$ values (-29.5‰ to -30.2‰) are the most negative among the homologues, followed by $\delta^{13}C_{n\text{-}31}$ (-28.1 to -29.1‰) and $\delta^{13}C_{n\text{-}33}$ (-24.2‰ to -25.1‰). During the Holocene, $\delta^{13}C_{n\text{-}31}$ becomes the most negative among the three (-31.2‰ to -33.9‰), followed by $\delta^{13}C_{n\text{-}29}$ (-30.7‰ to -32.1‰) and $\delta^{13}C_{n\text{-}33}$ (-26.7‰ to -31.5‰).

We conduct a concentration-weighted mixing model of the vegetation end-members to assess the impact of C3 versus C4 vegetation shift on the $\delta^{13}$C values of the homologues. The model is based on the concentrations and $\delta^{13}$C values of each *n*-alkane homologue of the two end-members (for C3 and C4 plants respectively). The $\delta^{13}$C values of each homologues are the concentration-weighted mix of the C3/C4 end-members. Due to limited data from modern East Javanese vegetation, the end-member concentrations and $\delta^{13}$C values are mean values derived from the tropical plant compilation (Table S1, references in the table caption).

$$\delta^{13}C_{29} = \frac{189 \times fC3 \times (-36.4‰) + 57 \times (1 - fC3) \times (-21.9‰)}{189 \times fC3 + 57 \times (1 - fC3)} \tag{3.5.2}$$

$$\delta^{13}C_{31} = \frac{119 \times fC3 \times (-36.7‰) + 161 \times (1 - fC3) \times (-22‰)}{119 \times fC3 + 161 \times (1 - fC3)} \tag{3.5.3}$$

$$\delta^{13}C_{33} = \frac{25 \times fC3 \times (-36.8‰) + 110 \times (1 - fC3) \times (-22.3‰)}{25 \times fC3 + 110 \times (1 - fC3)} \tag{3.5.4}$$

FC3 represents the relative contribution of C3 plants versus C4 plants, which is an integrating index of vegetation biomass, transport and deposition. fC3 ranges from 0 (full C4 vegetation) to 1 (full C3 vegetation). In a tropical ecosystem dominated by C3 plants (fC3 approaching 1), $\delta^{13}$C values *n*-C33 of are more sensitive to C4 vegetation expansion than those of *n*-C29 and *n*-C31, due to the high relative *n*-C33 concentrations in C4 plants. In a C4 dominated tropical ecosystem (f C3 approaching 0), $\delta^{13}$C values of *n*-C29 are more sensitive to C3/C4 vegetation type shifts than those of the other two homologues (Fig. 3.4).

We plot the $\delta^{13}$C values of the homologues from our sediment core during both the LGM and the Holocene onto the mixing curve (Fig. 3.4). The result shows that *n*-C31 and *n*-C33 share similar f C3 values during both the LGM (∼0.5) and the Holocene (0.7 to 0.9). Thus the Δf C3 for LGM-Holocene contrast ( 0.3) is similar for these two homologues. On the contrary, the f C3 values for *n*-C29 through the record (less than 0.4) are in a different range than the other two homologues; the LGM-Holocene Δf C3 ( 0.1) is also smaller. Please note that the absolute f C3 value needs to be taken with caution because this qualitative index depends on the actual end-members used. Instead, the Δf C3 values provide more robust information about the C3/C4 vegetation shift between the LGM and the Holocene. We are aware of the large ranges of *n*-alkane concentrations in plant types (Table S1). The ranges result from the compilation of data from various ecosystems [e.g. Diefendorf and Freimuth, 2017], and do not reflect the actual plant types within specific catchments. We expect smaller ranges at our site despite the lack of modern vegetation data from East Java. Nevertheless, despite these large ranges, the general trend how a C3/C4 vegetation type shift causes changes in $\delta^{13}$C values of different alkane homologues is obvious.

The ice volume adjusted $\delta$D values of the three *n*-alkane homologues (abbreviated to $\delta D_{n\text{-}29}$, $\delta D_{n\text{-}31}$ and $\delta D_{n\text{-}33}$) are most depleted during the LGM and most enriched through the Holocene. They differ, however, in their LGM-Holocene changes (Fig. 3.3j). The range of $\delta$D variation over the record is 12‰ for *n*-C29; in contrast, the range for *n*-C33 (31‰) is more than double, with *n*-C31 (20‰) in between. During the LGM, *n*-C33 has the most negative $\delta$D values (-175‰ to -168‰), followed by *n*-C31 (-171‰ to -167‰), then *n*-C29 (-165‰ to -161‰). During the Holocene, *n*-C29 and *n*-C31 have similar $\delta$D values of -158‰ to -152‰, which are generally more negative than that of *n*-C33 (-158‰ to -144‰).

During the LGM, the highest grass pollen (Poaceae) percentages (>35%), low representation of lowland rainforest taxa ( 20%) but high contributions from montane taxa occurred. In contrast, the Holocene is characterised by low grass pollen percentages (<20%), high values for lowland rainforest taxa (>50%) but low representation of montane taxa (Fig. 3.3b, c, d). Both the grass pollen percentage and the percentage of montane rainforest taxa to total rainforest taxa decrease stepwise during the deglaciation. The fern spores to pollen ratio shows a maximum during the Holocene but displays lowest values during the deglaciation, with LGM levels intermediate (Fig. 3.3g).

Two pollen types of woodland taxa in the core samples mainly originate from Aus-

tralia. Low percentages of Eucalyptus type pollen (Myrtaceae) fluctuate around 4 ± 2% throughout the core (Fig. 3.3e). Gyrostemon type pollen (Gyrostrmonaceae) also occur regularly through the record but with percentages lower than 0.9% (Fig. 3.3f). The only other pollen types that can be expected to originate from Australia are the grass pollen (Poaceae), Amaranthaceae and Asteraceae. The latter two types are hardly present in our sediment core.

## 3.6 Discussion

More positive leaf wax $\delta^{13}$C values in our record during the LGM indicate an expansion of more drought-tolerant C4 vegetation, which seem to contradict the more negative leaf wax $\delta$D values (indicating more rainfall according to the amount effect). Despite different regional settings, similar patterns are found in lake and marine sediments in Sulawesi from that period [Konecky et al., 2016; Wicaksono et al., 2017; Russell et al., 2014]. The contradiction between leaf wax $\delta^{13}$C and $\delta$D lies in the interpretation of both proxies. Unlike the relatively small catchment area of the lake sediments, the potential source area of the leaf waxes derived from a marine sediment core needs to be constrained. Thus, we first discuss the potential sources of pollen and leaf wax lipids. After that, we discuss the potential scenarios and deduce our interpretation.

### 3.6.1 Source of pollen and leaf wax lipids

We use the pollen data from the same core to constrain the sources of leaf wax lipids through the record. Although the quantity of production differs between leaf waxes and pollen, both reflect information on the same source vegetation. In particular, relative changes in vegetation will affect both pollen distribution and leaf wax lipid compositions.

Core-top pollen distributions from the south-eastern Indonesian waters imply that marine sediment pollen assemblages reflect the adjacent onshore vegetation types [Kershaw et al., 2007; van der Kaars et al., 2001]. Both the pollen percentages of rainforest angiosperm and rainforest conifer show high values along the coast of the Indonesian Archipelago and then decrease rapidly southward [Kershaw et al., 2007], implying a more local source of the rainforest taxa. Given the proximity of the core location to the East Javanese coastline, the rainforest taxa in the pollen record of GeoB10053-7 are likely to reflect the rainforest vegetation history of East Java. Due to the blocking effect of the 3000 km long volcanic arc mountain chains from Sumatra all the way to Java, we assume the contribution of pollen taxa from the exposed Sunda Shelf during the LGM to be minor.

Given the extensive eucalypt forests and woodlands in northern Australia, the south-east monsoon (AIWM) during the dry season may transport the Eucalyptus type pollen and Gyrostemon type pollen from Australia to East Java despite the long distance (>1,500 km). The existence of Eucalyptus and Gyrostemon type pollen throughout the GeoB10053-7 record implies that the Australian input cannot be excluded (Fig. 3.3e, f); however, the low percentages of both pollen types suggest

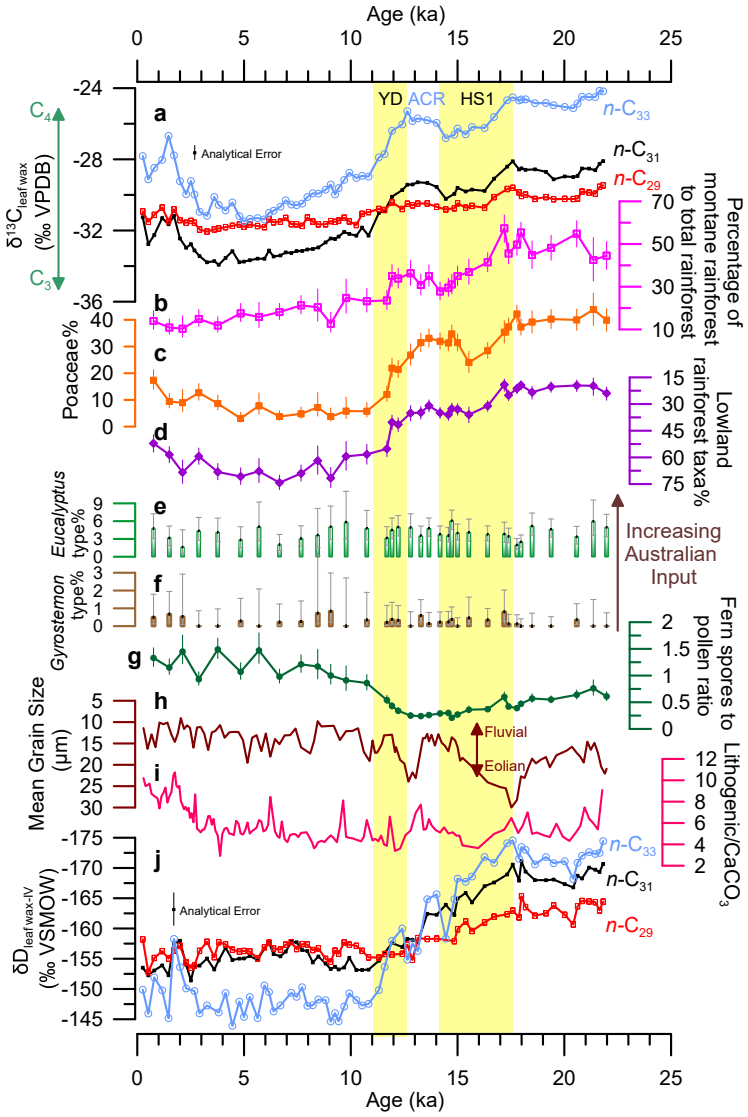


**Figure 3.3:** Various proxy records from sediment core GeoB10053-7. a) The $\delta^{13}$C values of the *n*-alkane homologues (red for *n*-C29, black for *n*-C31 and blue for *n*-C33). The analytical error (0.3‰) shows the long-term mean absolute deviation based on the external standard. b) The percentage of montane rainforest to total rainforest pollen counts. c) The percentage of grass pollen (Poaceae). d) The percentage of lowland rainforest pollen. The percentages of Eucalyptus type pollen (e) and Gyrostemon type pollen (f), which are mainly derived from Australia. g) The ratio of fern spores to pollen. Vertical error bars in b, c, d, e, f and g display 95% confidence limits [Maher, 1972]. h) The mean grain size distribution [Mohtadi et al., 2011]. i) The ratio of lithogenic particles to calcium carbonate as a proxy for river runoff [Mohtadi et al., 2011]. j) The ice volume adjusted $\delta$D values of the *n*-alkane homologues (red for *n*-C29, black for *n*-C31 and blue for *n*-C33). The analytical error (3‰) shows the long-term mean absolute deviation based on the external standard. The two vertical yellow bars correspond to Heinrich Stadial 1 (HS1) and the Younger Dryas (YD), with the Antarctic Cold Reversal (ACR) in between.

relatively minor and constant Australian contributions to the overall pollen counts. The Eucalyptus type percentages in GeoB10053-7 remain low as 4 ± 2% (Fig. 3.3f), similar to the core-top values in the open ocean and near the Indonesian coast but

much lower than the values near the north Australian source area [(>20%; van der Kaars et al., 2001; van der Kaars and De Deckker, 2003]. The lack of a clear glacial - interglacial pattern in both pollen percentages also suggests that the input from Australian savannah woodlands was not significant during the LGM, when the Sahul Shelf was exposed with a potentially expanded pollen source area.

The relatively low grass pollen percentages during the Holocene in the GeoB10053-7 record are consistent with the low percentages of Eucalyptus type and Gyrostemon type pollen. But unlike the latter two, grass pollen percentages reach high values around 40% during the LGM (Fig. 3.3c), which are close to the core-top percentages near the Australian source area. It is thus possible that the grass pollen are prone to longer transport than the two woodland pollen taxa, and/or the savannah grassland was more widespread than woodland during the LGM on the exposed Sahul Shelf. On the other hand, the high grass pollen percentages during the LGM may also be a local result, with a more open-canopy vegetation type in lowland East Java during that period.

The comparison of the grass pollen percentages with sedimentological indices from the same core supports the second scenario. The grain size distribution of the terrigenous fraction of core GeoB10053-7 (Fig. 3.3h) has been utilized to distinguish riverine vs. aeolian contributions; the lithogenic to $CaCO_3$ ratio (Fig. 3.3i) serves as a proxy for river runoff [Mohtadi et al., 2011]. Both indices show a minor LGM-Holocene difference [Mohtadi et al., 2011]. Without evidence for increased aeolian input during the LGM, a predominant contribution of grass pollen and waxes from northern Australia seems unlikely, despite a potential increase of grass source area on the exposed Sahul Shelf due to a lower sea level. During the deglaciation (18 - 12 ka) when the potential source area was still exposed, the peak in grass pollen percentages during 15 - 13 ka was actually accompanied by a major fluvial contribution inferred by both the mean grain size distribution and lithogenic to $CaCO_3$ ratios during that period (Fig. 3.3c, h, i). This synchrony suggests that Javanese fluvial contribution contained a high portion of grass pollen, in accordance with a much more open local vegetation type during the deglaciation.

Rhizophora type mangrove pollen grains are found throughout the sediment core. The mangrove to pollen ratio shows high values (20% to 40%) between 16 ka and 8 ka but generally low values (around or below 5%) for the rest of the record (data not shown). Rhizophora mangroves produce *n*-C29 and *n*-C31 like terrestrial plants and may potentially contribute to the isotope value shifts observed in the record [Ladd and Sachs, 2015, 2013; Mead et al., 2005]. However, the percentage of mangrove pollen does not correlate with the $\delta^{13}C$ or $\delta D$ values of any *n*-alkane homologue. The gradual trends in our leaf wax $\delta^{13}C$ and $\delta D$ records between 16 ka and 8 ka and the absence of abrupt changes before and after this period suggest that the contribution of leaf waxes from mangrove is minor.

In summary, East Java was the major source area of both rainforest pollen and grass pollen in sediments of core GeoB10053-7 throughout the entire record, with minor contributions from northern Australia (Sahul Shelf). We therefore infer that the leaf wax lipids are also derived predominantly from local source vegetation. The strong

similarity between the pollen records and the leaf wax $\delta^{13}$C (further discussion in 6.2) supports this conclusion.

### 3.6.2 $\delta^{13}$C of *n*-alkane homologues and vegetation changes at different altitudes

To solve the discrepancy between the leaf wax $\delta^{13}$C and $\delta$D signals, our $\delta^{13}$C records based on the *n*-alkane homologues in tandem with the pollen data provide a more detailed reconstruction of the vegetation changes in East Java since the LGM and yield a more solid climatic interpretation compared to approaches based solely on single compounds.

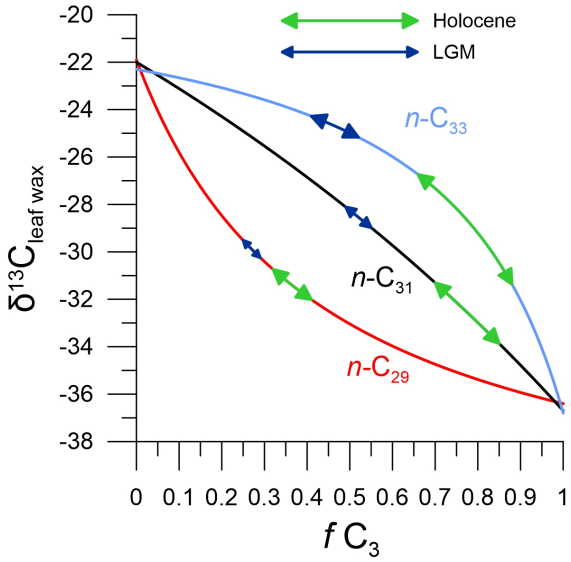


**Figure 3.4:** Concentration-weighted mixing model based on the concentrations and $\delta^{13}$C values of each *n*-alkane homologue of the two vegetation end-members (C3 and C4 plants). The $\delta^{13}$C values of each homologue are calculated according to the equation (3) to (5). f C3 (0 to 1) represents the relative contribution of C3 plants versus C4 plants. The $\delta^{13}$C values of the homologues from GeoB10053-7 during the LGM (dark blue arrows) and the Holocene (green arrows) are plotted onto the mixing curves.

The similar f C3 values and $\Delta$f C3 for LGM-Holocene contrast for *n*-C31 and *n*-C33 (Fig. 3.4) implies that the changes in $\delta^{13}C_{n\text{-}31/33}$ values are caused by a comparable C3/C4 vegetation type shift. Further comparison shows that the $\delta^{13}C_{n\text{-}31}$ and $\delta^{13}C_{n\text{-}33}$ records co-vary with the grass pollen percentages of the same core: the more positive $\delta^{13}C_{n\text{-}31/33}$ values during the LGM coincide with higher grass pollen percentages (Fig. 3.3a, c). The observed similarity fits the finding of higher concentrations of *n*-C31 and *n*-C33 in tropical C4 grasses [Bush and McInerney, 2013; Garcin et al., 2014; Rommerskirchen et al., 2006; Vogts et al., 2009; Wang et al., 2013].

In contrast, the $\delta^{13}C_{n\text{-}29}$ record displays a different pattern from $\delta^{13}C_{n\text{-}31/33}$. According to the mixing model, the f C3 values fall in a different range than those of the other two homologues, with a smaller LGM-Holocene contrast ($\sim$0.1 $\Delta$f C3) (Fig. 3.4). The *n*-C29 exception implies that the C3/C4 vegetation shift causing the changes of $\delta^{13}C_{n\text{-}31/33}$ in our record did not have the same impact on $\delta^{13}C_{n\text{-}29}$, and

that *n*-C29 was therefore derived from a relatively distinct vegetation source. Because *n*-C29 is the major *n*-alkane homologue in C3 rainforest plants [Garcin et al., 2014; Wu et al., 2017; Vogts et al., 2009], our $\delta^{13}C_{n\text{-}29}$ record most likely reflects the East Javanese rainforest. Besides, we detect similar trends in the $\delta^{13}C_{n\text{-}29}$ record and the relative changes in pollen percentages of montane rainforest taxa to total rainforest taxa (Fig. 3.3a, b). Higher $\delta^{13}C_{n\text{-}29}$ values during the LGM correspond to increased representations of montane rainforest, while more negative $\delta^{13}C_{n\text{-}29}$ values correlate to lower pollen percentages of montane taxa during the Holocene. This similarity suggests that the *n*-C29 predominantly reflected montane rainforest vegetation during the LGM and lowland rainforest during the Holocene. This pattern is in line with the observation of altitudinal leaf wax $\delta^{13}C_{n\text{-}29}$ distributions in tropical forests in the Andes: less negative $\delta^{13}$C values of leaf wax lipids are observed at higher altitudes [Wu et al., 2017]. Plant leaf $\delta^{13}$C values are likely to respond to water availability within a constant plant community [Diefendorf et al., 2010; Diefendorf and Freimuth, 2017]. But the source plant community for *n*-C29 through the record was not constant, with higher contributions of montane rainforest during the LGM. Given the relatively large variability in leaf $\delta^{13}$C values among vegetation types [Diefendorf et al., 2010], the response of $\delta^{13}C_{n\text{-}29}$ to water stress was highly uncertain. The recycling of $CO_2$ under the closed rainforest canopy causes accumulation of $CO_2$ depleted in $^{13}$C [Buchmann et al., 1997], which leads to negative leaf wax $\delta^{13}$C values as low as -40‰[Garcin et al., 2014; Wu et al., 2017; Vogts et al., 2009]. Such negative $\delta^{13}$C values are absent in our sediment core, implying the effect of $CO_2$ recycling is minor.

Due to the close relation between *n*-C29 and montane rainforest taxa, the relatively small range of $\delta^{13}C_{n\text{-}29}$ variation through the sediment core suggests that the canopy structure of montane rainforest remained relatively closed during the LGM. The significant increase in $\delta^{13}C_{n\text{-}31}$ and $\delta^{13}C_{n\text{-}33}$ values, a rise in grass pollen percentages but low representation of lowland rainforest taxa during the LGM reflect that the lowland vegetation in East Java was much more open during that period. This scenario further implies strongly enhanced rainfall seasonality in lowland areas but relatively unaltered montane rainfall seasonality during the LGM compared to the Holocene, in line with the interpretation of leaf wax $\delta^{13}$C as rainfall seasonality indicator Dubois et al. [2014]. Lower atmospheric $CO_2$ concentrations during the LGM [Monnin et al., 2001] may have favoured the C4 photosynthetic pathway due to its carbon-concentrating mechanism; but this factor alone can hardly cause vegetation shifts from trees to grasses indicated by our pollen records [Collatz et al., 1998; Ehleringer, 2005]. The increased contribution of montane rainforest in our pollen record during the LGM may be related to the downslope migration of montane rainforest, which is indicated by pollen records over the Maritime Continent during the LGM [Kershaw et al., 2007, and references therein].

The contrasting responses of low and high altitude ecosystems are observed across vegetation records from the Maritime Continent, with the higher elevations serving as rainforest refugia due to topographic control on rainfall [Qian, 2008; van der Kaars et al., 2010; Wicaksono et al., 2015]. Clouds are an important moisture source in montane regions. During the wet season, clouds cover the slopes and

peaks of mountains for days; in the dry season, a belt of clouds at around 2000 m is more common [Whitten et al., 1996]. Since plants can use the water droplets from the clouds that adhere to the leaf surfaces, montane plants are not water limited even though the actual rainfall amount is low [Goldsmith et al., 2013]. Due to the relatively steep coastline along southern Java, the cloud formations at mountain ranges is unlikely to be affected by the lower sea level during the LGM [Wicaksono et al., 2015].

### 3.6.3 $\delta$D of *n*-alkane homologues and hydrologic responses of different ecosystems

Similar to the carbon isotope compositions of the *n*-alkane homologues, the various homologues display different evolutions in the $\delta$D records. In contrast to the relatively small range of the variation in $\delta D_{n\text{-}29}$ through the record (12‰), we observe a significant D-depletion of 20‰ in $\delta D_{n\text{-}31}$ and 30‰ in $\delta D_{n\text{-}33}$ during the LGM compared to the Holocene (Fig. 3.3a). With the $\delta^{13}C_{n\text{-}29}$ correlated with representations of montane tropical rainforest and the $\delta^{13}C_{n\text{-}31/33}$ lowland grass expansion as discussed in the former section, we would expect that the $\delta$D values of the homologues reflect distinct hydrological responses of different ecosystems, which do not fit in the two existing scenarios ('dry convection' and 'moisture source change').

Our results do not support the 'dry convection' scenario for two reasons. Firstly, the climate was not overall arid in East Java during the LGM. The lithogenic to $CaCO_3$ ratio from core GeoB10053-7 (Fig. 3.3i) during the LGM is not lower than during the Holocene [Mohtadi et al., 2011], which suggests that the river discharge during the LGM was not reduced relative to the Holocene and contradicts an interpretation of overall aridity during the LGM. Secondly, the basin-wide regional convection would cause concurrent $\delta$D changes in precipitation, which contradicts the different $\delta$D patterns observed from the various homologues. Instead, our results imply that the $\delta$D values of the distinct homologues capture different rainfall regimes in montane vs. lowland ecosystems.

The 'moisture source change' scenario is also not applicable in our setting. The HYSPLIT4 trajectory analyses show that 90% of moisture sources remain proximally south off Java during both austral winter and summer (red parts in Fig. 3.2b, c). During austral summer, moisture from the Java Sea [Griffiths et al., 2009] or from the South China Sea [Konecky et al., 2016; Wicaksono et al., 2017] has minor contribution to our site (trajectory frequency <1%, Fig. 3.2b). Due to the blocking effect of the 3000 km long volcanic arc mountain chains from Sumatra all the way to Java, we assume that the modern austral summer moisture sources remained largely unchanged during the LGM. Timor Sea and Arafura Sea contribute less than 10% moisture to our site during austral winter (Fig. 3.2c, previously discussed in 2.3). We expect this contribution to be even less during the LGM. The lower sea level during the LGM likely reduced the areas of Arafura Sea and Timor Sea and caused less evaporation, less cloud formation and thus less precipitation. As proposed by Mohtadi et al. [2014], the mean ITCZ position stayed on the same latitude as today during the LGM and only moved southward during Heinrich Stadial 1. As the $\delta$D

values of each homologue remain basically identical from the LGM till Heinrich Stadial 1, the suggested reorganisation of the Hadley circulation does not seem to affect the rather proximal moisture sources to our site. Findings from a General Circulation Earth System model study using Vapour Source Distribution tracers support the inference of moisture sources being rather local during Heinrich Stadial 1 at two sites from the middle (Borneo) and the southern (Liang Luar cave) Maritime Continent [Lewis et al., 2010].

We propose another scenario to explain the observed trends in leaf wax isotopes during the LGM. The more positive $\delta^{13}C_{n\text{-}31/33}$ values indicate enhanced seasonality while the more negative $\delta D_{n\text{-}31/33}$ values reflect increased precipitation intensity in East Javanese lowland during the wet season of the LGM compared to the Holocene. The production, erosion and fluvial transport of leaf waxes favour a wet season biased $\delta$D signal in the sedimentary leaf wax lipids in East Java. The wet season bias is supported by a study from offshore West Africa, where the sedimentary leaf wax $\delta$D values closely match the instrumental record of the rainy season precipitation in the catchment area [Niedermeyer et al., 2016]. Since the river runoff of East Java during the LGM remained similar to that during the Holocene as reflected by the lithogenic to $CaCO_3$ ratios [Mohtadi et al., 2011], the wet season with enhanced rainfall intensity during the LGM was likely to be shorter, compensated by a longer dry season. High fern-spores/pollen ratios in the Maritime Continent indicate increased moisture availability [Turney et al., 2006] or increased riverine input [van der Kaars et al., 2010]. The prolonged dry season and the more open-canopy vegetation in the East Javanese lowland during the LGM probably caused the relatively low fern-spore/pollen ratio compared to the Holocene. The complex ecological preferences of different fern species may also play a role. Prolonged dry seasons in Sumba, southern Indonesia during the LGM are also proposed by Dubois et al. [2014], who attribute grassland expansion to increased dry season water stress. In accordance with the interpretation of $\delta^{13}C_{n\text{-}29}$, our $\delta D_{n\text{-}29}$ record potentially reflects lowland rainfall intensity during the Holocene and montane rainfall intensity during the LGM. The slightly lower $\delta D_{n\text{-}29}$ values during the LGM correspond to higher portions of montane rainforest taxa. This pattern is in line with the observation of D-depleted rainfall at higher elevations [Gonfiantini et al., 2001], although the downslope migration of montane rainforest during the LGM may have dampened this effect.

A strong dry season in the lowlands and less seasonality at higher altitudes are also observed by studies of modern climate in the Maritime Continent. For example, satellite observations and climate model results [Qian et al., 2010; Rauniyar and Walsh, 2013] show overall drier lowlands but high rainfall in montane regions. Our inference for the LGM climate is in accordance with modern observations with a decreased lowland rainfall during a longer and more severe dry season, and intensified rainfall during a shorter rainy season. The D-depletion of lowland precipitation reflected by *n*-C33 supports this scenario during the LGM. On the other hand, leaf wax $\delta$D of highland vegetation reflected by *n*-C29 during the LGM integrates both the D-depleted rainfall of the rainy season and the relatively D-enriched precipitation during the drier seasons, when rainfall still occurred sporadically at high altitudes.

This explains the dampened LGM-Holocene contrast in $\delta D_{n\text{-}29}$ compared to $\delta D_{n\text{-}31/33}$.

This scenario is supported by a multi-model ensemble study of the Australian-Indonesian monsoon during the LGM, which shows enhanced seasonality with a shorter but more intense wet season in the Australian-Indonesian monsoon region of the Maritime Continent [Yan et al., 2018]. The model ensemble shows an anomalous low sea level pressure over northwest Australia during the early wet season (November to December), accompanied by strong low-level westerlies from the exposed Sunda Shelf to the exposed Sahul Shelf; this pattern is favourable for moisture convergence and thus increased rainfall [Yan et al., 2018]. Another Earth system model study focusing on the lowered sea level of the Indo-Pacific warm pool area during the LGM simulates increased rainfall in the Australian-Indonesian monsoon region from September to November [DiNezio et al., 2016]. The increase in wet season rainfall is a relatively local phenomenon between the two exposed shelves (Sunda Shelf and Sahul Shelf) during the LGM [Yan et al., 2018].

## 3.7 Conclusions

We present paired leaf wax $\delta^{13}C$ and $\delta D$ records as well as pollen data from a sediment core dating back to 22 ka collected south off East Java. Instead of the commonly used single-compound approach, we use multiple *n*-alkane homologues (*n*-C29, *n*-C31 and *n*-C33) to evaluate potential scenarios regarding the past hydroclimatic evolution in this region. Our results show the great potential of multi-homologue leaf wax isotope analyses in settings with mixed vegetation types.

Comparison of the multi-homologue $\delta^{13}C$ records and the pollen records implies a dominant local source vegetation; *n*-C29 mainly reflects lowland (montane) rainforest during the Holocene (LGM), while *n*-C31 and *n*-C33 predominantly reflect lowland vegetation. A concentration-weighted mixing model supports the assumption that different homologues predominantly reflect distinct ecosystems. The $\delta^{13}C_{n\text{-}31/33}$ record reflects a grassland expansion and enhanced rainfall seasonality in lowland East Java during the LGM, when the canopy structure of montane rainforest reflected by $\delta^{13}C_{n\text{-}29}$ remained closed with relatively unaltered montane rainfall seasonality.

The leaf wax $\delta D$ records the precipitation $\delta D$ in East Java, which mostly reflects the rainfall intensity during the wet season. The variation in $\delta D_{n\text{-}29}$ through the record is small; increased contribution from montane rainforest caused a slight D-depletion during the LGM. In contrast, the significant decrease of $\delta D_{n\text{-}31}$ and $\delta D_{n\text{-}33}$ values during the LGM implies a wet season with enhanced rainfall intensity in the lowlands compared to the Holocene. Although we find no glacial-interglacial change in integrated rainfall, strongly enhanced lowland rainfall seasonality is detected for East Java during the LGM.

# Acknowledgements

We acknowledge MARUM – Center for Marine Environmental Sciences, University of Bremen. This work was funded by the Deutsche Forschungsgemeinschaft (DFG) Research Centre/Cluster of Excellence 'The Ocean in the Earth System'. We thank two anonymous reviewers for their constructive comments. SvdK, funded by the DFG grant BE2116/10-1, carried out initial pollen counting of core GeoB10053-7 at the Department of Palynology and Climate Dynamics of the University of Göttingen. YR is funded by CSC – the China Scholarship Council and supported by GLOMAR – Bremen International Graduate School for Marine Sciences. Samples were provided by the GeoB Core Repository at MARUM. We thank Ralph Kreutz for laboratory support, Lydia Gerullis for dataset preparation and Dr. Jennifer Wurtzel for helpful advice. The CMAP Precipitation data and the NCEP Reanalysis derived wind vector data are provided by the NOAA/OAR/ESRL PSD, Boulder, Colorado, USA (https://www.esrl.noaa.gov/psd/). The Global Historical Climatology Network data are retrieved from the KNMI Climate Explorer (https://climexp.knmi.nl). Datasets related to this study can be found at doi.pangaea.de/10.1594/PANGAEA.896146.

# Supplementary Information

Table S1. End-member information for $C_3$ and $C_4$ plants in tropical locations: concentration (µg/g leaf) and $\delta^{13}C$ values in ‰ against Vienna PeeDee Belemnite (VPDB) of the *n*-$C_{29}$, *n*-$C_{31}$ and *n*-$C_{33}$ alkane homologues. Average values, standard deviations and lower/upper quartiles are based on global compilations from Sachse et al. (2012) and Diefendorf and Freimuth (2017) plus the data from tropical South America (Wu et al., 2017). Only the data from tropical locations (between 30°N/30°S) are considered (Badewien et al., 2015; Bezabih et al., 2011; Bi et al., 2005; Bush and McInerney, 2015; Chikaraishi and Naraoka, 2003; Duan and He, 2011; Garcin et al., 2014; Krull et al., 2006; Liu and Yang, 2008; Mortazavi et al., 2012; Rommerskirchen et al., 2006; Vogts et al., 2009; Wu et al., 2017).

| | | *n*-$C_{29}$ | *n*-$C_{31}$ | *n*-$C_{33}$ |
|---|---|---|---|---|
| Tropical $C_3$ plants | Average concentration (µg/g leaf) | 189 | 119 | 25 |
| | Lower – upper quartiles of concentration (µg/g leaf) | 21 – 216<br>n = 551 | 12 – 144<br>n = 549 | 1 – 17<br>n = 547 |
| | $\delta^{13}C$ value (‰) (Mean ± 1σ) | −36.4 ± 3.1<br>n = 302 | −36.7 ± 3.2<br>n = 284 | −36.8 ± 3.2<br>n = 139 |
| Tropical $C_4$ plants | Concentration (µg/g leaf) | 57 | 161 | 110 |
| | Lower – upper quartiles of concentration (µg/g leaf) | 27 – 75<br>n = 77 | 61 – 202<br>n = 77 | 26 – 170<br>n = 77 |
| | $\delta^{13}C$ value (‰) (Mean ± 1σ) | −21.9 ± 2.7<br>n = 81 | −22.0 ± 2.6<br>n = 83 | −22.3 ± 2.4<br>n = 76 |

Table S2. Apparent hydrogen isotope fractionation between *n*-alkane homologues and mean annual precipitation. Average values and standard deviations are obtained from a global compilation from Sachse et al. (2012) plus the data from tropical South America (Feakins et al., 2016). Only the data from tropical locations (between 30°N/30°S) are considered (Bi et al., 2005; Chikaraishi and Naraoka, 2003; Feakins et al., 2016; Krull et al., 2006; Liu and Yang, 2008).

| | $\varepsilon C_{29}$/MAP (‰) (Mean ± 1σ) | $\varepsilon C_{31}$/MAP (‰) (Mean ± 1σ) | $\varepsilon C_{33}$/MAP (‰) (Mean ± 1σ) |
|---|---|---|---|
| $C_3$ plants | −129 ± 23<br>n = 168 | −123 ± 40<br>n = 154 | −130 ± 23<br>n = 26 |
| $C_4$ plants | −131 ± 32<br>n = 18 | −136 ± 28<br>n = 21 | −128 ± 19<br>n = 7 |

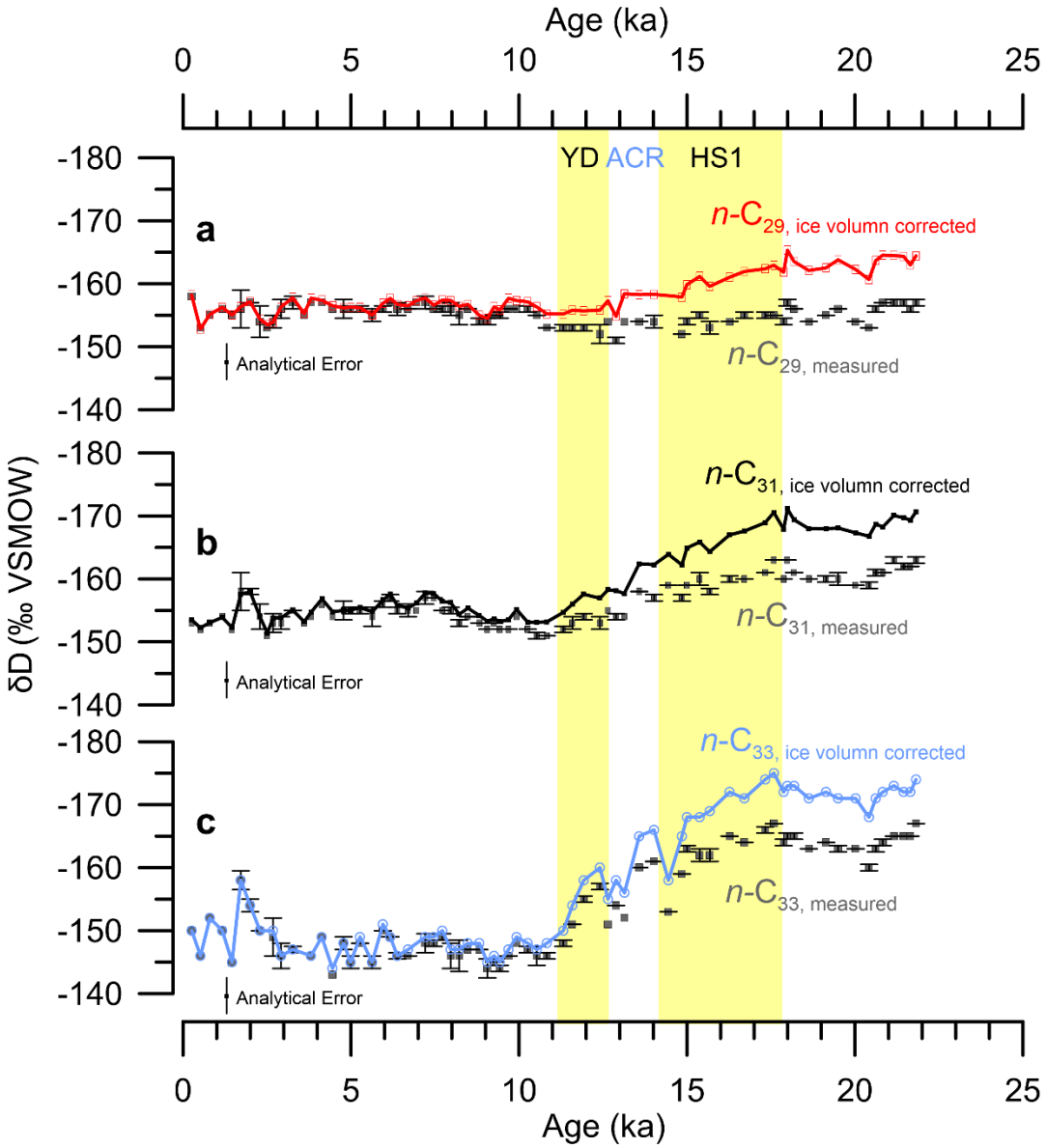


Figure S1. δD values of the *n*-alkane homologues before and after the ice volume correlation: a for *n*-$C_{29}$, b for *n*-$C_{31}$ and c for *n*-$C_{33}$. The grey dots represent either the measured δD values for the samples that were analysed only once or the mean δD values of the duplicates with vertical error bars displaying the difference between duplicates. The analytical error (3‰) shows the long-term mean absolute deviation based on the external standard. The two vertical yellow bars correspond to Heinrich Stadial 1 (HS1) and the Younger Dryas (YD), with the Antarctic Cold Reversal (ACR) in between.

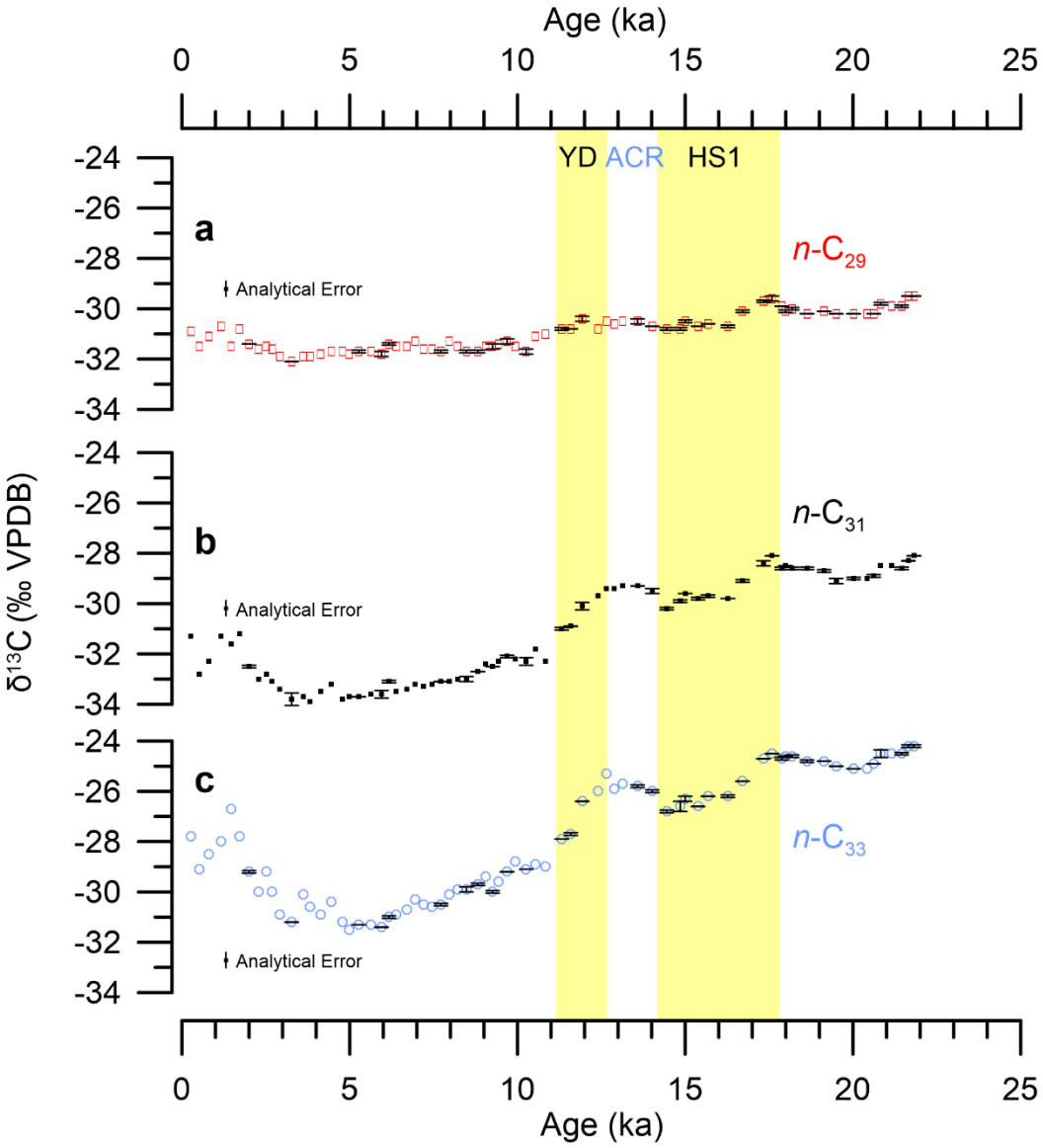


Figure S2. $\delta^{13}C$ values of the *n*-alkane homologues: a for *n*-$C_{29}$, b for *n*-$C_{31}$ and c for *n*-$C_{33}$. The dots represent either the $\delta^{13}C$ values of the samples that were analysed only once or the mean $\delta^{13}C$ values of duplicates with vertical error bars displaying the difference between duplicates. The analytical error (0.3‰) shows the long-term mean absolute deviation based on the external standard. The two vertical yellow bars correspond to Heinrich Stadial 1 (HS1) and the Younger Dryas (YD), with the Antarctic Cold Reversal (ACR) in between.

Table S3. Lists of pollen taxa

**Lowland rainforest taxa**

*Acalypha* type (Euphorbiaceae)
Acanthaceae
*Adenanthera* type (Mimosaceae)
*Aglaia* type (Meliaceae)
*Alchornea* (Euphorbiaceae)
*Allophylus racemosus* (Sapindaceae)
*Alnus* (Betulaceae)

Anacardiaceae
*Antidesma* type (Euphorbiaceae)
*Baccaurea* type (Euphorbiaceae)
*Barringtonia* (Lecythidaceae)
*Blumeodendron* type (Euphorbiaceae)
*Bombax* type (Bombacaceae)
Burseraceae
Cupressaceae)
*Calophyllum* (Guttiferae)
*Campnosperma* (Anacardiaceae)
Caprifoliaceae
*Celtis* (Ulmaceae)
*Cephalomappa* (Euphorbiaceae)
*Clematis* type (Ranunculaceae)
*Clerodendrum* type (Verbenaceae)
Combretocarpus rotundatus (Rhizophoraceae)
*Croton* type (Euphorbiaceae)
Cunoniaceae
*Cycas* type (Cycadaceae)
*Dillenia* type (Dilleniaceae)
*Diospyros* type (Ebanaceae)
Dipterocarpaceae
*Duabanga* type (Sonneratiaceae)
Elaeocarpaceae
Ericaceae
*Euphorbia* type (Euphorbiaceae)
*Fagraea* (Loganiaceae)
*Ficus* (Moraceae)
*Freycinetia* type (Pandanaceae)
*Ganophyllum* type (Sapindaceae)
*Garcinia cuspidata* type (Guttiferae)
*Garcinia dives* type (Guttiferae)
*Gironniera* type (Ulmaceae)
*Glochidion* (Euphorbiaceae)
*Gluta* type (Anacardiaceae)
*Gnetum* type (Gnetaceae)
*Guioa* type (Sapindaceae)
*Ilex* (Aquifoliaceae)
*Ixora* type (Rubiaceae)
*Kleinhovia* (Sterculiaceae)
*Lagerstroemia* (Lythraceae)

Leguminosae
Loranthaceae
Macaranga type (Euphorbiaceae)
Malpighiaceae
Malvaceae
Melanorrhoea type (Anacardiaceae)
Moraceae/Urticaceae
Myristicaceae
*Decaspermum* type (Myrtaceae)
*Nauclea* type (Rubiaceae)
*Neesia* type (Bombacaceae)
*Neoscortechinia* type (Euphorbiaceae)
Oleaceae
Palmae *Arenga* type
Palmae *Areca* type
Palmae *Borassus* type
Palmae *Calamus* type
Palmae *Caryota* type
Palmae *Cococ nucifera* type
Palmae *Iguanura* type
Palmae *Korthalsia* type
Palmae *Metroxylon* type
Palmae *Oncosperma* type
Palmae not differentiated
*Pandanus* (Pandanaceae)
*Pentace* type (Tiliaceae)
*Phyllanthus* type (Euphorbiaceae)
*Pinus* (Pinaceae)
*Piper* type (Piperaceae)
*Polyosm*a (Escalloniaceae)
*Pometia* (Sapindaceae)
Proteaceae
*Pterospermum* (Sterculiaceae)
*Randia* type (Rubiaceae)
Rhamnaceae
Rosaceae
Rutaceae
Sapotaceae/Meliaceae
*Stemonurus* (Icacinaceae)
*Pterocymbium* type (Sterculiaceae)
*Reevesia* type (Sterculiaceae)

*Symplocos* (Symplocaceae)
*Terminalia* type (Combretaceae)
*Tinospora* type (Menispermaceae)
Theaceae
*Trema* (Ulmaceae)
*Triumfetta* type (Tiliaceae)
*Ulmus* (Ulmaceae)
Winteraceae

**Montane rainforest taxa**
*Altingia* (Hamamelidaceae)
Araliaceae
*Dacrycarpus* (Podocarpaceae)
*Distylium* (Hamamelidaceae)
*Dodonaea* (Sapindaceae)
*Engelhardia* (Juglandaceae)
*Lithocarpus* type (Fagaceae)
*Myrica* (Myricaceae)
*Myrsine* (Myrsinaceae)
*Eugenia* (Myrtaceae)
*Nothofagus* (Fagaceae)
*Phyllocladus* (Podocarpaceae)
*Podocarpus* (Podocarpaceae)
*Quercus* (Fagaceae)

**Fern spores**
*Aspidium* type
*Asplenium* type
Cyatheaceae
*Davallia* type
*Lycopodium cernuum*
*Lycopodium phlegmaria*
*Lygodium microphyllum*
Polypodiaceae
psilamonolete fernspores
*Pteris*
*Selaginella*
*Stenochlaena palustris* type
Pteridophyta spores not differentiated

The assignment of pollen taxa to ecological groups was based on Huang, 1972; Kodela, 2006 and Tissot et al., 1994. The pollen reference collections at the School of Earth, Atmosphere and Environment at Monash University were also used.

References for this supplementary material

Badewien, T., Vogts, A., Rullkötter, J., 2015. n-Alkane distribution and carbon stable isotope composition in leaf waxes of C3 and C4 plants from Angola. Org. Geochem. 89–90, 71–79. https://doi.org/10.1016/J.ORGGEOCHEM.2015.09.002

Bezabih, M., Pellikaan, W.F., Tolera, A., Hendriks, W.H., 2011. Evaluation of n-alkanes and their carbon isotope enrichments (δ13C) as diet composition markers. animal 5, 57–66. https://doi.org/10.1017/S1751731110001515

Bi, X., Sheng, G., Liu, X., Li, C., Fu, J., 2005. Molecular and carbon and hydrogen isotopic composition of n-alkanes in plant leaf waxes. Org. Geochem. 36, 1405–1417. https://doi.org/10.1016/j.orggeochem.2005.06.001

Bush, R.T., McInerney, F.A., 2015. Influence of temperature and C4 abundance on n-alkane chain length distributions across the central USA. Org. Geochem. 79, 65–73. https://doi.org/10.1016/J.ORGGEOCHEM.2014.12.003

Chikaraishi, Y., Naraoka, H., 2003. Compound-specific δD-δ13C analyses of n-alkanes extracted from terrestrial and aquatic plants. Phytochemistry 63, 361–371. https://doi.org/10.1016/S0031-9422(02)00749-5

Diefendorf, A.F., Freimuth, E.J., 2017. Extracting the most from terrestrial plant-derived n-alkyl lipids and their carbon isotopes from the sedimentary record: A review. Org. Geochem. 103, 1–21. https://doi.org/10.1016/j.orggeochem.2016.10.016

Duan, Y., He, J., 2011. Distribution and isotopic composition of n-alkanes from grass, reed and tree leaves along a latitudinal gradient in China. Geochem. J. 45, 199–207. https://doi.org/10.2343/geochemj.1.0115

Feakins, S.J., Bentley, L.P., Salinas, N., Shenkin, A., Blonder, B., Goldsmith, G.R., Ponton, C., Arvin, L.J., Wu, M.S., Peters, T., West, A.J., Martin, R.E., Enquist, B.J., Asner, G.P., Malhi, Y., 2016. Plant leaf wax biomarkers capture gradients in hydrogen isotopes of precipitation from the Andes and Amazon. Geochim. Cosmochim. Acta 182, 155–172. https://doi.org/10.1016/j.gca.2016.03.018

Garcin, Y., Schefuß, E., Schwab, V.F., Garreta, V., Gleixner, G., Vincens, A., Todou, G., Séné, O., Onana, J.M., Achoundong, G., Sachse, D., 2014. Reconstructing C3 and C4 vegetation cover using n-alkane carbon isotope ratios in recent lake sediments from Cameroon, Western Central Africa. Geochim. Cosmochim. Acta 142, 482–500. https://doi.org/10.1016/j.gca.2014.07.004

Huang, T.C., 1972. Pollen flora of Taiwan. National Taiwan University, Botany Dept. Press.

Kodela, P., 2006. Pollen morphology of some rainforest taxa occurring in the Illawarra region of New South Wales, Australia. Telopea 346–389. https://doi.org/10.7751/telopea20065734

Krull, E., Sachse, D., Mügler, I., Thiele, A., Gleixner, G., 2006. Compound-specific δ13C and

δ2H analyses of plant and soil organic matter: A preliminary assessment of the effects of vegetation change on ecosystem hydrology. Soil Biol. Biochem. 38, 3211–3221. https://doi.org/10.1016/j.soilbio.2006.04.008

Liu, W., Yang, H., 2008. Multiple controls for the variability of hydrogen isotopic compositions in higher plant n-alkanes from modern ecosystems. Glob. Chang. Biol. 14, 2166–2177. https://doi.org/10.1111/j.1365-2486.2008.01608.x

Mortazavi, B., Conte, M.H., Chanton, J.P., Weber, J.C., Martin, T.A., Cropper, W.P., 2012. Variability in the carbon isotopic composition of foliage carbon pools (soluble carbohydrates, waxes) and respiration fluxes in southeastern U.S. pine forests. J. Geophys. Res 117, 2009. https://doi.org/10.1029/2011JG001867

Rommerskirchen, F., Plader, A., Eglinton, G., Chikaraishi, Y., Rullkötter, J., 2006. Chemotaxonomic significance of distribution and stable carbon isotopic composition of long-chain alkanes and alkan-1-ols in C4 grass waxes. Org. Geochem. 37, 1303–1332. https://doi.org/10.1016/j.orggeochem.2005.12.013

Sachse, D., Billault, I., Bowen, G.J., Chikaraishi, Y., Dawson, T.E., Feakins, S.J., Freeman, K.H., Magill, C.R., McInerney, F.A., van der Meer, M.T.J., Polissar, P., Robins, R.J., Sachs, J.P., Schmidt, H.-L., Sessions, A.L., White, J.W.C., West, J.B., Kahmen, A., 2012. Molecular Paleohydrology: Interpreting the Hydrogen-Isotopic Composition of Lipid Biomarkers from Photosynthesizing Organisms. Annu. Rev. Earth Planet. Sci. 40, 221–249. https://doi.org/10.1146/annurev-earth-042711-105535

Tissot, C., Chikhi, H., Nayar, T.S., Garden, T.B., Research Institute (Trivandrum, I., français de Pondichéry, I., 1994. Pollen of wet evergreen forests of the Western Ghats, India, Publications du Département d'écologie. Institut français de Pondichéry.

Vogts, A., Moossen, H., Rommerskirchen, F., Rullkötter, J., 2009. Distribution patterns and stable carbon isotopic composition of alkanes and alkan-1-ols from plant waxes of African rain forest and savanna C3 species. Org. Geochem. 40, 1037–1054. https://doi.org/10.1016/j.orggeochem.2009.07.011

Wu, M.S., Feakins, S.J., Martin, R.E., Shenkin, A., Bentley, L.P., Blonder, B., Salinas, N., Asner, G.P., Malhi, Y., 2017. Altitude effect on leaf wax carbon isotopic composition in humid tropical forests. Geochim. Cosmochim. Acta 206, 1–17. https://doi.org/10.1016/j.gca.2017.02.022

# Chapter 4

# Interaction of fire, vegetation and climate in tropical ecosystems: a multi-proxy study over the past 22,000 years

Yanming Ruan[a], Mahyar Mohtadi[a], Lydie M. Dupont[a], Dierk Hebbeln[a], Sander van der Kaars[b,c,d], Ellen C. Hopmans[e], Stefan Schouten[e,f], Edward J. Hyer[g], Enno Schefuß[a]

a MARUM – Center for Marine Environmental Sciences, University of Bremen, D-28359 Brmen, Germany
b School of Earth, Atmosphere and Environment, Monash University, Clayton, VIC 3800, Australia
c Cluster Earth and Climate, Faculty of Earth and Life Sciences, Vrije Universiteit, 1081 HV Amsterdam, Netherlands
d Department of Palynology and Climate Dynamics, Albrecht-von-Haller Institute for Plant Sciences, University of Göttingen, 37073 Göttingen, Germany
e NIOZ Royal Netherlands Institute for Sea Research, Department of Microbiology and Biogeochemistry, and Utrecht University, P.O. Box 59, 1790 AB Den Burg, Texel, The Netherlands.
f Department of Earth Sciences, Utrecht University, P.O. Box 80.121, 3508 TA Utrecht, The Netherlands.
g Naval Research Laboratory, Marine Meteorology Division, Monterey, CA 93943, United States.

Submitted to *Global Biogeochemical Cycles*

**Abstract:** Fire causes dramatic energy and matter exchanges between biosphere and atmosphere on a regional to global scale. Predicting fires, however, is hindered by the complex interplay of fire, climate and vegetation. Paleo-fire records provide critical information beyond instrumental records that cover only the past few decades, and may be used to assess the role of fire in large-scale and long-term environmental changes. Here we present a 22,000-year multi-proxy record of fire regime from a sediment core retrieved offshore South Java, Indonesia. We use micro-charcoal in combination with two molecular markers of burning, levoglucosan and polycyclic aromatic hydrocarbons, to reconstruct fire occurrence as well as fire intensity in the past. We show that fire occurrence and intensity were high during the Last Glacial Maximum (LGM, around 21,000 years ago) and low during the Heinrich Stadial 1, the Younger Dryas and the early Holocene. Both fire regime and vegetation in tropical regions with high annual rainfall were primarily controlled by rainfall seasonality. However, fire additionally stabilized the savannah (rainforest)-dominated ecosystem during the LGM (early Holocene) but caused transitions between the two vegetation types during the deglaciation and the late Holocene.

**Keywords:** fire regime; vegetation; precipitation

## 4.1 Introduction

Fire is a ubiquitous component of almost every terrestrial ecosystem on Earth [Bowman et al., 2009]. Emissions from biomass burning such as aerosols, greenhouse gases and chemically active gases change the chemical composition of the atmosphere and play a significant role in regional and global biogeochemical cycles [Ramanathan et al., 2001; Santín et al., 2016]. Fire frequency and fire intensity are two important fire regime characteristics in describing fire patterns [Bond and Keeley, 2005; Gill, 1975]. They are related to both vegetation type and hydro-climate [Archibald et al., 2013; Murphy and Bowman, 2012]. While fires in tropical moist broadleaf forests are predominantly of low intensity (burning temperature) and low to intermediate frequency, tropical grassland fires are more frequent and tend to reach higher intensity (burning temperature) [Archibald et al., 2013]. It is proposed that rarer but more intense fires dominate the tropical regions under a drier climate [Hantson et al., 2017]. Therefore, climate and vegetation are two important factors in understanding how fire interacts with environmental changes, although only about half of the existing studies about fire feedbacks tackle both factors [Archibald et al., 2018]. Paleo-fire records are essential in providing data beyond the timeframe of modern observations and to assess the role of fire in large-scale and long-term ecological changes. However, multi-proxy paleo-records integrating fire, climate and vegetation are sparse [Shanahan et al., 2016; Dupont and Schefuß, 2018].

Changes in fire regime are often not resolved in paleo-records [Archibald et al., 2018; Han et al., 2016]. Charcoal, commonly used as a proxy to indicate past fire activity, is a carbonaceous material produced by incomplete combustion of biomass with temperatures between 280 °C and 500 °C [Whitlock and Larsen, 2001]. Micro-charcoal abundance in marine sediments reflects general fire occurrence on a regional scale, representing fire frequency, intensity and extent [Power et al., 2008; Daniau

et al., 2010, 2012]. Combining sedimentary charcoal record with combustion-derived molecular markers, such as levoglucosan (a monosaccharide anhydrate compound) and/or polycyclic aromatic hydrocarbons (PAHs), is a promising new way of reconstructing fire intensity [Sikes et al., 2013; Schüpbach et al., 2015; Shanahan et al., 2016; Battistel et al., 2017; Miller et al., 2017; Argiriadis et al., 2018; Dietze et al., 2019; Schreuder et al., 2019]. Levoglucosan (1,6-anhydro-$\beta$-D-glucopyranose), a product of cellulose combustion, is a tracer for biomass burning due to its high emission factor and specific pyrogenic sources [Simoneit et al., 1999; Schkolnik and Rudich, 2006; Bhattarai et al., 2019; Suciu et al., 2019]. It is only formed at low burning temperatures (150-350 °C) and thus reflects low intensity fires [Kuo et al., 2008]. Pyrogenic PAHs are formed at a wider range of higher burning temperatures (200-700 °C) [Lu et al., 2009; Keiluweit et al., 2012]. According to an in-situ forest fire emission study, more particle-associated PAHs are produced during the flaming phase of combustion (with higher burning intensity) than during the smouldering phase of combustion (with lower burning intenstiy), while higher emission of levoglucosan occurs during the smouldering phase than during the flaming phase [Wang et al., 2007].

Modern ecological studies show that tropical forest and savannah are two alternative stable states which can co-exist under similar environmental conditions, despite distinct ecological structures, biodiversity and carbon storage [Hirota et al., 2011; Staver et al., 2011]. According to the alternative stable state theory, stabilizing feedbacks maintain these two ecosystems: high tree cover and rare fires are typical for tropical forest, while open-canopy with grassy ground layer and frequent fires characterize the savannah [Murphy and Bowman, 2012; Ondei et al., 2017]. Shifts between these two ecosystems occur if the feedback processes are disturbed [Murphy and Bowman, 2012]. Several multi-decadal fire-exclusion experiments show the tendency for forest species to invade and replace savannahs when fires are absent or of low frequency and/or intensity [Veenendaal et al., 2018, and references therein]. In this study, we reconstruct 22,000 years of fire regime changes by analyzinging micro-charcoal, levoglucosan and PAHs from a sediment core. The accumulation rate of micro-charcoal reflects general fire occurrence, while the two novel molecular markers of burning shed light on changes in fire intensity. The study area experienced shifts in rainfall seasonality and vegetation (savannah-rainforest transition) through the past 22,000 years [Ruan et al., 2019]. This multi-proxy study aims to evaluate the role of fire in the ecotone from savannah- to rainforest-dominated ecosystems in tropical regions on the time scale from the Last Glacial to the present.

## 4.2 Materials and Methods

### 4.2.1 Modern fire distribution in the study area

Modern fires in Java, Indonesia display a distinct seasonal pattern as detected by satellite observations (Fig. 4.1), with high fire occurrence during the dry season and low fire occurrence during the wet season, since a sufficient amount of dry fuel for ignition is the prerequisite for fires [Reid et al., 2012]. Thus, we assume a dry season

biased production of micro-charcoal particles and fire-induced molecular markers. Riverine discharge, the major transport process in wet areas, is postulated to bring micro-charcoal and molecular markers deposited in soils or rivers of East Java into the marine environment year-round with peaks during the wet season. During the dry season transport by aerosols may play a role. The prevailing wind direction during the dry (fire) season (Fig. 4.1a) is southeast [Kalnay et al., 1996]; therefore, the inclusion of material from Australia cannot be ruled out but is expected to be minor due to the transport distance of over 1500 km today, and over 900 km during the LGM when lower sea level exposed the Sahul Shelf.

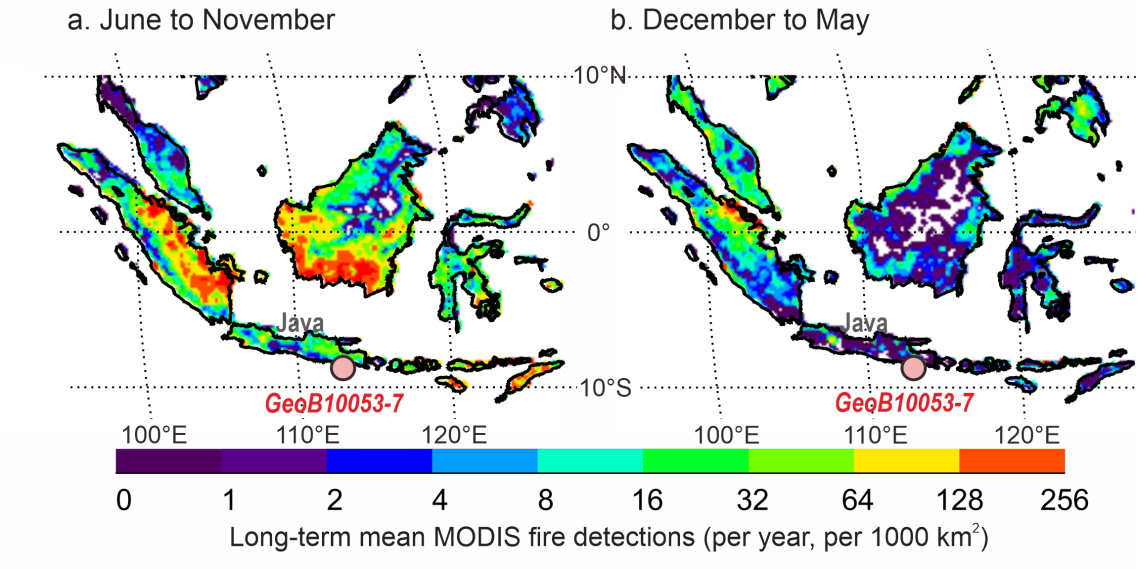


**Figure 4.1:** Seasonal distribution of MODIS active fire hotspot: a) for June to November (dry season), b) for December to May (wet season). Long-term mean results from 2003 to 2018 are based on the fire products of Aqua MODIS Collection 6 [Giglio et al., 2016]. Location of the sediment core GeoB10053-7 (pink dot) is shown.

### 4.2.2 Site description

Sediment core GeoB 10053-7 (8° 40.59'S; 112° 52.35' E, 1,375 m water depth; 750 cm core length; Fig. 4.1) was retrieved off south Java, Indonesia during the SO-184 "PABESIA" expedition in 2005 [Hebbeln and cruise participants, 2006]. According to the previously published age model based on 19 accelerator mass spectrometry (AMS) $^{14}$C dates [Mohtadi et al., 2011], the sediment core covers the past 22,000 years. The stable hydrogen and carbon isotope composition of long chain *n*-alkanes together with pollen data from this sediment core were reported by Ruan et al. [2019]. Analyses of micro-charcoal and fire-induced molecular markers (levoglucosan and PAHs) will be described here.

### 4.2.3 Micro-charcoal analysis

For charcoal analysis, 34 sediment samples were collected at depth intervals of 3 to 40 cm. For each sample an amount between 4.8 and 6.0 ml of sediment was sus-

pended in approximately 40 ml of tetra-sodium-pyrophosphate (±10%) then sieved over 200 and 7 micrometre screens, followed by hydrochloric acid (10%) treatment, heavy liquid separation (sodium-polytungstate, SG 2.0, 20 min at 2,000 rpm, twice), acetolysis and sodium carbonate (20%) treatment. The resulting organic residues were mounted in glycerol on microscope slides sealed with paraffin wax. Charcoal particles >10 $\mu$m were counted along three evenly spaced transects in every slide. To account for biases due to sediment rates, the accumulation rate of charcoal particles was calculated by multiplying the charcoal count (particles $cm^{-3}$) with the sedimentation rate (cm $kyr^{-1}$) based on the age model.

### 4.2.4 Analysis of PAHs

A DIONEX Accelerated Solvent Extractor (ASE 200) was used for lipid extractions with a mixture of dichloromethane:methanol (DCM:MeOH 9:1, v:v) at 1000 psi and 100°C (three cycles, 5 minutes each). An internal standard (2-Nonadecanone) was added to each sample prior to extraction. Saponification was carried out with 0.1M KOH-solution. Neutral fractions were recovered by *n*-hexane. Further separation of the neutral fractions was achieved by a 5 cm silica gel column: subsequent elution with *n*-hexane, DCM and DCM to MeOH (1:1, v:v) yielded the apolar, ketone and polar fractions, respectively. The ketone fractions, containing the PAHs, were dissolved in 50 $\mu$l dilute internal standard solution, i.e. 1 ng/$\mu$l 2-Fluorofluorene (Sigma-Aldrich Co.) in toluene, before PAH analysis. We used an Agilent 7820A Gas Chromatograph (GC) equipped with an Rxi-PAH capillary column (40 m, 0.18 mm i.d., 0.07 $\mu$m) coupled to a 5977E Mass Selective Detector (MSD) quadrupole mass spectrometer to determine the concentrations of PAHs. Injection volume was 1 $\mu$l (splitless mode; 275°C); helium was used as carrier gas with a flow rate of 1.4 ml min-1. GC oven temperature was programmed to 110°C for 1 min, then ramped to 210°C at 37°C per min, to 260°C at 3°C per min, to 350°C at 11°C per min and held for 8 min. The MSD transfer line was held at 280°C and the ion source temperature was 230°C. Electron ionization was accomplished with an electron energy of 70 eV in single ion monitoring (SIM) mode (masses shown in Table 4.1).

Linearity of mass spectrometer performance was evaluated using standard solutions (a mixture of 9 PAHs) (PAH Kit 610-N, SUPELCO) with seven concentration levels. Injections of PAHs of 0.05 ng, 0.1 ng, 0.5 ng, 1 ng, 2 ng, 4 ng and 5 ng on column resulted in a linear response with R2 >0.99 for all individual PAHs (Table 4.1). Instrument performance and relative response factors (RRF) for PAHs compared to 2-Fluorofluorene were monitored by repetitive measurements of one standard mixture solution before, between and after samples. The precision and accuracy for each analyzed PAH are shown in Table 4.1.

We identified each peak according to the SIM mass (m/z shown in Table 4.1) and retention time of the standard mixture. Quantification was determined by comparing the peak area of the target compound to that of the internal standard (2-Fluorofluorene) and applying the RRFs. Duplicate measurements on five samples revealed an average relative difference between 4% for BaA/Chry/BF (name abbreviations shown in Table 4.1) and 10% for BaP (Table 4.1).

Relative difference was calculated as the difference of two measured concentrations divided by the average of the two. To account for biases due to sediment properties and sediment rates, the accumulation rate of PAHs (ng $cm^{-2}$ $kyr^{-1}$) was calculated by multiplying the concentration (ng $g^{-1}$) with the dry bulk density of the sediment (g $cm^{-3}$), and the sedimentation rate (cm $kyr^{-1}$) based on the age model.

| PAH name and abbreviation | Qualitative ion (m/z) | Linear Range (ng/$\mu$l) | Linear Coefficient (%) (n=21) | Precision of standard % (n=15) | Accuracy of standard % (n=15) | Relative difference of duplicate % |
|---|---|---|---|---|---|---|
| Benzo(a)anthracene (BaA) | 228 | 0.05 - 5 | 99.5 | 1.9 | 1.2 | 4 |
| Chrysene (Chry) | 228 | 0.05 - 5 | 99.6 | 1.8 | 0.7 | 4 |
| Benzo(b/j/k)fluoranthene (BF) | 252 | 0.05 - 5 | 99.2 | 2.7 | 1.1 | 4 |
| Benzo(a)pyrene (BaP) | 252 | 0.05 - 5 | 99.5 | 2.1 | 0.9 | 10 |
| Indeno(1,2,3-cd)-pyrene (IP) | 276 | 0.05 - 5 | 99.1 | 1.8 | 0.5 | 8 |
| Dibenzo(a,h)-anthracene (DBA) | 278 | 0.05 - 5 | 99.5 | 2.6 | 1 | 6 |
| Benzo(g,h,i)perylene (BghiP) | 276 | 0.05 - 5 | 99.5 | 2.3 | 0.5 | 6 |

**Table 4.1:** PAH name abbreviations, range and linear regression of calibration curves, precision and accuracy of standards, and reproducibility of duplicates

### 4.2.5 Source of PAHs

PAHs are ubiquitous in the environment. Apart from incomplete combustion (pyrogenic PAHs), other origins include petroleum (petrogenic PAHs) and diagenesis of biogenic precursors [Lima et al., 2005, and references therein]. Petrogenic PAHs enter the environment directly through either human-induced oil spill or natural oil seepage [Lima et al., 2005, and references therein]. Biogenic PAHs occur as a localized source, and only types of PAHs not analyzed in this study are generated (perylene, phenanthrene homologs etc.) [Wakeham et al., 1980].

The suite of PAHs is always emitted as a mixture. Therefore, diagnostic ratios are commonly used to distinguish petrogenic and pyrogenic sources and to further identify emission sources of combustion (biomass or fossil fuels) [Tobiszewski and Namieśnik, 2012]. Diagnostic ratios mostly involve pairs of PAHs which have the same molecular weight, similar physical and chemical properties, and undergo comparable environmental fates [Tobiszewski and Namieśnik, 2012]. Pyrogenic input is inferred from an increase in the proportion of the less stable isomer relative to the more stable isomer compared to petrogenic input [Yunker et al., 2002]. With the same molecular weight, Indeno(1,2,3-cd)pyrene (IP) is less stable than Benzo(g,h,i)perylene (BghiP); thus, an increase in the IP/(IP+BghiP) ratio in-

dicates more contribution from combustion than petroleum. Petrogenic input is generally featured by IP/(IP+BghiP) ratios <0.2 [Yunker et al., 2002].

### 4.2.6 Analysis of levoglucosan

After the ASE extraction with a mixture of DCM:MeOH (9:1, v:v), the residual sediments were further extracted using a DIONEX Accelerated Solvent Extractor (ASE 200) with MeOH at 1000 psi and 100°C (three cycles, 5 minutes each). The methanol extracts were passed over cotton wool to eliminate large salt particles. A known amount of deuterated (D7) levoglucosan (dLVG, Cambrige Isotope Laboratories, Inc.) (usually 0.25 ng) was added as an internal standard to 1/10 aliquot of each extract. The extracts were eluted over a small $Na_2SO_4$ Pasteur pipette column with dichloromethane to methanol (9:1, v:v) to further remove salt. After being dried under N2, each extract was dissolved in acetonitrile:$H_2O$ (95:5, v:v) and filtered through a polytetrafluoroethylene (PTFE) filter (0.45 $\mu$m; 13 mm diameter) before analysis.

Levoglucosan analysis was performed as described in detail by Schreuder et al. [2018]. The extracts were analyzed using an Agilent 1290 Infinity Ultra-High Performance Liquid Chromatography (UHPLC) coupled to an Agilent 6230 Time-Of-Flight (TOF) mass spectrometer. Separation was achieved with two Aquity BEH amide columns (150 mm, 2.1 mm i.d., 1.7 $\mu$m, Waters Chromatography) in series with a 50 mm guard column. Linearity of mass spectrometer performance was evaluated using 9 point standard curve; injections of levoglucosan (Sigma-Aldrich Co.) or dLVG of 12.5 pg, 25 pg, 50 pg, 125 pg, 250 pg, 0.5 ng, 1.25 ng, 2.5 ng and 5 ng on column resulted in a linear response with R2 >0.99. Instrument performance and relative response factors (RRF) for levoglucosan compared to dLVG were monitored by repetitive measurements of one standard solution before, after and between samples. Quantification was based on peak integrations of mass chromatograms within 10 ppm mass accuracy using an exact mass of 161.0445 m/z for levoglucosan and 168.0884 m/z for dLVG. Duplicate measurements on 10% of all samples revealed an average relative difference of 2.5% for levoglucosan. To account for biases due to sediment properties and sediment rates, the accumulation rate of levoglucosan (ng $cm^{-2}$ $kyr^{-1}$) was calculated by multiplying the concentration (ng $g^{-1}$) with the dry bulk density of the sediment (g $cm^{-3}$), and the sedimentation rate (cm $kyr^{-1}$) based on the age model.

To estimate the extraction loss of levoglucosan due to prior extraction using DCM: MeOH (9:1, v:v), we measured the levoglucosan concentrations in the DCM:MeOH (9:1, v:v) extracts of 13 samples from the sediment core, and compared each concentration with that of the MeOH extract from the same sample. The extracts of DCM:MeOH (9:1, v:v) contain on average 17 ± 8% (average ± standard deviation, n=13) of the concentrations of levoglucosan in the MeOH extracts. This indicates that the MeOH extracts contain a relatively consistent and major portion of the total levoglucosan content in the samples. In order to correct for this loss due to prior DCM:MeOH (9:1, v:v) extractions, we calculated the total concentrations (Fig. S1d) and accumulation rates (Fig. 4.2d) of levoglucosan in the samples using the

average and standard deviation above.

### 4.2.7 Fire regime reconstruction and comparison with vegetation and hydro-climatic proxies

The ratio between levoglucosan and the pyrogenic PAHs (abbreviated as LVG/(LVG+PAHs) ratio) from marine sediments has the potential to reflect the intensity of source fires, because these two molecular markers share similar environmental fates before being deposited in marine sediments. The two types of compounds are emitted into the atmosphere mainly attached to particles from fires [Wang et al., 2017]. Both undergo photochemical alterations in the atmosphere [Lima et al., 2005; Bhattarai et al., 2019] before dry deposition in the marine environment. An alternative transport route is via aerosol deposition in soils and subsequent river transport into the marine environment. In this regard, both types of compounds are transported similarly by river systems [Myers-Pigg et al., 2017]. Particularly, the steep topography from the volcanic arc to the core site in East Java without a delta system favors relatively fast transport and sedimentary deposition of fire-induced molecular markers [Hunsinger et al., 2008]. It is noteworthy that levoglucosan in marine sediments is prone to degradation at the seawater-sediment interface [Schreuder et al., 2018], which is substantially less for PAHs due to their more stable chemical structures. Such a degradation could bias the concentration of levoglucosan and its ratio to PAHs, if preservational conditions (e.g. oxygen exposure time) have substantially changed through the sediment core. When this 'preservation effect' (Section 3.3) is absent, the LVG/(LVG+PAHs) ratio represents the relative intensity of past fires recorded in marine sediments: high (low) intensity fires produce high (low) relative abundances of PAHs but low (high) relative abundances of levoglucosan [Wang et al., 2017].

To calculate the LVG/(LVG+PAHs) ratio, the concentration of levoglucosan/PAHs is firstly normalised in the same range of 0 to 1, respectively:

$$Norm_{LVG} = \frac{X}{X_{max} - X_{min}} \tag{4.2.1}$$

$$Norm_{PAHs} = \frac{Y}{Y_{max} - Y_{min}} \tag{4.2.2}$$

Xmax/Xmin represents the maximum/minimum concentration of levoglucosan in the sediment core; Ymax/Ymin represents the maximum/minimum total concentration sum of PAHs in the sediment core. Then the ratio LVG/(LVG+PAHs) is calculated based on NormLVG and NormPAHs. A ratio of 0.5 is a boundary: ratios $<0.5$ represent a major contribution of PAHs (high intensity fires); ratios $>0.5$ reflect a major contribution of levoglucosan (low intensity fires).

Micro-charcoal particles are produced by both low intensity and high intensity, the accumulation rate of which thus indicates general fire occurrence. Together with the LVG/(LVG+PAHs) ratio, past fire regime in East Java over the past 22,000 years is reconstructed. Proxies for hydro-climate and vegetation from the same sediment

core are compared [Ruan et al., 2019]. The proxies include the lithogenic particles to $CaCO_3$ ratio and the leaf wax $\delta$D (stable hydrogen isotope composition) reflecting riverine runoff and wet season rainfall intensity in East Java, respectively [Ruan et al., 2019; Mohtadi et al., 2011]. The leaf wax $\delta^{13}$C (stable carbon isotope composition) and pollen percentages reflect regional vegetation changes [Ruan et al., 2019]. Specifically, $\delta^{13}C_{n\text{-}33}$ (the $\delta^{13}$C value of leaf wax *n*-C33 alkane) predominantly reflects the contribution of C3 versus C4 plant types in East Javanese lowland vegetation; higher values indicate C4 grass (savannah) expansion at the cost of lowland rainforest [Ruan et al., 2019]. The $\delta$D value of leaf wax *n*-C33 alkane ($\delta D_{n\text{-}33}$) predominantly reflects wet season rainfall intensity in the East Javanese lowlands [Ruan et al., 2019].

## 4.3 Results

### 4.3.1 Pyrogenic source of PAHs

The IP/(IP+BghiP) ratios through the sediment core remain higher than 0.2 (Section 4.2.4; Fig. S1), indicating that the PAHs analyzed are mainly pyrogenic. The minor input from petroleum is also supported by the relatively high carbon preference index (CPI) values of the *n*-alkanes throughout the core [Ruan et al., 2019].

### 4.3.2 Accumulation rate of micro-charcoal, levoglucosan and PAHs

In sediment core GeoB10053-7, the highest accumulation rates of micro-charcoal particles (Fig. 4.2f) occurred during the LGM. They displayed millennial-scale variations during the deglaciation, with peaks in the Bølling-Allerød period (B-A, 14.6-12.9 ka) but low values during the Heinrich Stadial 1 (HS1, 17.5-14.6 ka) and the Younger Dryas (YD, 12.9-11.6 ka). According to the micro-charcoal accumulation rates we divide the Holocene into two parts, with low values during the early Holocene (10 ka to 3 ka) and high values during the late Holocene (3 ka till now).

The levoglucosan accumulation rates showed a general increase through the sediment core, similar with the trend of sedimentation rates (Fig. 4.2d, h). In contrast, there is a clear LGM-Holocene contrast in the accumulation rates of the PAHs, with high fluxes for the LGM part but low fluxes for the early Holocene part (Fig. 4.2e). Despite the relatively low sedimentation rates during the LGM, the high concentrations of all 7 PAHs resulted in high accumulation rates during that period (Fig. S1).

### 4.3.3 Minor preservation effect on levoglucosan and the LVG/(LVG+PAHs) ratio

Sedimentation rate potentially impacts the sedimentary levoglucosan concentrations since faster sediment burial leads to shorter oxygen exposure time and better preservation [Hartnett et al., 1998]. However, the very weak correlation between levoglu-

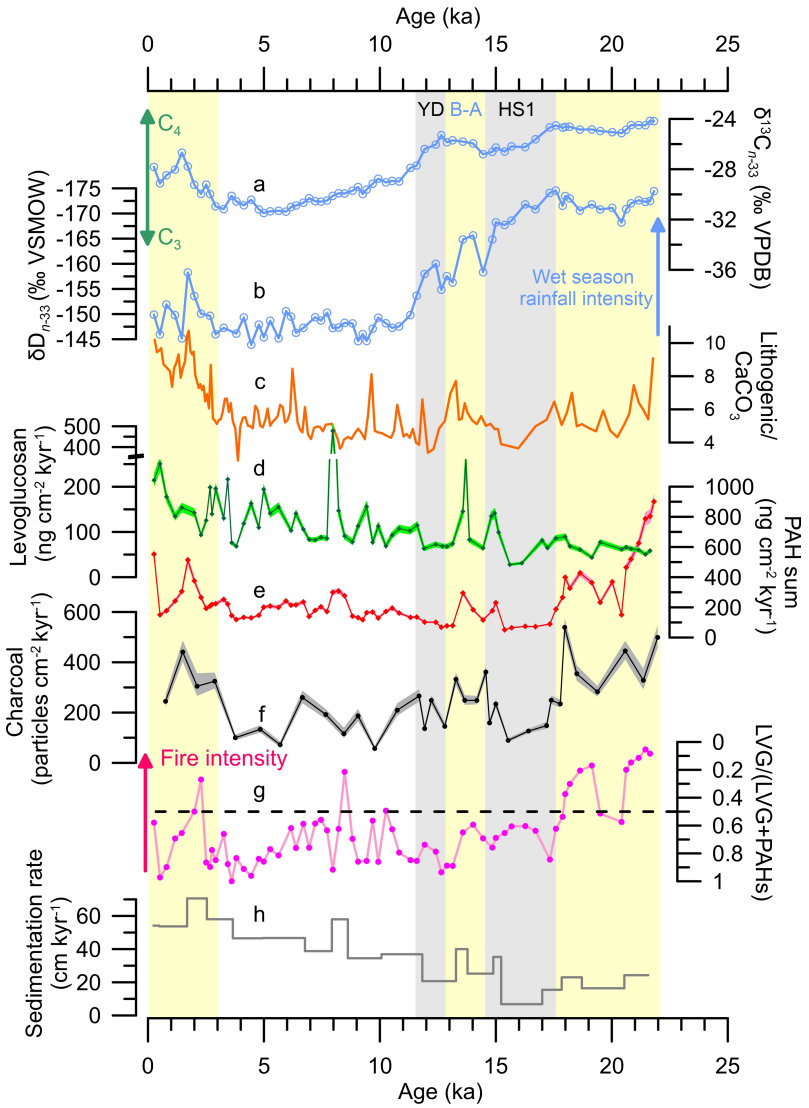


**Figure 4.2:** Comparison of various proxy records from sediment core GeoB10053-7. a) The $\delta^{13}$C values of the *n*-C33 alkane as proxy for lowland vegetation in East Java; C4 grass expansion during LGM is shown [Ruan et al., 2019]. b) The ice volume adjusted $\delta$D values of the *n*-C33 alkane as proxy for wet season rainfall intensity in East Java lowlands [Ruan et al., 2019]. c) The ratio of lithogenic particles to calcium carbonate as a proxy for river runoff [Mohtadi et al., 2011]. According to b) and c), rainfall seasonality in East Java lowlands was enhanced during the LGM, with a shorter but wetter rainy season. d) Accumulation rates of levoglucosan with error ranges based on the determined extraction efficiency. The dark green dots show the levoglucosan accumulation rates of each methanol extract multiplied by 1.17. The error envelope represents the lower and upper limit of total levoglucosan accumulation rates, i.e. accumulation rates of each methanol extract multiplied by 1.09 and 1.25, respectively. e) Accumulation rates of total PAHs with error ranges based on the relative difference of duplicate (Table 4.1). f) Accumulation rates of micro-charcoal particles with 95% confidence limits. The ratio of LVG/(LVG+PAHs) (g) reflects fire intensity. (h) Sedimentation rate based on the age model [Mohtadi et al., 2011]. Three vertical yellow bars show periods of peaks in micro-charcoal accumulation rates, which correspond to the LGM, the Bølling-Allerød period (B-A) and the late Holocene. Two vertical grey bars correspond to the Heinrich Stadial 1 period (HS1) and the Younger Dryas period (YD), during which the micro-charcoal accumulation rates were relatively low.

cosan concentrations and sedimentation rates from the sediment core (R=0.040, p=0.745) rules out this impact. Therefore, we infer a minor, if at all, preservation effect on levoglucosan concentrations and thus on the ratio of levoglucosan over PAHs in sediment core GeoB10053-7. The LVG/(LVG+PAHs) ratio was generally lower than 0.5 during the LGM and higher than 0.5 after the LGM (Fig. 4.2g).

## 4.4 Discussion

### 4.4.1 Last Glacial Maximum

High fire occurrence in East Java during the LGM is indicated by high abundances of micro-charcoal particles (Fig. 4.2f), with the dominance of high intensity fires as revealed by the low LVG/(LVG+PAHs) values (Fig. 4.2g). Thus, the fire regime during that period was characterized by frequent intense fires.

The vegetation reconstruction from the same sediment core shows that extensive C4 grasses in East Javanese lowlands were present during the LGM [Ruan et al., 2019, ; Fig. 4.2a]. The frequent and intense fire regime effectively limited tree cover and maintained an open canopy vegetation. As a positive feedback, the presence of a grassy ground layer significantly increases the flammability of the ecosystem; grasses regrow and regain the flammability quickly after burning, allowing frequent and high intensity fires to occur [Stott, 2000; Bond, 2008; Hoffmann et al., 2012a].

Proxies from the sediment core indicate that the runoff remained intermediate during the LGM (Fig. 4.2c) while the wet season rainfall was intensified in East Java lowlands (Fig. 4.2b). Consequently, strong rainfall seasonality prevailed during that period, with a long dry season and a short but intense wet season [Ruan et al., 2019]. The pronounced rainfall seasonality favored an increase in both fire frequency and intensity. Satellite observations show that more frequent fires occur in years with extended dry seasons, which more efficiently dry out potential fuels and make them prone to ignition [van der Werf et al., 2008]. Fire experiments in savannah ecosystems observe high fire intensity when the fuel moisture content is low [Govender et al., 2006]. The short but intense wet season likely facilitated the rapid regrowth of grasses, producing enough potential fuel for frequent fires in the dry season.

### 4.4.2 The deglaciation

A shift in regional fire regime occurred around 18 ka: a substantial decrease in both fire occurrence and fire intensity occurred, reflected by a drop in the accumulation rate of micro-charcoal particles and a rise of LVG/(LVG+PAHs) (Fig. 4.2f, g). While the fire intensity remained generally low during the deglaciation (Fig. 4.2g), millennial-scale oscillations occurred in fire occurrence: accumulation rates of micro-charcoal, levoglucosan and PAHs were relatively high during the B-A but low during the HS1 and the YD (Fig. 4.2d, e, f).

The millennial-scale change in fire occurrence coincided with changes in the lowland vegetation of East Java. The vegetation reconstruction shows two major transitions

from savannah towards rainforest in lowland East Java over the course of the HS1 and the YD, with a reverse trend during the B-A [Ruan et al., 2019]. Over the course of the HS1 and the YD, a sharp decrease in both fire occurrence and fire intensity compared to the LGM level likely facilitated the change from grass- to tree-dominated vegetation. With the fire intensity remaining low, an increase in fire occurrence during the B-A likely caused a slight increase in grass cover. Such a pattern can be explained by different growth patterns of grasses vs. trees. Unlike fast-growing grasses, tree saplings need a fire-free interval to reach certain sizes to escape flame damage of subsequent fires and continue growing [Bond and Midgley, 2000; Hoffmann et al., 2012a]. Additionally, trees of certain sizes are more likely to survive low intensity fires than high intensity fires [Hoffmann et al., 2012a]. Therefore, a combination of both low fire occurrence and low fire intensity during the HS1 and the YD was crucial for increasing the survival chances of trees, which was not the case during the B-A. The low intensity fire regime was still able to ignite grasses during the dry season, which potentially created space for trees. The rising atmospheric $CO_2$ concentration during the HS1 and the YD potentially also facilitated the vegetation transition by accelerating the growth rates of trees [Bond and Midgley, 2000].

The riverine runoff from East Java during the deglaciation was at a generally similar level as during the LGM, while the wet season rainfall intensity in the lowlands gradually declined as reflected by the rising $\delta D_{n\text{-}33}$ values [Ruan et al., 2019]. Consequently, the lowland dry (fire) season was getting shorter in the course of the deglaciation, which dried out potential fuels less efficiently. On the millennial time scale, there was more runoff during the B-A than during the HS1 and the YD [Fig. 4.2c; Mohtadi et al., 2011]. The $\delta D_{n\text{-}33}$ values for the B-A sediments were relatively low (Fig. 4.2b), implying that intense rainfall in the wet season caused the enhanced runoff during that period. The intense wet season likely increased the grass fuel load that were prone to ignite during the dry season.

### 4.4.3 Holocene

Fire occurrence was generally low in East Java at the onset of the Holocene before a rise from  3 ka onwards as reflected by micro-charcoal accumulation rates (Fig. 4.2f). The fire intensity remained generally constant through the Holocene, since the LVG/(LVG+PAHs) ratios rarely fell below 0.5 (Fig. 4.2g). During the early Holocene, rainforest continued to replace grass and became widespread both in lowland and montane areas of East Java [Ruan et al., 2019]. The rainforest dominated vegetation coincided with rare fires of low intensity. The dense canopy of tropical rainforest suppresses fires by reducing grass fuel loads and maintaining a humid and low-wind micro-climate (Hoffmann et al., 2012b). Since  3 ka, however, C4 grass expanded at the expense of rainforest in the East Javanese lowlands, while fire occurrence also increased (Fig. 4.2a).

Rainfall intensity of the wet season in East Java through the Holocene was generally low except for a peak at  2 ka as reflected by the $\delta D_{n\text{-}33}$ values (Fig. 4.2b), while the runoff was intermediate during the early Holocene and increased after  3 ka (Fig.

4.2c) [Ruan et al., 2019]. These proxies indicate a moist early Holocene climate with low rainfall seasonality, making it difficult for fuels to dry sufficiently for ignition.

In assessing the fire history of East Java during the late Holocene, human influences have to be considered. Humans affect fire occurrence in either a positive or a negative way, by increasing ignition or supressing/eliminating fires [Whitlock et al., 2010]. Modern humans are believed to have been present in East Java since at least the LGM, based on findings of human skull fragments dated back to 37-29 ka [Storm et al., 2013]. Pottery fragments first appeared around 4.7 ka and their numbers started to increase around 2.6 ka in a cave in Southeast Java, implying intensified human activity and use of fire [Morwood et al., 2008]. The increase in fire occurrence and expansion of lowland C4 grass since 3 ka could be related to anthropogenic burning practices, which are generally more frequent than naturally occurring fires [Veenendaal et al., 2018]. However, the spatial extent of human impact remains unknown, which makes it difficult to attribute the regional signal recorded in our sediment core to human activity.

### 4.4.4 Feedbacks

The results from our study show a strong feedback loop between regional fire regime and mosaic lowland rainforest-savannah vegetation over the past 22,000 years (black loop in Fig. 4.3), while regional rainfall seasonality exerted an impact on both (blue arrows in Fig. 4.3).

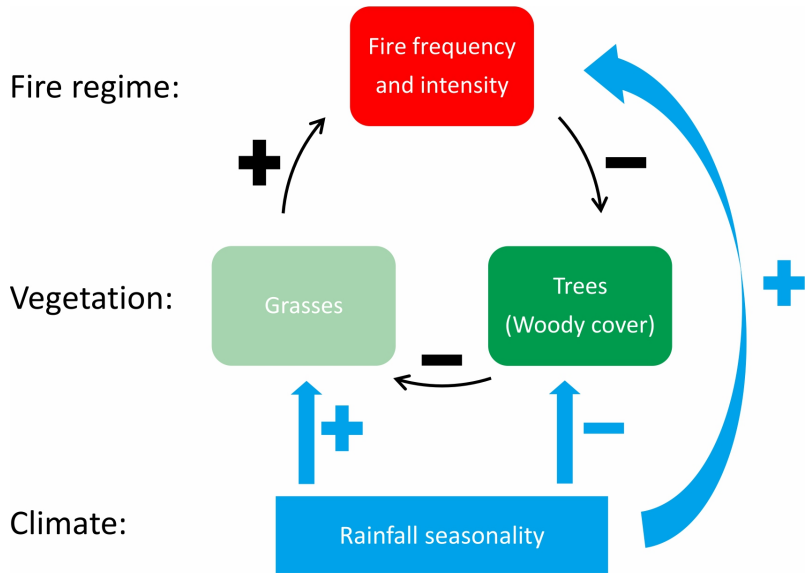


**Figure 4.3:** Conceptual diagram illustrating the interaction between fire regime, vegetation and climate (positive feedback: '+'; negative feedback: '-'). The feedbacks between fire and vegetation, composed of trees and grasses, are shown in the black loop: tree growth is impeded by more frequent and/or intense fires (negative feedback); a decrease in woody cover allows an increase in grass cover (negative feedback); the flammable grasses lead to an increase in fire frequency and/or intensity (positive feedback). Rainfall seasonality serves as a first order control on both fire regime and vegetation (blue arrows). Seasonal drought limits tree growth and canopy closure (negative feedback) but efficiently dry out fuels for fires (positive feedback); intense wet season facilitate fast growth of grasses (positive feedback), providing enough fuels for fires (positive feedback).

A series of feedbacks maintained two alternative stable ecosystems in East Java lowlands: savannah-dominated vegetation during the LGM and rainforest-dominated vegetation during the early Holocene. During the LGM, fires of high frequency and intensity impeded the growth of tree saplings and created space for grasses. The highly flammable nature of C4 grasses further enhanced this fire regime [Stott, 2000; Bond, 2008; Hoffmann et al., 2012a]. The LGM climate with a drier and longer dry season [Ruan et al., 2019] was a prerequisite for potential fuels to dry out and for frequent fires to occur [van der Werf et al., 2008]. An increase in water stress during the dry season favored expansion of drought tolerant C4 grasses [Dubois et al., 2014]. Meanwhile, the short but intense wet season during the LGM [Ruan et al., 2019] allowed for the quick regrowth of grasses, the retained flammability of which further promotes more fires in the dry season. During the early Holocene, low occurrence of fires with low intensity allowed the growth of trees and the closure of the canopy, limiting the growth of grasses due to low light penetration into the understorey. The climate during the early Holocene was characterized by low rainfall seasonality [Ruan et al., 2019], which favored the tropical rainforest vegetation over savannah [Murphy and Bowman, 2012; Dubois et al., 2014]. The relatively evenly distributed rainfall and the rainforest vegetation reduced the amount and the flammability of potential fuels, maintaining a fire regime of low frequency and low intensity [Hoffmann et al., 2012a; Archibald et al., 2013]. A similar coupling of vegetation changes and fire occurrence is recorded in several tropical lowland sites, i.e. a swamp in West Java [van der Kaars et al., 2001], lakes in Sulawesi [Hamilton et al., 2019] and West Africa [Shanahan et al., 2016], respectively. These records indicate that high representation of grass corresponded with high fire occurrence, although fire intensity was not resolved in those studies.

During the deglaciation and the late Holocene, the above feedbacks were disturbed. Under changing rainfall seasonality, fires played an important role in changing vegetation between the two stable states earlier described. Different combinations of frequency and intensity of fires determined whether trees could escape the 'fire trap' and compete with grasses, which led to a shift in regional vegetation cover. A fire regime of low intensity but high frequency during the B-A and the late Holocene was concurrent with C4 grass expansion, implying that such a fire regime was still strong enough to ignite both trees and grasses. In contrast, a fire regime of low frequency and low intensity during the HS1 and the YD potentially facilitated the change from savannah-dominated vegetation to rainforest-dominated vegetation by selectively clearing grasses and creating space for trees. As a feedback, the gradual increase in tree cover at the expense of lowland C4 grasses reduced the availability of a flammable grass layer for fires to spread, which further decreased regional fire occurrence. Such a fire regime is an analogue for that in West Africa during the early Holocene [Dupont and Schefuß, 2018] and that in Southwest Africa during the late Miocene [Hoetzel et al., 2013]. Fire disturbance during the African Humid Period likely created a mosaic vegetation structure and facilitated high density of woody species [Dupont and Schefuß, 2018].

Our results indicate that rainfall seasonality has been a first order control on fire regime and vegetation changes in East Java since the LGM. They are consistent with

findings from other studies that enhanced rainfall seasonality has a two-fold effect of maintaining savannah by reducing tree growth and canopy closure while increasing the probability of fire occurrence [Lehmann et al., 2011]. High rainfall seasonality significantly increases the fire frequency in regions experiencing high annual rainfall by drying out large quantities of fuels and limiting tree cover [Staal et al., 2018]. Our multi-proxy study indicates the importance of rainfall seasonality in modifying fire regime and vegetation types over a broad region and on long periods. An amplified rainfall seasonality was present in the southern part of the Maritime Continent (from southern Indonesia to northern Australia) during the LGM, as shown by a multi-model numerical simulation of the Australian-Indonesian monsoon system [Yan et al., 2018]. The exposure of the Sunda and Sahul Shelves during the LGM played an important role by changing regional atmospheric circulation [DiNezio et al., 2016]: weakened upward air mass motion in austral winter decreased dry season rainfall, while enhanced moisture convergence in austral summer increased wet season rainfall intensity [Yan et al., 2018]. Apart from East Java, the expansion of C4 grass vegetation during the LGM was evident in Sulawesi [Russell et al., 2014; Wicaksono et al., 2017], southern Borneo [Wurster et al., 2019] and Sumba [Dubois et al., 2014]. Fires thus likely also played a significant role in maintaining savannah ecosystem there.

Our results provide a long-term context to assess potential changes in fire regime and tropical ecosystems in the future, a time when human activities are the most extensive and intensive over the past 22,000 years. Under a scenario of continuing anthropogenic greenhouse gas emission, global climate models predict a trend of increasing rainfall seasonality and a more prolonged dry season over most of the tropical regions by the end of the century [Pascale et al., 2016]. Such a change would favor higher fire frequency and intensity while threatening tropical forests as shown in the results during the LGM. Moreover, the forest loss in the tropics is increasing by 2101 square kilometers per year over the 21st Century [Hansen et al., 2013]. The increased flammability of the tropical ecosystems due to lower tree covers would make fires more prone to evade control, especially during the dry season. However, this trend could also be slowed by actively reducing fire frequency and intensity via changing burning practices and patterns, since fire exclusion experiments provide evidence of forest encroachment into savannah [Veenendaal et al., 2018].

## 4.5 Conclusions

In this study, we present accumulation rates of micro-charcoal and two molecular burning markers (levoglucosan and PAHs) from a sediment core covering the past 22,000 years. While the micro-charcoal accumulation rate reflects general fire occurrence in East Java, the ratio of levoglucosan vs. PAHs indicates relative fire intensity. The regional fire occurrence was highest during the LGM and showed two additional maxima during the Bølling-Allerød and the late Holocene, while the fire level was low during the Heinrich Stadial 1, the Younger Dryas and the early Holocene. Fire intensity was high during the LGM but remained low since 18 ka. The combination of charcoal and molecular markers shows great potential for detailed paleo-fire

regime reconstructions.

A series of feedbacks of fire with hydro-climate and vegetation stablized two alternative stable ecosystems in East Javanese lowlands during the LGM and during the early Holocene, respectively. The LGM was characterized by high rainfall seasonality, high occurrence of intense fires and savannah-dominated vegetation, while the early Holocene was characterized by low rainfall seasonality, low occurrence of fires of low intensity and rainforest-dominated vegetation. The deglaciation and the late Holocene were transition periods between the two stable states. A fire regime of low frequency and low intensity during the Heinrich Stadial 1 and the Younger Dryas coincided with major transitions from savannah towards rainforest, while a reverse change in vegetation during the Bølling-Allerød was concurrent with a fire regime of low intensity but high frequency. Hydro-climatic changes in rainfall seasonality thus have the potential to facilitate large-scale vegetation changes mediated by changes in fire regime. Our results implicate more frequent and intense fires in the future in light of the projected increase in the seasonality of the tropical climate.

# Acknowledgements

This work was funded through the German Ministry of Education and Research (BMBF) grants 03G0184A (PABESIA) and 03G0864F (CAHOL). Support was provided through the Cluster of Excellence 'The Ocean Floor – Earth's Uncharted Interface' in Bremen. YR is funded by CSC - the China Scholarship Council and supported by GLOMAR – Bremen International Graduate School for Marine Sciences. SvdK was funded by the Deutsche Forschungsgemeinschaft (DFG) grant BE2116/10-1. SS and ECH are supported by the Netherlands Earth System Science Center (NESSC) funded by the Dutch Ministry for Education and Science. EJH acknowledges the support of the NASA FIREX-AQ program, grant #NNH17ZDA001N. We thank Ralph Kreutz (MARUM), Denise Dorhout (NIOZ) and Monique Verweij (NIOZ) for laboratory support. Lydia Gerullis is acknowledged for dataset preparation. Datasets related to this study can be found at doi.pangaea.de/10.1594/PANGAEA.915962.

Supporting Information for

**Interaction of fire, vegetation and climate in tropical ecosystems: a multi-proxy study over the past 22,000 years**

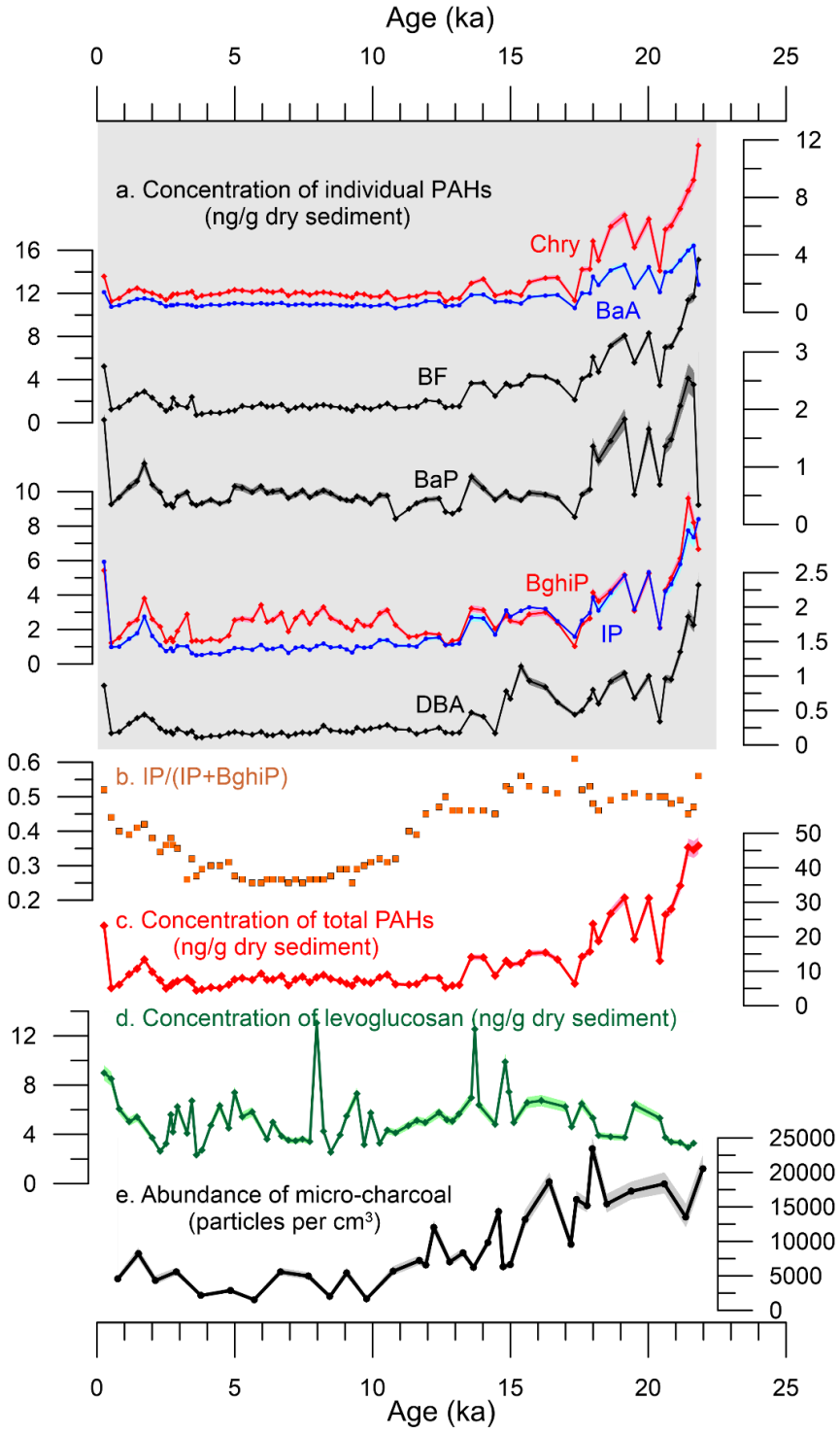

**Figure S1.** Original data of multi-fire proxies from sediment core GeoB10053-7. a) Concentrations of individual PAHs (name abbreviations shown in Table 1). The error envelopes are based on the relative difference of duplicate (Table 1) of each PAH. b) Diagnostic ratio IP/(IP+BghiP). c) Sum of individual PAH concentrations. d) Concentration of levoglucosan. Based on the determined extraction efficiency, the dark green dots show the measured levoglucosan concentrations of each methanol extract multiplied by 1.17. The error envelope represents the lower and upper limit of total levoglucosan concentrations, i.e. measured concentrations of each methanol extract multiplied by 1.09 and 1.25, respectively. e) Abundance of micro-charcoal particles with 95% confidence limits.

# Chapter 5

# Interplay of climate, fire and human activities on land cover and fluvial erosion in East Java over the past 5,000 years

Yanming Ruan[a], Mahyar Mohtadi[a], Lydie M. Dupont[a], Dierk Hebbeln[a], Sander van der Kaars[b,c,d], Matthias Prange[a], Ellen C. Hopmans[e], Stefan Schouten[e,f], Enno Schefuß[a]

a MARUM – Center for Marine Environmental Sciences, University of Bremen, D-28359 Brmen, Germany
b School of Earth, Atmosphere and Environment, Monash University, Clayton, VIC 3800, Australia
c Cluster Earth and Climate, Faculty of Earth and Life Sciences, Vrije Universiteit, 1081 HV Amsterdam, Netherlands
d Department of Palynology and Climate Dynamics, Albrecht-von-Haller Institute for Plant Sciences, University of Göttingen, 37073 Göttingen, Germany
e NIOZ Royal Netherlands Institute for Sea Research, Department of Microbiology and Biogeochemistry, and Utrecht University, P.O. Box 59, 1790 AB Den Burg, Texel, The Netherlands.
f Department of Earth Sciences, Utrecht University, P.O. Box 80.121, 3508 TA Utrecht, The Netherlands.

*In preparation*

**Abstract:** Today, human land use has profoundly induced land cover change and soil erosion. The linkages between land cover, climate and human is essential for projections of future sustainable development. Information about the long-term land cover-climate-human interactions, which go beyond the past decades of instrumental records, however, is limited. In this study, we present the history of land use/land cover (vegetation cover, fluvial erosion and fire disturbance) in East Java, Indonesia over the past 5,000 years, and compare it with regional rainfall reconstructions and archaeologic records, respectively. We find that the fluvial erosion co-varied with the annual rainfall amount of the region through the record, while the highest erosion between 2,800 and 1,800 years ago occurred with a gradual increase in both C4 vegetation and high intensity fire occurrence. Our results suggest that the hydroclimate had a primary control on the East Javanese fluvial system over the past 5,000 years. In the meanwhile, the prehistoric human society of East Java potentially caused deforestation by swidden cultivation using fire as a tool, which enhanced soil erosion. Such a human impact became stepwise profound through the record as reflected by the increasing occurrence of high intensity fires.

## 5.1 Introduction

Land cover, including its vegetation and fluvial system, is the basis of human livelihoods. In turn, humans are significantly exerting impact on land cover. Among the total global ice-free land surface by 2015, about three-quarters of it has been affected by human use, while 12-14% of it has been used as croplands [IPCC, 2019]. In the tropics, humans have long been transforming forest for agriculture and settlement purposes (deforestation), using fires as a tool [Ellis et al., 2013, and references therein]. Swidden cultivation (also called shifting cultivation or slash-and-burn) has been one of the most important land use systems in the tropics for centuries and is still practiced today, in which areas of vegetation (including forest) are burned and then used for cultivation before left fallow [Mertz et al., 2009]. Soil erosion is a severe consequence of land use/land cover changes. Mean soil loss (an indicator for the degree of soil erosion) for croplands are about double the amount for grasslands and about ten times as much as that for forests in the tropics [Labrière et al., 2015].

Climate serves as another important factor on land cover by shaping the vegetation and altering the water balance through hydrological processes. In the tropics, rainfall largely determines the vegetation distribution [Peel, 2007]. Rainfall seasonality has an impact on tropical C3/4 vegetation composition since C4 plants are generally more drought tolerant than C3 plants [e.g. Collins et al., 2011; Dubois et al., 2014]. Furthermore, rainfall of high intensity in the tropics can cause dramatic levels of riverine runoff [van Noordwijk et al., 2017] and soil erosion [Labrière et al., 2015].

Long-term interactions between land cover, climate and human, which cannot be resolved by the short instrumental records only covering only the past decades [Alkama and Cescatti, 2016], are essential for making projections on sustainable future developments. A key problem is that the extent and intensity of prehistoric human impact on land cover is difficult to quantify [Stephens et al., 2019]. Human land use generally evolved from the less intensive form of foraging (practices of foraging,

hunting and gathering) to more intensive forms of agriculture, pastoralism and even urbanization [Stephens et al., 2019]. Integrating paleoclimatology based on multiple proxies with archaeological results is a promising way to study long-term land cover-climate-human interactions on a regional scale [Ellis et al., 2013]. East Java in Indonesia is a suitable region for this purpose, as human prehistory there in the late Holocene is relatively well documented in several archaeological records [e.g. Morwood et al., 2004; Sémah et al., 2016; Simanjuntak and Asikin, 2004]. Here, we reconstruct 5,000 years of land use/land cover history using proxies of vegetation, fluvial erosion riverine detrital flux and fires, and compare it with rainfall reconstructions and archaeological evidence to elucidate the past climatic vs. human impact on the landscape.

## 5.2 Modern environmental setting of the study area

### 5.2.1 Modern rainfall and runoff distribution

Modern rainfall has a distinct seasonal pattern in Java. High rainfall amounts occur during the northwestly Australian-Indonesian summer monsoon (AISM) season, when the Intertropical Convergence Zone (ITCZ) is situated above the Maritime Continent; drier conditions accompany the southeastly Australian-Indonesian winter monsoon (AIWM) season, when the ITCZ migrates towards the north with a mean position near 12°N [Kalnay et al., 1996]. Similar to rainfall, riverine runoff in East Java displays a seasonal pattern with low (high) values during the dry (wet) season [Aldrian et al., 2008; Jennerjahn et al., 2004].

The state of the Pacific/Indian Ocean exerts important impacts on the climate of Java through inter-annual and decadal coupled atmosphere-ocean oscillations, i.e. El Niño and Southern Oscillation (ENSO) and the Indian Ocean Dipole (IOD). The average (composite) progression of El Niño involves two consecutive years, with an onset in April to its peak in December and a transition to La Niña in August of the subsequent year. El Niño events induce a decrease in precipitation in Java, which occurs mostly in the dry season but is not significant and spatially coherent in the wet season [As-syakur et al., 2014; Supari et al., 2018]. Instead, El Niño events cause a positive rainfall anomaly over the large islands of the Maritime Continent (including Java) during the wet season [Rauniyar and Walsh, 2013]. IOD is seasonally phase-locked to the dry season of Java [Cai et al., 2013; Saji et al., 1999]; positive IOD events cause a decrease in Javanese rainfall in the dry season [As-syakur et al., 2014].

### 5.2.2 Modern vegetation distribution

The distribution of natural vegetation types of East Java depends on the rainfall distribution as well as elevation. Six major natural vegetation types are mapped by Whitten et al. [1996] based on elevation, annual rainfall amount and dry month length (Fig. 5.1c). Both distributed in areas with high annual rainfall (over 2,000 mm), evergreen rainforests experience less than two dry months (with monthly rain-

fall <100 mm), while semi-evergreen rainforests (with a few deciduous trees) experience two to four dry months. Moist deciduous forests (where at least half of the trees are deciduous) are distributed in areas with an annual rainfall amount between 1,500 and 4,000 mm and four to six dry months. Dry deciduous forests (where almost all the trees are deciduous) occur in coastal areas with less than 1,500 mm annual rainfall amount and over six dry months. With the former four vegetation types growing below 1,200 m, aseasonal/seasonal montane forests are distributed on mountainous areas higher than 1,000 m [Whitten et al., 1996].

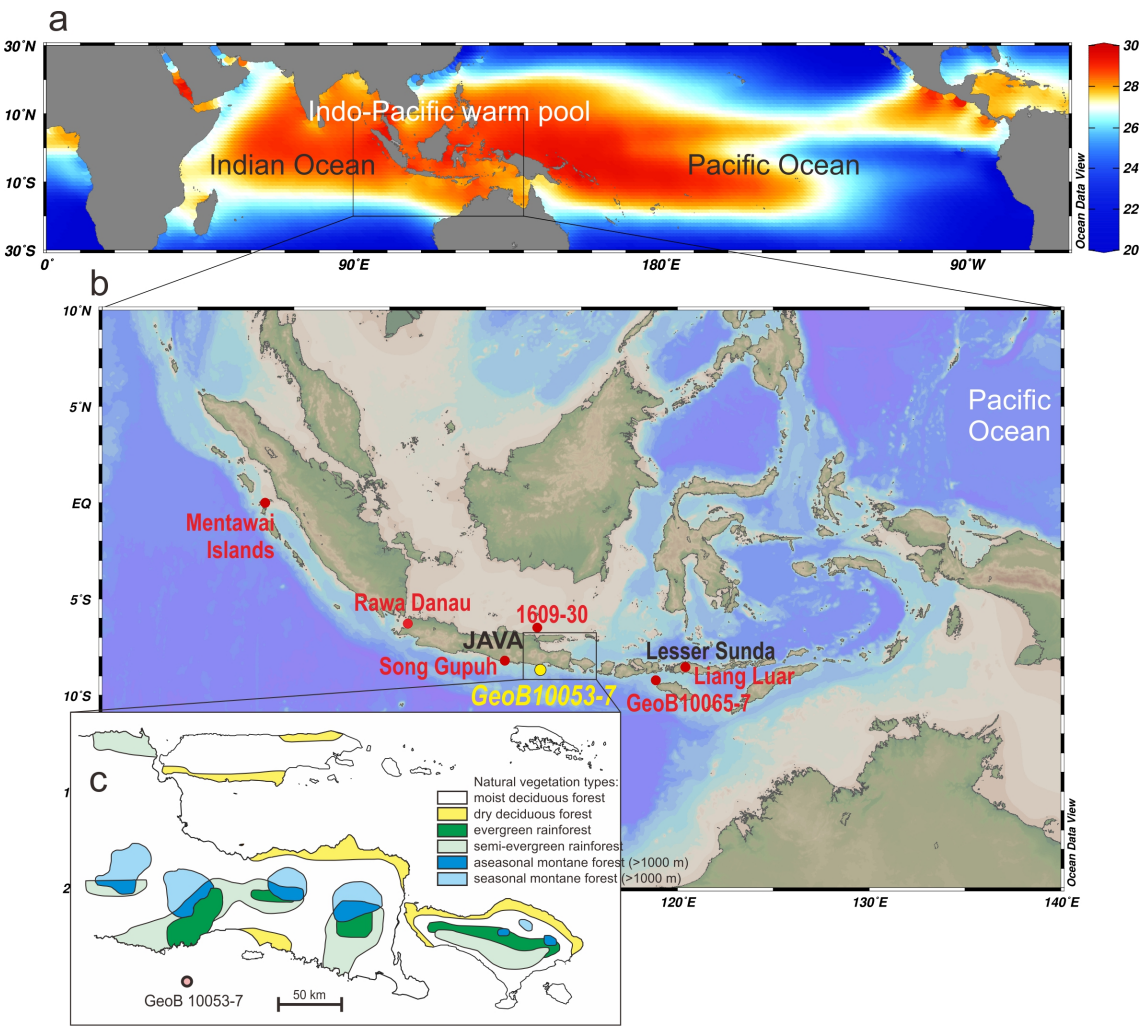


**Figure 5.1:** a) The annual sea surface temperature distribution of the tropical oceans [World Ocean Atlas 2013; Locarnini et al., 2013]. The Indo-Pacific Warm Pool, located between the tropical Indian Ocean and Pacific Ocean, is characterized by high annual sea surface temperatures. b) The location of the sediment core GeoB10053-7 (yellow dot) and other sites discussed in the text (red dots). c) Natural vegetation distribution of East Java and Bali, modified from Whitten et al. (1996).

Since Java is one of the most densely populated areas of the world today, most of the natural vegetation has been replaced by rice fields, grasslands, urban areas etc. [Stibig et al., 2002]. The only remaining rainforests are restricted to isolated montane patches [Collins et al., 1991]. Fire occurrence also plays a role in modifying the vegetation distribution, resulting in montane grasslands in Java as an example

[Collins et al., 1991].

### 5.2.3 Modern fire pattern

Fires in Java display a distinct seasonal pattern despite a large part of the fires are human-induced in modern times. The fire occurrence there is high during the dry (AIWM) season and low during the wet (AISM) season, since a sufficient amount of dry fuel for ignition is the prerequisite for fires [Reid et al., 2012]. There is an increase in fire occurrence of Java during El Niño events [Reid et al., 2012]. During extreme drought events, fire usage tends to evade control more often [Page et al., 2002]. The most extensive fires are potentially associated with the co-occurrence of a positive IOD event and an El Niño event, when reduced Walker Circulations of both the Pacific and the Indian Ocean resulted in severe drought conditions in Indonesia as a whole (e.g. 1972, 1982-83 and 1997-98)[Saji and Yamagata, 2003; Field et al., 2009; Field and Shen, 2008].

## 5.3 Material and Methods

### 5.3.1 Sample information and lipid extraction

Sediment core GeoB 10053-7 (8° 40.59'S; 112° 52.35' E; 1,375 m water depth; 750 cm core length) was retrieved offshore south Java, Indonesia during the SO-184 "PABESIA" expedition in 2005 [Hebbeln and cruise participants, 2006]. Fourty samples were collected from the upper 250 cm of the sediment core, covering the past 5,000 years according to five accelerator mass spectrometry (AMS) $^{14}C$ dates [Mohtadi et al., 2011]. The average sample resolution is around 120 years. Lipid analyses are performed for paleo-climate and fire regime reconstructions. After adding an internal standard to each sample, lipid extractions were carried out using a DIONEX Accelerated Solvent Extractor (ASE 200) first with a mixture of dichloromethane to methanol (9:1) and then with methanol, both at 1000 psi and 100°C (three cycles, 5 minutes each).

For the extracts with dichloromethane to methanol (9:1), desulphurisation was carried out before water was removed using 2-cm $Na_2SO_4$ columns. Saponification was carried out with 0.1M KOH-solution, after which neutral fractions were recovered by *n*-hexane. Silica gel columns (5-cm) were used to separate the neutral fractions: elution with *n*-hexane, dichloromethane and dichloromethane to methanol (1:1) yielded the apolar, ketone and polar fractions, respectively. The apolar fractions were additionally eluted with *n*-hexane over 5-cm $AgNO_3$-coated silica columns to remove unsaturated compounds. The hydrogen and carbon isotopes of leaf wax *n*-alkanes were measured using the apolar fractions. The PAH analysis was based on the ketone fractions. Levoglucosan analysis was based on the methanol extracts as described by Ruan et al. (Chapter 4).

### 5.3.2 Hydrogen and carbon isotopes of leaf wax lipids

Long chain leaf wax lipids, transported by rivers or wind before deposition in sedimentary archives, provide information of the continental vegetation that biosynthesized them [e.g. Eglinton and Eglinton, 2008]. The leaf wax $\delta$D changes in response to changes in the $\delta$D values of precipitation [Sachse et al., 2012, and references therein], which primarily reflect rainfall intensity via the 'amount effect' in the study area, i.e. more negative precipitation $\delta$D values suggest higher rainfall intensity [Belgaman et al., 2017; Suwarman et al., 2013]. The leaf wax $\delta^{13}$C mostly reflects the regional vegetation composition in terms of C3 and C4 plants, which in tropical regions are typically woody plants (trees/shrubs) and grasses/sedges, respectively [Ehleringer et al., 1997; Diefendorf and Freimuth, 2017]. The leaf wax $\delta^{13}$C is further linked to rainfall seasonality in the study area, since C4 plants are generally more drought tolerant than C3 plants [Dubois et al., 2014].

The analyses of leaf wax lipids and their isotopes were performed as described in detail by Ruan et al. [2019]. Contents of the *n*-alkanes were determined by a ThermoFisher Scientific Focus Gas Chromatography (GC) coupled with a flame ionization detector. $\delta$D values of the *n*-alkanes were measured using a Thermo Trace GC coupled via a pyrolysis reactor (1420 °C) to a Thermo Fisher MAT 253 isotope ratio mass spectrometer. An external standard (a mixture of 12 *n*-alkanes of known isotope compositions) was measured between every six sample measurements to monitor machine performance. The long-term mean absolute deviation based on the external standard was 3‰. The analyses of the internal standard (squalene, $\delta$D = -180‰) in all samples revealed a precision of 1‰ and an accuracy of 1‰ (n = 81). The $H_3^+$ factor, which was determined on a daily basis, had a mean value of 4.77 (n = 15) and varied between 4.67 and 4.85 throughout measurements. Samples were analyzed in duplicate, except for five samples that were analyzed only once because of low compound abundances. The difference between the duplicates ranges from <1‰ to 4‰ with a mean value of 1‰ for each homologue (*n*-C29, *n*-C31 and *n*-C33). The $\delta$D values were calibrated against the external $H_2$ reference gas, and are reported in ‰ against Vienna Standard Mean Ocean Water (VSMOW). $\delta^{13}$C values of *n*-alkanes were measured using a Thermo Trace GC coupled via a combustion interface (1000 °C) to a ThermoFinnigan MAT 252 isotope ratio mass spectrometer. The long-term mean absolute deviation based on the external standard was 0.3‰. The $\delta^{13}$C values were calibrated against the external $CO_2$ reference gas, and are reported in ‰ against Vienna PeeDee Belemnite (VPDB). The external standard was routinely measured similar to the $\delta$D analyses. The analyses of the internal standard (squalene, $\delta^{13}$C = -19.8‰) across the measurements corroborated a precision of 0.1‰ and an accuracy of <0.1‰ (n = 64). Samples were analyzed in duplicate, except for 13 samples that were measured only once due to low compound abundances after $\delta$D analyses. The difference between the duplicates ranges from <0.1‰ to 0.4‰ with a mean value of 0.1‰ for each homologue (*n*-C29, *n*-C31 and *n*-C33).

### 5.3.3 Levoglucosan and PAHs

Levoglucosan (1,6-anhydro-$\beta$-D-glucopyranose) is a product of cellulose combustion only produced in low burning temperatures (150-350 °C), and thus reflects low intensity fires [Kuo et al., 2008]. Pyrogenic PAHs, on the other hand, are formed at higher burning temperatures (200-700 °C) and reflect high intensity fires [Lu et al., 2009; Keiluweit et al., 2012].

The PAH analysis was performed as described in detail by Ruan et al. (Chapter 4). Briefly, the ketone fractions which containing the PAHs were analyzed using an Agilent 7820A Gas Chromatograph (GC) equipped with an Rxi-PAH capillary column (40 m, 0.18 mm i.d., 0.07 μm) coupled to a 5977E Mass Selective Detector (MSD) quadrupole mass spectrometer. Electron ionization was accomplished with an electron energy of 70 eV in single ion monitoring (SIM) mode.

We identified each peak according to the SIM mass and retention time of the standard mixture. Quantification was determined by comparing the peak area of the target compound to that of the internal standard (2-Fluorofluorene) and applying the Relative Response Factors. Duplicate measurements on 30 samples revealed an average relative difference of 4% for Chrysene/Benzo(b/j/k)fluoranthene, 5% for Benzo(a)anthracene/Benzo(g,h,i)perylene, 7% for Dibenzo(a,h)anthracene/ Indeno(1,2,3-cd)pyrene and 8% for Benzo(a)pyrene. In order to account for biases due to sediment properties and sediment rates, the accumulation rate of PAHs (ng $cm^{-2}$ $kyr^{-1}$) was calculated by multiplying the content (ng $g^{-1}$) with the dry bulk density of the sediment (g $cm^{-3}$), and the sedimentation rate (cm $kyr^{-1}$) based on the age model.

The analysis of levoglucosan was performed as described in detail by Schreuder et al. [2018]. Briefly, the MeOH extracts were analyzed using an Agilent 1290 Infinity Ultra-High Performance Liquid Chromatography (UHPLC) coupled to an Agilent 6230 Time-Of-Flight (TOF) mass spectrometer. Separation was achieved with two Aquity BEH amide columns in series with a 50 mm guard column. Quantification was based on peak integrations of mass chromatograms within 10 ppm mass accuracy using an exact mass of 161.0445 m/z for levoglucosan and 168.0884 m/z for dLVG. Duplicate measurements on 15 samples revealed an average relative difference of 3% for levoglucosan. In order to account for biases due to sediment properties and sediment rates, the accumulation rate of levoglucosan (ng $cm^{-2}$ $kyr^{-1}$) was calculated by multiplying the content (ng $g^{-1}$) with the dry bulk density of the sediment (g $cm^{-3}$), and the sedimentation rate (cm $kyr^{-1}$) based on the age model.

### 5.3.4 Palynological analysis

Six samples were used for palynological analysis as described in Ruan et al. [2019].

## 5.4 Results

### 5.4.1 Source of leaf wax *n*-alkanes

The long chain *n*-alkane homologues show a distinct odd-over-even predominance, a feature of higher plant leaf waxes [Eglinton and Hamilton, 1967]. The predominance is quantified by the carbon preference index (CPI) calculated based on the contents of individual *n*-alkane homologues:

$$CPI_{27\text{-}33} = \frac{1}{2} \times \frac{[n\text{-}27] + [n\text{-}29] + [n\text{-}31] + [n\text{-}33]}{[n\text{-}26] + [n\text{-}28] + [n\text{-}30] + [n\text{-}32]} + \frac{1}{2} \times \frac{[n\text{-}27] + [n\text{-}29] + [n\text{-}31] + [n\text{-}33]}{[n\text{-}28] + [n\text{-}30] + [n\text{-}32] + [n\text{-}34]} \tag{5.4.1}$$

Strong degradation of organic matter can result in low CPI values [Bray and Evans, 1961] that approach CPI = 1 for petroleum as an extreme [Kolattukudy, 1967]. The overall high CPI values of the samples analyzed in this study, ranging from 4 to 5.8, indicate the dominance of relatively non-degraded plant-derived long chain *n*-alkanes.

### 5.4.2 Vegetation reconstruction based on leaf wax $\delta^{13}$C and pollen data

The $\delta^{13}$C values of the three homologues (abbreviated to $\delta^{13}C_{29}$, $\delta^{13}C_{31}$ and $\delta^{13}C_{33}$) show similar trends throughout the past 5,000 years (Fig. 5.2a). The weighted-average $\delta^{13}$C record is thus calculated based on the $\delta^{13}$C values and contents of the three homologues:

$$\delta^{13}C_{weighted-average} = \frac{\delta^{13}C_{29} \times [n\text{-}29] + \delta^{13}C_{31} \times [n\text{-}31] + \delta^{13}C_{33} \times [n\text{-}33]}{[n\text{-}29] + [n\text{-}31] + [n\text{-}33]} \tag{5.4.2}$$

The lowest $\delta^{13}$C values occurred from 5 ka (thousand years ahead of 1950 AD) to 3 ka, followed by a general increase from 3 ka to 2 ka. The highest $\delta^{13}$C values occurred around 1.8 ka and 0.2 ka, respectively (Fig. 5.3a).

Based on the polynological record with a lower sample resolution, the representation of herbaceous taxa (herbs) display a general increase from 10% to 30% over the past 5 kyr. The pollen of herbs were dominated by Poaceae (grass) and Cyperaceae (sedges), with an increase in the representation of the former from 5% to 17% and the latter from 5% to 10%, respectively, over the past 5 kyr. The Palmae Arenga type pollen was present but rare in the sample dated to 3.8 ka. Its percentage rose to 5% around 2.9 ka and then above 10% in the samples younger than 2.1 ka.

### 5.4.3 Rainfall intensity reconstruction based on leaf wax $\delta$D

The $\delta$D values of the three *n*-alkane homologues (abbreviated to $\delta D_{29}$, $\delta D_{31}$ and $\delta D_{33}$) were in a similar range from 4.5 ka to 2.5 ka (Fig. 5.2b). After 2.5 ka the $\delta$D values of the three homologues became more divergent but still displayed similar trends (Fig. 5.2b). The weighted-average $\delta$D record is thus calculated based on the

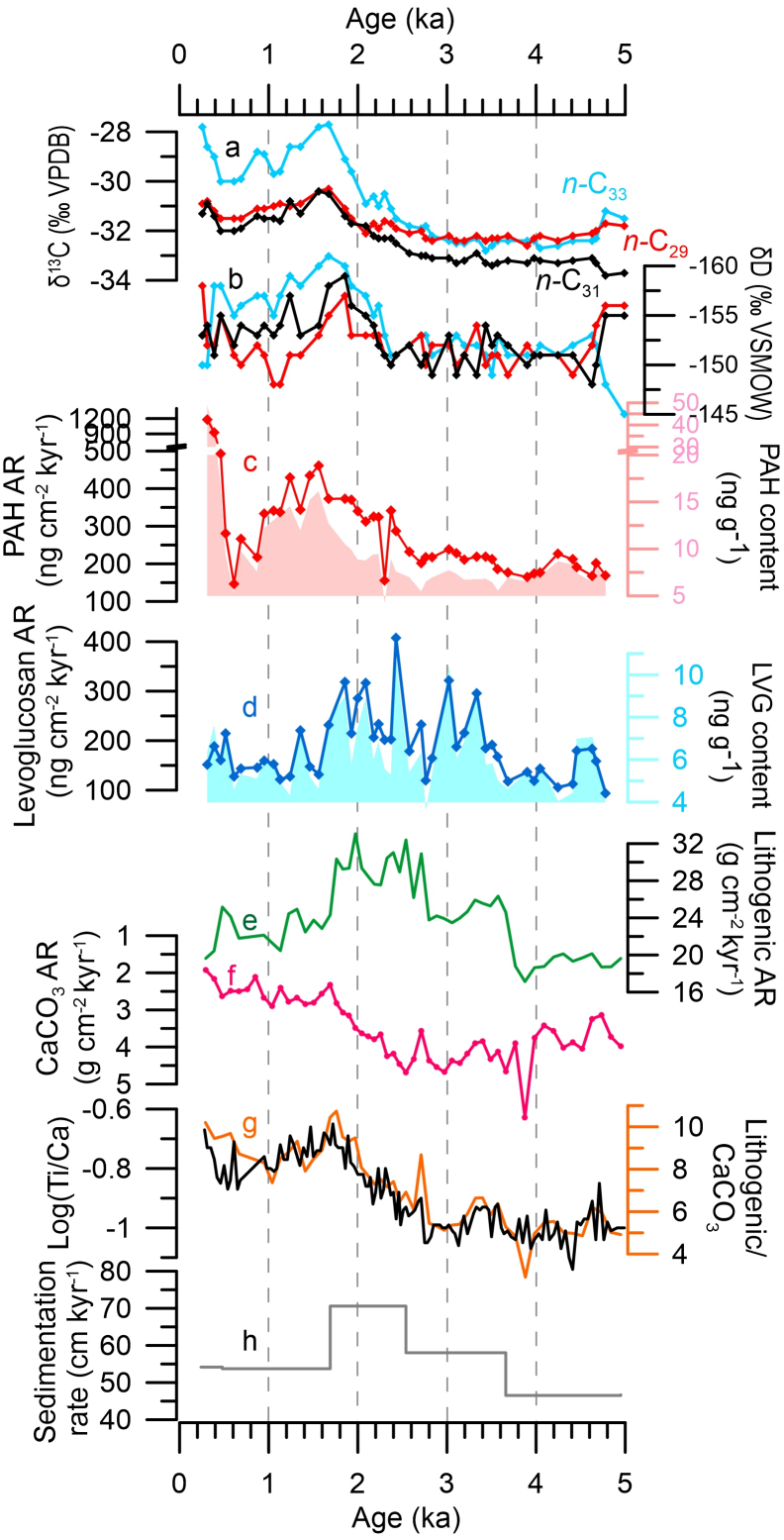


**Figure 5.2:** Comparison of various proxy records from sediment core GeoB10053-7. The $\delta^{13}C$ (a) and $\delta D$ (b) values of the *n*-alkane homologues (red for *n*-C29, black for *n*-C31 and blue for *n*-C33). c) Accumulation rates (line) and contents (shadow) of PAHs. d) Accumulation rates (line) and contents (shadow) of levoglucosan. Accumulation rates of the lithogenic fraction (e) and the $CaCO_3$ content (f) of the sediment [Mohtadi et al., 2011]. g) Ti/Ca ratios and lithogenic/$CaCO_3$ ratios [Mohtadi et al., 2011]. h) Sedimentation rate of the sediment core.

$\delta$D values and concentrations of the three homologues:

$$\delta D_{weighted-average} = \frac{\delta D_{29} \times [n\text{-}29] + \delta D_{31} \times [n\text{-}31] + \delta D_{33} \times [n\text{-}33]}{[n\text{-}29] + [n\text{-}31] + [n\text{-}33]} \quad (5.4.3)$$

All three homologues showed an $\delta$D minima around 1.8 ka, which is the most distinct feature of the $\delta$D records over the past 5 ka (Fig. 5.3c).

### 5.4.4 Source and environmental fates of levoglucosan and PAHs

Levoglucosan and PAHs share similar environmental fates before being deposited in marine sediments. Both types of compounds are emitted into the atmosphere mainly attached to particles from fires [Wang et al., 2017]. Riverine discharge, the major transport process in wet areas, is postulated to bring the two kinds of molecular markers deposited in soils or rivers of East Java into the marine environment. In this regard, both are transported similarly by river systems [Myers-Pigg et al., 2017]. Particularly, the steep topography from the volcanic arc to the core site in East Java without a delta system favors relatively fast transport and sedimentary deposition of fire-induced molecular markers [Hunsinger et al., 2008]. During the dry season, transport by aerosols may play a role. The prevailing wind direction during the dry (fire) season is southeast [Kalnay et al., 1996]; the inclusion of material from Australia cannot be ruled out but is expected to be minor due to the transport distance of over 1500 km. It is noteworthy that levoglucosan in marine sediments is prone to degradation at the seawater-sediment interface [Schreuder et al., 2018], which is substantially less for PAHs due to their more stable chemical structures. The very weak correlation between levoglucosan concentrations and sedimentation rates of the samples ($R^2$=0.17), however, implies a minor degradation of levoglucosan in the seawater-sediment interface.

### 5.4.5 Accumulation rates of levoglucosan and PAHs

The accumulation rates of both levoglucosan and PAHs show similar variations with the contents of the compounds (Fig. 5.2c, d). The accumulation rate of the PAHs shows a similar trend of changes as the $\delta^{13}$C record, with low values before 3 ka, an increase from 3 ka to 2 ka and high values around 1.5 ka and in the shallowest part of the sediment core (Fig. 5.2a, c). The PAH accumulation rates were, however, significantly higher since 0.5 ka than the rest of the record (Fig. 5.2c).

The accumulation rate of levoglucosan showed an earlier increase (at around 3.6 ka) than that of the PAHs. The levoglucosan accumulation rate reached the highest values between 3 ka and 2 ka before a general decrease to low values since 1 ka (Fig. 5.2d).

## 5.5 Discussion

### 5.5.1 Regional vegetation cover (land cover)

The leaf wax $\delta^{13}C$ record displays an increase around 3 ka (Fig. 5.3a), implying for an expansion of regional C4 vegetation. Such an expansion in C4 vegetation continued till 1.6 ka before a reduction until 0.5 ka (Fig. 5.3a). The positive leaf wax $\delta^{13}C$ values between 3 and 0.5 ka implies a relatively open canopy vegetation cover during that period, which is supported by the spread of grasses (Poaceae) and sedges (Cyperaceae) and the decline of trees and shrubs based on palynological evidence from the same sediment core. It is, however, noteworthy that the palynological record, with a lower sample resolution than the leaf wax $\delta^{13}C$ record, displays a continuous increase (decrease) in the representation of Poaceae and Cyperaceae (trees and shrubs) through the past 5 kyr.

Our vegetation cover reconstruction since 5 ka shows comparative patterns with a leaf wax $\delta^{13}C$ record from a marine sediment core GeoB 10065-7 offshore Sumba (a Lesser Sunda Island, location shown in Fig. 5.1b) [Fig. 5.3b; Dubois et al., 2014] and palynological data from a marine sediment core 1609-30 off the Solo River mouth (offshore northern Java, location shown in Fig. 5.1b) covering the last 3,500 years [Poliakova et al., 2017]. The latter study shows that forest canopy opening started around 3 ka and became more significant between 2 and 1 ka, with the evidence for a decline in primary forest taxa but a development of secondary vegetation pioneer taxa and herbs [Poliakova et al., 2017]. In a lowland swamp Rawa Danau, West Java (location shown in Fig. 5.1b), a similar increase in Poaceae and Cyperaceae pollen occurred but with a different timing: a maxima around 2 ka and highest over the last few hundred years [van der Kaars et al., 2001].

The palynological data show a rise in both the percentage of Palmae Arenga type pollen and micro-charcoal accumulation rate after 3.8 ka, together with the evidence of spread of grasses and sedges. This pattern can be interpreted as an increase in local swidden cultivation activities according to existing palynological studies on Java Island [van der Kaars and van den Bergh, 2004; Poliakova et al., 2017], although the impact of rainfall seasonality potentially also played a role (see 5.5.6 for more discussion). A similar pattern is observed in the Solo River catchment but with a later onset, i.e. after 1 ka [Poliakova et al., 2017].

### 5.5.2 Fire history (land use)

The early onset of low intensity fires around 3.8 ka is reflected by the accumulation rate of levoglucosan; while the occurrence of high intensity fires reflected by PAHs rose later around 3 ka (Fig. 5.3h, i). When the occurrence of low intensity fires decreased between 2 and 1 ka, the occurrence of intense fires was high during that period (Fig. 5.3h, i), indicating a shift in fire regime towards higher fire intensity. Another interesting feature about the PAH record is the sharp 2-fold increase in accumulation rates around 0.5 ka (Fig. 5.3h). The micro-charcoal concentration based on the sediment core off the Solo River mouth [Poliakova et al., 2017] shares similar patterns of our PAH record. The lowland swamp site of West Java sees a

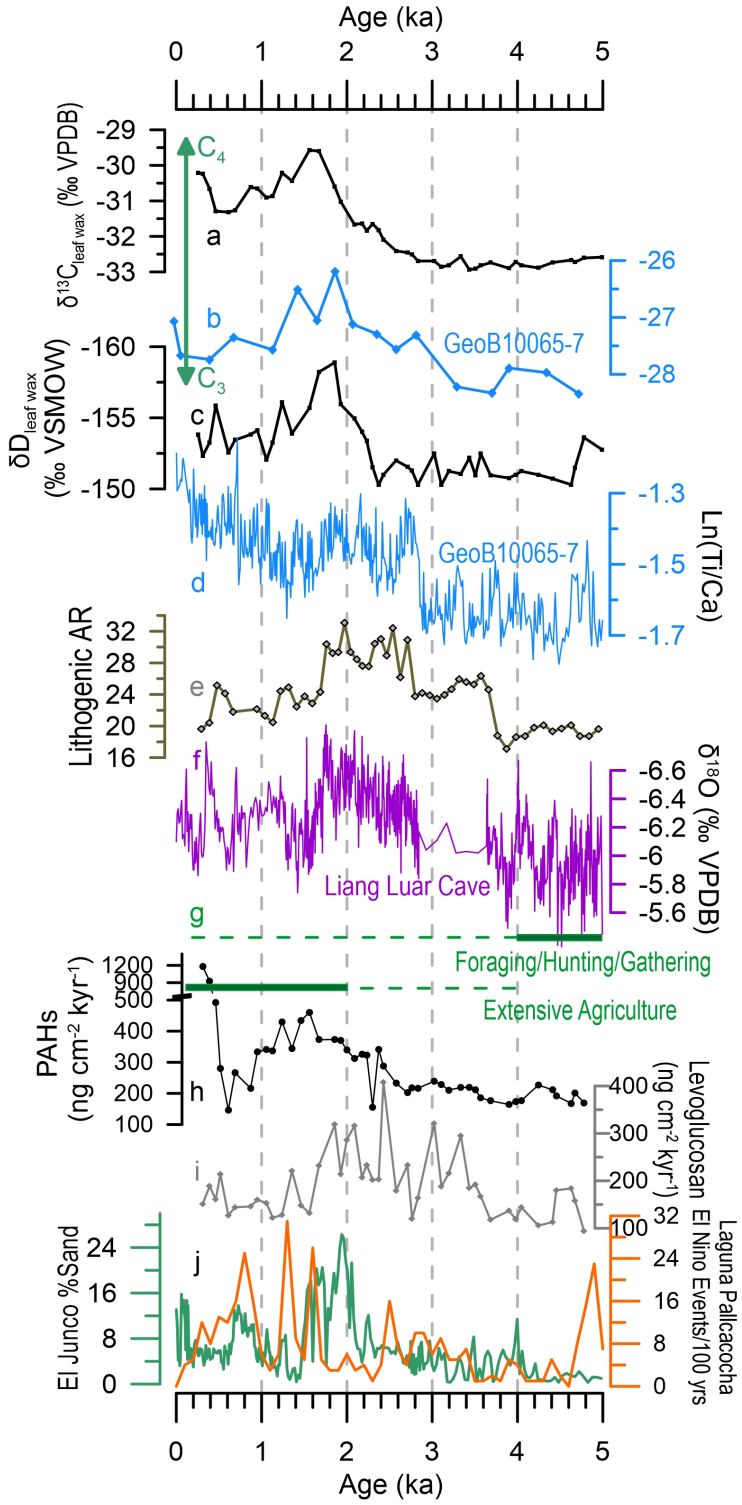


**Figure 5.3:** Comparison of various proxy records from sediment core GeoB10053-7 and other sites. a) The weighted-average $\delta^{13}C$ values of three *n*-alkane homologues. b) The $\delta^{13}C$ values of C30 *n*-alkanoic fatty acid from the sediment core GeoB10065-7 [Dubois et al., 2014]. c) The weighted-average $\delta D$ values of three *n*-alkane homologues. d) Ti/Ca ratios from GeoB10065-7 [Steinke et al., 2014]. e) Accumulation rates of the lithogenic fraction [Mohtadi et al., 2011]. f) Spliced $\delta^{18}O$ values of Liang Luar Cave speleothems in Flores [Griffiths et al., 2009]. g) Broad-scale archaeological assessment of pre-historic human evolution in Java and Timor: foraging was widespread (>20% regional land area) before 4 ka and became common (>1 to 20% regional land area) after 4 ka; extensive agriculture started around 4 ka and became widespread since 2 ka [Stephens et al., 2019]. Accumulation rates of PAHs (h) and levoglucosan (i). j) El Niño reconstructions from two eastern tropical Pacific sites: Laguna Pallcacocha, Ecuador [Moy et al., 2002] and El Junco lake, Galapagos [Conroy et al., 2008].

significant increase in micro-charcoal to pollen ratio since 0.5 ka, similar to what is observed in our PAH record during the same period [van der Kaars et al., 2001].

Our results show a coupling between vegetation and intense fires, with a higher portion of C4 vegetation mirrored by high occurrence of intense fires from 2 to 1 ka and after 0.5 ka (Fig. 5.3a, h). Such a relationship agrees with modern observations: fires in tropical moist broadleaf forests are predominantly of low intensity and low to intermediate frequency, while tropical grassland fires are more frequent and tend to reach higher intensity [Archibald et al., 2013].

The different pattern of levoglucosan accumulation rate from the above two implies a limited impact of low intensity fires on changing regional C3/4 vegetation. An explanation is that trees of certain sizes are more likely to survive low intensity fires than high intensity fires [Hoffmann et al., 2012a]. It is, however, noteworthy that the leaf wax $\delta^{13}$C record is not so detailed as pollen data and may thus not be sensitive enough to resolve a slight expansion of herbs.

### 5.5.3 Fluvial erosion

The marine sediments deposited in the core site over the past 5,000 years are characterized by a fine grained terrigenous fraction which is interpreted as river-derived [Mohtadi et al., 2011]. The accumulation rate of the lithogenic particles based on the sediment core thus quantitatively reflects the riverine detrital flux to the core site over the past 5 kyr, which shows an increase starting around 3.8 ka, highest values between 2.8 ka and 1.8 ka, before a decrease from 2 ka to 1.6 ka (Fig. 5.2e, Fig. 5.3e). The highest amounts of riverine detrital flux between 2.8 ka and 1.8 ka are consistent with high Ti/Ca values from the core GeoB10065-7 offshore Sumba [Steinke et al., 2014] (Fig. 5.3d), although the Ti/Ca ratio can also be affected by the Ca part related with marine productivity.

Two major factors contribute to an increase in fluvial erosion reflected by the riverine detrital flux: 1) high runoff induced by precipitation which enhances the transport capacity of the river [Aldrian et al., 2008; Jennerjahn et al., 2004]; 2) stronger erosion due to weaker soil stability induced by land use/land cover changes [Labrière et al., 2015]. Hydro-climate exclusively controls the first factor while plays a potential part in the second factor. Anthropogenic deforestation and agriculture cultivation cause changes in the second factor. Below, we first discuss the regional climatic forcing and then the potential impact of human activities on East Javanese landscapes, before evaluating the land cover-climate-human interactions.

### 5.5.4 Regional hydro-climate history

The leaf wax $\delta$D of the sediment core GeoB10053-7 is used to reflect the $\delta$D values of the monsoonal rainfall of East Java over the past 5,000 years. It is not influenced by human activities, thus can be used to assess the climatic impact on land cover. Similarly, the $\delta^{18}$O values of Liang Luar Cave speleothems in Flores indicate the $\delta^{18}$O values of the past monsoonal rainfall [Griffiths et al., 2009]. Both indices share similar variations over the past 5,000 years, with the most negative values around

1.8 ka (Fig. 5.3c, f). The general decrease in Liang Luar Cave $\delta^{18}O$ from 4 to 3 ka is however not present in our leaf wax $\delta D$ record (Fig. 5.3c, f). Although both are water isotope based proxies for rainfall in the Australian-Indonesian monsoon region, the leaf wax $\delta D$ is proposed to reflect wet season rainfall intensity whereas the speleothem $\delta^{18}O$ likely reflects annual rainfall amount. The production [Moser et al., 2014; Rowland et al., 2014; Wiegand et al., 2004], erosion and fluvial transport [Bird et al., 1995; Aldrian et al., 2008] of leaf waxes favor a wet season $\delta D$ signal in the sedimentary leaf wax lipids in East Java. Thus, the leaf wax $\delta D$ of the sediment core GeoB10053-7 is proposed to reflect wet season rainfall intensity via the 'amount effect' [Belgaman et al., 2017; Suwarman et al., 2013; Ruan et al., 2019]. Groundwater as the source water for speleothems is more likely an annually integrated pool and less sensitive to rainfall intensity. Therefore, the $\delta^{18}O$ of Liang Luar Cave speleothems is expected to be an annual rainfall amount signal.

There is a strong coupling between the lithogenic accumulation rates and the $\delta^{18}O$ of Liang Luar Cave speleothems through the record despite the growth hiatus in stalagmite from 3.6 to 2.8 ka (Fig. 5.3e, f). This implies the annual rainfall amount as a significant control on East Javanese riverine detrital flux. Although the East Javanese riverine runoff and thus fluvial transport capacity is seasonal [Aldrian et al., 2008; Jennerjahn et al., 2004], the soil erosion occurs over the entire year.

### 5.5.5 Regional prehistoric human activities

The broad-scale pre-historic human development in the study area is inferred by archaeological data (Fig. 5.3g): foraging was widespread (>20% regional land area) in Java and Timor before 4 ka and became less prominent (>1 to 20% regional land area) after that; in contrast, the onset of extensive agriculture was around 4 ka, which later became widespread since 2 ka [Stephens et al., 2019].

The Neolithic period (also called the Gupuh Phase after the cave Song Gupuh) in East Java is dated from 4 to 2 ka [Simanjuntak and Asikin, 2004]. This period is associated with the arrival and expansion of Austronesian-speaking people, who carried a fully agricultural economy and introduced pottery use and stone adze manufacture [Bellwood, 2007]. Swidden cultivation must have been the norm for early farming in the beginning of the settlement [Christie, 2007]. Before the Neolithic period was the pre-neolithic layer in archaeological sites of East Java (also called the Keplek Phase after the cave Song Keplek) dated from 12 to 4 ka. This pre-neolithic layer is characterized by lithic artefacts and bone tools, with shell tools especially abundant in coastal regions [Simanjuntak and Asikin, 2004]. The pre-Austronesian inhabitants during that period were mostly hunters and gatherers, who used stone axes and shell adzes but did not use pottery [Bellwood, 2007]. Charred materials found in the pre-neolithic layer [Simanjuntak and Asikin, 2004] imply that the inhabitants already used fire as a tool by then, but likely not so intense as in the swidden cultivation later during the Neolithic period.

Therefore, the transition from the pre-neolithic period to the Neolithic period was an expansion of swidden cultivation by the Austronesian-speaking people, while pre-Austronesian hunters and gatherers survived in ever-diminishing numbers [Bell-

wood, 2007]. The rise in levoglucosan accumulation rates around 4 ka based on our sediment core coincides with such a transition, which may be induced by the burning practices related with early swidden cultivation. The regional vegetation based on our leaf wax $\delta^{13}$C record did not respond until 3 ka, probably because swidden cultivation was characterized of relatively small spatial scale during the early settlement, which did not substantially change the vegetation cover, especially regarding C3 vs. C4 plant types.

Human population growth and intensification of agricultural practices in East Java around 2.6 ka were indicated by an archaeological record with high temporal resolution at Song Gupuh: a signifidant increase in pottery fragments as well as a progressive loss of faunal species [Morwood et al., 2008]. Intensified human activities during that period likely induced the vegetation cover (Fig. 5.3a) and the fire regime change with an increasing occurrence of high intensity fires at that time (Fig. 5.3h). The abrupt increase in high intensity fire occurrence around 0.5 ka was synchronous with the civilization of the Majapahit Kingdom in East Java around the 14th century [Bellwood, 2007]. Islamic influence and the European colonization afterwards likely contributed to the consistently high occurrence of intense fires reconstructed from the shallowest (most recent) part of the sediment core (Fig. 5.3h).

### 5.5.6 Hydro-climatic vs. anthropogenic impact on land cover

The close correlation between the riverine detrital fluxes in our sediment core and the regional annual rainfall amounts based on Liang Luar $\delta^{18}$O suggests a primary hydroclimatic impact on the East Javanese landscape throughout the past 5,000 years. In the meanwhile, the prehistoric human society of East Java potentially modified the regional vegetation by swidden cultivation using fire as a tool, which further induced soil erosion and enhanced riverine detrital fluxes. Such a human impact became stepwise profound reflected by the change in fire regime: the early settlement and expansion of Austronesian-speaking people around 4 ka were synchronous with a rise in low intensity fire occurrence but without a response of the leaf wax $\delta^{13}$C record; the intensification of human activities around 2.6 ka occurred with more frequent high intensity fires and an expansion of C4 vegetation; further development in human societies since 0.5 ka was concurrent with a fire regime dominated by frequent high intensity fires.

Although the joint increase in Palmae Arenga type pollen, representation of herbs and micro-charcoal accumulation rate after 3.8 ka based on our sediment core can be interpreted as human distribution [van der Kaars and van den Bergh, 2004; Poliakova et al., 2017], the hydro-climate potentially also played a role. The period around 2 ka, as an example, was characterized by a peak in C4 vegetation cover, high occurrence of both low and high intensity fires, yet the highest riverine detrital flux and a peak in rainfall intensity ever since 5 ka (Fig. 5.3a, c, e, h, i). The ENSO-IOD variability might cause such a distinct period reconstructed by GeoB10053-7.

A suite of records based on different proxies from eastern tropical Pacific sites indicate a high frequency and magnitude of El Niño events around 2 ka [Moy et al., 2002; Conroy et al., 2008; Thompson et al., 2017]. El Niño events are known to induce a

decrease in precipitation in the western tropical Pacific, such a drying impact occurs mostly in the dry season of the region but is not significant and spatially coherent in the wet season [As-syakur et al., 2014; Supari et al., 2018]. Instead, El Niño events cause a positive rainfall anomaly over the large islands of the Maritime Continent (including Java, Sumatra and Papua New Guinea) during the wet season [Rauniyar and Walsh, 2013]. Thus, higher frequency and magnitude of El Niño events around 2 ka could enhance the rainfall seasonality by making the dry season drier but the wet season wetter in East Java.

The estimates of sea surface temperature anomalies based on fossil coral Sr/Ca at the Mentawai Islands (location shown in 5.1b) around 2 ka yield -0.9 ± 0.6 °C, which are generally cooler and with greater variability than the present-day coral SST estimates (0.1± 0.3 °C, based on modern coral samples) [Abram et al., 2009]. This indicates more frequent positive IOD events or enhanced IOD variability during that period, since positive IOD upwelling events produce negative sea surface temperature anomalies at the Mentawai Islands [Abram et al., 2007]. The impact of such an IOD pattern on past precipitation in East Java around 2 ka was likely significant during the dry season (by making it drier) but minor during the wet season, since positive IOD events are seasonally phase locked with the dry season of Java [As-syakur et al., 2014].

Therefore, high frequency and/or magnitude of El Niño events and positive IOD events around 2 ka could cause a drier dry season, which favored deforestation and high occurrence of both low and high intensity fires. In the meanwhile, El Niño events during that period could enhance the wet season rainfall, which is recorded in the leaf wax $\delta$D values and the proxy for riverine detrital flux in GeoB10053-7. However, Steinke et al. [2014] found no statistical correlation between the high-resolution Ti/Ca record from the sediment core GeoB10065-7 and the ENSO records [Moy et al., 2002; Conroy et al., 2008], suggesting a minor control of ENSO on riverine detrital supply and the AISM variability. Instead, a grand minimum in solar activity around 2.8 ka was proposed to cause an enhanced riverine detrital flux and rainfall based on the statistically significant correlation between the Ti/Ca record and the sunspot number record [Steinke et al., 2014].

## 5.6 Conclusions

In this study, we use multi-proxies based on a sediment core south off East Java to discuss the land cover-climate-human interactions in East Java over the past 5,000 years. The accumulation rate of the lithogenic particles reflects the riverine detrital flux to the core site, which shows an increase starting around 3.8 ka, highest values between 2.8 ka and 1.8 ka, before a decrease from 2 ka to 1.6 ka. The highest fluxes between 2.8 ka and 1.8 ka occurred with a gradual increase in both C4 vegetation and high intensity fire occurrence.

Increases in riverine detrital fluxes co-varied with higher annual rainfall amount of the region through the record, suggest a primary hydro-climatic impact on the East Javanese fluvial system throughout the past 5,000 years.

The prehistoric human society in East Java potentially modified the regional vegetation by swidden cultivation using fire as a tool, which further induced soil erosion. The changes in fire regime, i.e. low intensity fire occurrence around 4 ka, a shift from low to high intensity fires around 2.6 and the dominance of frequent high intensity fires since 0.5 ka, were concurrent with the stepwise development in human society.

# Acknowledgements

This work was supported by the German Ministry of Education and Research (BMBF) grants 03G0184A (PABESIA), 03G0864F (CAHOL) and the Cluster of Excellence 'The Ocean Floor – Earth's Uncharted Interface' in Bremen. YR is funded by CSC - the China Scholarship Council and supported by GLOMAR – Bremen International Graduate School for Marine Sciences. SvdK was funded by the Deutsche Forschungsgemeinschaft (DFG) grant BE2116/10-1. SS and ECH are supported by the Netherlands Earth System Science Center (NESSC) funded by the Dutch Ministry for Education and Science. We thank Ralph Kreutz (MARUM), Denise Dorhout (NIOZ) and Monique Verweij (NIOZ) for laboratory support.

# Chapter 6

# Systhesis and Outlook

This thesis applied a multi-proxy methodology (see Chapter 2) to a sediment core collected off the southern shore of East Java covering the past 22,000 years. The main conclusions of the thesis are summarized below each Scientific question listed in Section 1.5. Perspectives of future work are discussed.

- Did a savannah vegetation expansion occur in East Java during the Last Glacial? Did the vegetation in lowland and highland ecosystems evolve differently?

Synthesis: In Chapter 3, by comparing the $\delta^{13}C$ records based on multiple leaf wax *n*-alkane homologues with the pollen records, we find that *n*-C29 alkane mainly reflects East Javanese lowland (montane) rainforest during the Holocene (LGM), while *n*-C31 and *n*-C33 alkanes predominantly reflect lowland vegetation of East Java through the record. A concentration-weighted mixing model supports the assumption that different leaf wax *n*-alkane homologues predominantly reflect distinct ecosystems. During the LGM, a savannah expansion occurred in lowland East Java, while the canopy structure of East Javanese montane rainforest remained closed.

Outlook: This study shows the great potential of multi-homologue leaf wax isotope analyses in settings with mixed vegetation types. In accordance with studies that propose to use *n*-C29 alkane as an indicator for C3 vegetation and *n*-C33 alkane as a C4 plant biomarker Diefendorf and Freimuth [2017]; Garcin et al. [2014], future paleo-studies may use this method to disentangle changes in different ecosystems based on one climate archive.

Comparison with the pollen data and sedimentological indices (such as grain size distribution and the lithogenic/$CaCO_3$ ratio) is important to constrain the source of leaf wax lipids, which is a prerequisite for further discussions. The complex source regions (including the exposed Sunda Shelf and Sahul Shelf as additional ones during periods with low sea levels) and transport pathways (fluvial and aeolian) call for a multi-proxy methodology when conducting future paleo-studies in the Maritime Continent.

A concentration-weighted mixing model was conducted in Chapter 3 to assess the

impact of C3 versus C4 vegetation shift on the $\delta^{13}$C values of the different *n*-alkane homologues. This model is based on a tropical compilation of existing literature (e.g. Fig. 2.1) due to the limited vegetation data from the Maritime Continent. The large ranges of *n*-alkane contents in plant types (Fig. 2.1) result from the compilation of data from various ecosystems [e.g. Diefendorf and Freimuth, 2017], and do not reflect the actual plant types within specific catchments. Thus modern ecosystem-scale studies in the Maritime Continent based on plant and soil samples [e.g. Wu et al., 2017, in tropical South America] will serve as the foundation for paleo-studies. Moreover, modern catchment-scale studies based on soil samples, river samples and surface sediments [e.g. Herrmann et al., 2017, in South Africa] will improve the understanding of source-to-sink processes in the Maritime Continent.

- Did the 'amount effect' remain the dominant control on the rainfall $\delta$D values in East Java during the LGM? How did the past rainfall (seasonality) in such a monsoonal region of the Maritime Continent evolve and respond to various forcings since the LGM?

Synthesis: In Chapter 3, the multi-homologue methodology enables an evaluation of the existing scenarios on the LGM hydro-climate in the Maritime Continent. We propose a dominant control of the 'amount effect' through the record, and that the leaf wax $\delta$D mostly reflects the rainfall intensity during the wet season. The variation in $\delta D_{n\text{-}29}$ through the record is small; increased contribution from montane rainforest caused a slight D-depletion during the LGM. In contrast, the significant decrease of $\delta D_{n\text{-}31}$ and $\delta D_{n\text{-}33}$ values during the LGM implies a wet season with enhanced rainfall intensity in the lowlands compared to the Holocene. Although we find no glacial-interglacial change in integrated rainfall, strongly enhanced lowland rainfall seasonality is detected for East Java during the LGM. This enhanced seasonality during the LGM is supported by the simulations of multiple climate models; the phenomenon was of a relatively local spatial scale between the two exposed shelves (Sunda Shelf and Sahul Shelf)[Yan et al., 2018].

Outlook: Rainfall changes in monsoon regions of the Earth are related with changes in seasonality, e.g. the length of the rainy season and the rainfall intensity [Mohtadi et al., 2016]. This study supports that the paired analyses of leaf wax $\delta^{13}$C and $\delta$D are a promising approach to distinguish past wet season length from wet season intensity [Mohtadi et al., 2016]. Their future applications in monsoon regions are expected. The source region of leaf wax lipids and the moisture source of the precipitation, however, need to be constrained before the actual applications.

Knowledge about hydrogen isotope fractionations from precipitation to leaf wax lipids is especially limited for C4 plants in the tropics (Table 2.1). Modern studies based on tropical C4 plants will provide important information for the application of leaf wax $\delta$D in paleo-studies.

Climate models are powerful tools to understand the climatic processes, such as differentiating the dynamic vs. thermodynamic effects on monsoonal rainfall [Mohtadi et al., 2016]. Climate models are essential in deciphering the underlying mechanisms of the climatic patterns reflected by proxy results. Thus, integrating both proxy reconstructions and model simulations is necessary to a better understanding of the

various forcings on the paleo-climate in the Maritime Continent.

- How did the fire regime, i.e. frequency and intensity of fires, change in East Java since the Last Glacial?
- How did fire interact with vegetation and climate?

Synthesis: In Chapter 4, the micro-charcoal accumulation rate is used to reconstruct general fire occurrence in East Java, while the ratio of levoglucosan vs. PAHs indicates relative fire intensity. The regional fire occurrence was highest during the LGM and showed two additional maxima during the Bølling-Allerød and the late Holocene, while the fire level was low during the Heinrich Stadial 1, the Younger Dryas and the early Holocene. Fire intensity was high during the LGM but remained low since 18 ka.

Further comparison shows that fires of different frequencies and intensities were capable of either stabilizing or destabilizing savannah/rainforest vegetation. The LGM was characterized by high rainfall seasonality, high occurrence of intense fires and savannah-dominated vegetation, while the early Holocene was characterized by low rainfall seasonality, low occurrence of fires of low intensity and rainforest-dominated vegetation. The deglaciation and the late Holocene were transition periods between the two stable states. A fire regime of low frequency and low intensity during the Heinrich Stadial 1 and the Younger Dryas coincided with major transitions from savannah towards rainforest, while a reverse change in regional vegetation during the Bølling-Allerød was concurrent with a fire regime of low intensity but high frequency. Hydro-climatic changes in rainfall seasonality have the potential to facilitate large-scale vegetation changes mediated by changes in fire regime.

Outlook: The combination of charcoal and molecular markers in this study shows great potential for detailed fire regime reconstructions when they share the same fire source. Further applications are expected in paleo-fire studies.

The reconstructed fire history of East Java in the thesis do not have a peatland origin. The lowland peatlands in the Maritime Continent are the the largest peatland area in the tropics [Dommain et al., 2011]. The peatland fires turn the terrestrial carbon reservoir of peatlands into a significant source of atmospheric carbon [Dommain et al., 2011]. Further studies integrating peatland formation, peat fires and climate variability in the past are particularly important in terms of the global carbon cycle.

- How did prehistoric human activities influence land cover and fluvial erosion in East Java over the past 5,000 years?

Synthesis: In Chapter 5, we find that the prehistoric human society in East Java potentially modified the regional vegetation by swidden cultivation using fire as a tool, which further induced soil erosion. The changes in fire regime, i.e. low intensity fire occurrence around 4 ka, a shift from low to high intensity fires around 2.6 and the dominance of frequent high intensity fires since 0.5 ka, were concurrent with the stepwise development in human society. In the meanwhile, hydro-climate is proposed to have a primary impact on the East Javanese fluvial system throughout the past 5,000 years.

Outlook: It remains challenging to determine the timing, intensity and distribution of human impact, and to disentangle natural variability and anthropogenic disturbance recorded in integrative archives such as sedimentary deposits [Dubois et al., 2018]. To tackle this question, either a careful selection of sites or a selection of proxies serves as a potential approach [Dubois et al., 2018, and references therein]. In the former case, pairs of non-human-impacted and human-impacted sites under similar climate conditions can be compared, although such straightforward pre-conditions are often not easy to be met [e.g. Moorhouse et al., 2014]. Another way is to combine sites covering a certain spatial scale. For example, a review of fluvial sedimentology in central Europe shows that sediment fluxes in small catchments are highly sensitive to local human land use changes while river sediments integrate both regional land use and climate variability [Dotterweich, 2008]. In the latter case, proxies either reflect environmental changes that can be linked to human disturbation (such as biomass burning, vegetation shift, soil erosion and water quality degradation) or are specific to certain human activities (such as cultivation and pastoralism) [Dubois and Jacob, 2016, and references therein]. Macrofossils from cereals, novel molecular biomarkers indicative of cultivation and/or grazing, or new ancient DNA techniques, may offer new perspectives in this regard [e.g. Slatkin and Racimo, 2016; Dubois and Jacob, 2016; Deng et al., 2020].

# Bibliography


Abram, N. J., Gagan, M. K., Liu, Z., Hantoro, W. S., McCulloch, M. T., and Suwargadi, B. W. (2007). Seasonal characteristics of the indian ocean dipole during the holocene epoch. *Nature*, 445(7125):299–302.

Abram, N. J., Hargreaves, J. A., Wright, N. M., Thirumalai, K., Ummenhofer, C. C., and England, M. H. (2020). Palaeoclimate perspectives on the Indian Ocean Dipole. *Quaternary Science Reviews*, 237:106302.

Abram, N. J., McGregor, H. V., Gagan, M. K., Hantoro, W. S., and Suwargadi, B. W. (2009). Oscillations in the southern extent of the Indo-Pacific Warm Pool during the mid-Holocene. *Quaternary Science Reviews*, 28(25-26):2794–2803.

Aldrian, E., Chen, C.-T. A., Adi, S., Prihartanto, Sudiana, N., and Nugroho, S. P. (2008). Spatial and seasonal dynamics of riverine carbon fluxes of the Brantas catchment in East Java. *Journal of Geophysical Research*, 113(G3):G03029.

Alkama, R. and Cescatti, A. (2016). Climate change: Biophysical climate impacts of recent changes in global forest cover. *Science*, 351(6273):600–604.

Archibald, S., Lehmann, C. E. R., Belcher, C. M., Bond, W. J., Bradstock, R. A., Daniau, A.-L., Dexter, K. G., Forrestel, E. J., Greve, M., He, T., Higgins, S. I., Hoffmann, W. A., Lamont, B. B., McGlinn, D. J., Moncrieff, G. R., Osborne, C. P., Pausas, J. G., Price, O., Ripley, B. S., Rogers, B. M., Schwilk, D. W., Simon, M. F., Turetsky, M. R., Van der Werf, G. R., and Zanne, A. E. (2018). Biological and geophysical feedbacks with fire in the Earth system. *Environmental Research Letters*, 13(3):033003.

Archibald, S., Lehmann, C. E. R., Gomez-Dans, J. L., and Bradstock, R. A. (2013). Defining pyromes and global syndromes of fire regimes. *Proceedings of the National Academy of Sciences*, 110(16):6442–6447.

Argiriadis, E., Battistel, D., McWethy, D. B., Vecchiato, M., Kirchgeorg, T., Kehrwald, N. M., Whitlock, C., Wilmshurst, J. M., and Barbante, C. (2018). Lake sediment fecal and biomass burning biomarkers provide direct evidence for prehistoric human-lit fires in New Zealand. *Scientific Reports*, 8(1).

As-syakur, A. R., Adnyana, I. W. S., Mahendra, M. S., Arthana, I. W., Merit, I. N., Kasa, I. W., Ekayanti, N. W., Nuarsa, I. W., and Sunarta, I. N. (2014). Observation of spatial patterns on the rainfall response to ENSO and IOD over Indonesia

using TRMM Multisatellite Precipitation Analysis (TMPA). *International Journal of Climatology*, 34(15):3825–3839.

Badewien, T., Vogts, A., and Rullkötter, J. (2015). *n*-alkane distribution and carbon stable isotope composition in leaf waxes of C3 and C4 plants from Angola. *Organic Geochemistry*, 89-90:71–79.

Battistel, D., Argiriadis, E., Kehrwald, N., Spigariol, M., Russell, J. M., and Barbante, C. (2017). Fire and human record at Lake Victoria, East Africa, during the Early Iron Age: Did humans or climate cause massive ecosystem changes? *The Holocene*, 27(7):997–1007.

Beaufort, L., de Garidel-Thoron, T., Linsley, B., Oppo, D., and Buchet, N. (2003). Biomass burning and oceanic primary production estimates in the Sulu Sea area over the last 380 kyr and the East Asian monsoon dynamics. *Marine Geology*, 201(1-3):53–65.

Belgaman, H. A., Ichiyanagi, K., Suwarman, R., Tanoue, M., Aldrian, E., Utami, A. I., and Kusumaningtyas, S. D. (2017). Characteristics of seasonal precipitation isotope variability in Indonesia. *Hydrological Research Letters*, 11(2):92–98.

Bellwood, P. (2007). *Prehistory of the Indo-Malaysian Archipelago: revised edition*. ANU Press.

Bezabih, M., Pellikaan, W. F., Tolera, A., and Hendriks, W. H. (2011). Evaluation of *n*-alkanes and their carbon isotope enrichments ($\delta^{13}$C) as diet composition markers. *animal*, 5(01):57–66.

Bhattarai, H., Saikawa, E., Wan, X., Zhu, H., Ram, K., Gao, S., Kang, S., Zhang, Q., Zhang, Y., Wu, G., Wang, X., Kawamura, K., Fu, P., and Cong, Z. (2019). Levoglucosan as a tracer of biomass burning: Recent progress and perspectives. *Atmospheric Research*, 220:20–33.

Bi, X., Sheng, G., Liu, X., Li, C., and Fu, J. (2005). Molecular and carbon and hydrogen isotopic composition of *n*-alkanes in plant leaf waxes. *Organic Geochemistry*, 36(10):1405–1417.

Bird, M. I., Summons, R. E., Gagan, M. K., Roksandic, Z., Dowling, L., Head, J., Keith Fifield, L., Cresswell, R. G., and Johnson, D. P. (1995). Terrestrial vegetation change inferred from *n*-alkane $\delta^{13}$C analysis in the marine environment. *Geochimica et Cosmochimica Acta*, 59(13):2853–2857.

Bond, W. J. (2008). What Limits Trees in C 4 Grasslands and Savannas? *Annual Review of Ecology, Evolution, and Systematics*, 39(1):641–659.

Bond, W. J. and Keeley, J. E. (2005). Fire as a global 'herbivore': The ecology and evolution of flammable ecosystems. *Trends in Ecology and Evolution*, 20(7):387–394.

Bond, W. J. and Midgley, G. F. (2000). A proposed $CO_2$-controlled mechanism of woody plant invasion in grasslands and savannas. *Global Change Biology*, 6(8):865–869.

Bowman, D. M. J. S., Balch, J. K., Artaxo, P., Bond, W. J., Carlson, J. M., Cochrane, M. A., D'Antonio, C. M., DeFries, R. S., Doyle, J. C., Harrison, S. P., Johnston, F. H., Keeley, J. E., Krawchuk, M. A., Kull, C. A., Marston, J. B., Moritz, M. A., Prentice, I. C., Roos, C. I., Scott, A. C., Swetnam, T. W., van der Werf, G. R., and Pyne, S. J. (2009). Fire in the Earth System. *Science*, 324(5926):481–484.

Box, E. O. (1995). Factors determining distributions of tree species and plant functional types. *Vegetatio*, 121(1-2):101–116.

Bray, E. and Evans, E. (1961). Distribution of *n*-paraffins as a clue to recognition of source beds. *Geochimica et Cosmochimica Acta*, 22(1):2–15.

Buchmann, N., Guehl, J.-M., Barigah, T. S., and Ehleringer, J. R. (1997). Interseasonal comparison of $CO_2$ concentrations, isotopic composition, and carbon dynamics in an Amazonian rainforest (French Guiana). *Oecologia*, 110(1):120–131.

Bush, R. T. and McInerney, F. A. (2013). Leaf wax *n*-alkane distributions in and across modern plants: Implications for paleoecology and chemotaxonomy. *Geochimica et Cosmochimica Acta*, 117:161–179.

Bush, R. T. and McInerney, F. A. (2015). Influence of temperature and C4 abundance on *n*-alkane chain length distributions across the central USA. *Organic Geochemistry*, 79:65–73.

Cai, W., Wu, L., Lengaigne, M., Li, T., McGregor, S., Kug, J.-S., Yu, J.-Y., Stuecker, M. F., Santoso, A., Li, X., Ham, Y.-G., Chikamoto, Y., Ng, B., McPhaden, M. J., Du, Y., Dommenget, D., Jia, F., Kajtar, J. B., Keenlyside, N., Lin, X., Luo, J.-J., Martín-Rey, M., Ruprich-Robert, Y., Wang, G., Xie, S.-P., Yang, Y., Kang, S. M., Choi, J.-Y., Gan, B., Kim, G.-I., Kim, C.-E., Kim, S., Kim, J.-H., and Chang, P. (2019). Pantropical climate interactions. *Science*, 363(6430):eaav4236.

Cai, W., Zheng, X.-T., Weller, E., Collins, M., Cowan, T., Lengaigne, M., Yu, W., and Yamagata, T. (2013). Projected response of the indian ocean dipole to greenhouse warming. *Nature geoscience*, 6(12):999–1007.

Carolin, S. A., Cobb, K. M., Adkins, J. F., Clark, B., Conroy, J. L., Lejau, S., Malang, J., and Tuen, A. A. (2013). Varied response of western Pacific hydrology to climate forcings over the last glacial period. *Science*, 340(6140):1564–1566.

Chiang, J. C. (2009). The Tropics in Paleoclimate. *Annual Review of Earth and Planetary Sciences*, 37(1):263–297.

Chikaraishi, Y. and Naraoka, H. (2003). Compound-specific $\delta$D-$\delta^{13}$C analyses of *n*-alkanes extracted from terrestrial and aquatic plants. *Phytochemistry*, 63(3):361–371.

Chikaraishi, Y., Naraoka, H., and Poulson, S. R. (2004). Hydrogen and carbon isotopic fractionations of lipid biosynthesis among terrestrial (C3, C4 and CAM) and aquatic plants. *Phytochemistry*, 65(10):1369–1381.

Christie, J. W. (2007). Water and rice in early java and. In *A World of Water*, pages 235–258. Brill.

Collatz, G. J., Berry, J. A., and Clark, J. S. (1998). Effects of climate and atmospheric $CO_2$ partial pressure on the global distribution of C4 grasses: present, past, and future. *Oecologia*, 114(4):441–454.

Collins, J. A., Schefuß, E., Heslop, D., Mulitza, S., Prange, M., Zabel, M., Tjallingii, R., Dokken, T. M., Huang, E., MacKensen, A., Schulz, M., Tian, J., Zarriess, M., and Wefer, G. (2011). Interhemispheric symmetry of the tropical African rainbelt over the past 23,000 years. *Nature Geoscience*, 4(1):42–45.

Collins, J. A., Schefuß, E., Mulitza, S., Prange, M., Werner, M., Tharammal, T., Paul, A., and Wefer, G. (2013). Estimating the hydrogen isotopic composition of past precipitation using leaf-waxes from western Africa. *Quaternary Science Reviews*, 65:88–101.

Collins, N. M., Sayer, J. A., and Whitmore, T. C., editors (1991). *The Conservation Atlas of Tropical Forests Asia and the Pacific*. Palgrave Macmillan UK, London.

Conroy, J. L., Overpeck, J. T., Cole, J. E., Shanahan, T. M., and Steinitz-Kannan, M. (2008). Holocene changes in eastern tropical Pacific climate inferred from a Galápagos lake sediment record. *Quaternary Science Reviews*, 27(11-12):1166–1180.

Craig, H. (1961). Isotopic variations in meteoric waters. *Science*, 133(3465):1702–1703.

Daniau, A. L., Bartlein, P. J., Harrison, S. P., Prentice, I. C., Brewer, S., Friedlingstein, P., Harrison-Prentice, T. I., Inoue, J., Izumi, K., Marlon, J. R., Mooney, S., Power, M. J., Stevenson, J., Tinner, W., Andrič, M., Atanassova, J., Behling, H., Black, M., Blarquez, O., Brown, K. J., Carcaillet, C., Colhoun, E. A., Colombaroli, D., Davis, B. A., D'Costa, D., Dodson, J., Dupont, L., Eshetu, Z., Gavin, D. G., Genries, A., Haberle, S., Hallett, D. J., Hope, G., Horn, S. P., Kassa, T. G., Katamura, F., Kennedy, L. M., Kershaw, P., Krivonogov, S., Long, C., Magri, D., Marinova, E., McKenzie, G. M., Moreno, P. I., Moss, P., Neumann, F. H., Norstrm, E., Paitre, C., Rius, D., Roberts, N., Robinson, G. S., Sasaki, N., Scott, L., Takahara, H., Terwilliger, V., Thevenon, F., Turner, R., Valsecchi, V. G., Vannière, B., Walsh, M., Williams, N., and Zhang, Y. (2012). Predictability of biomass burning in response to climate changes. *Global Biogeochemical Cycles*, 26(4):1–12.

Daniau, A.-L., Desprat, S., Aleman, J. C., Bremond, L., Davis, B., Fletcher, W., Marlon, J. R., Marquer, L., Montade, V., Morales-Molino, C., Naughton, F., Rius, D., and Urrego, D. H. (2019). Terrestrial plant microfossils in palaeoenvironmental studies, pollen, microcharcoal and phytolith. Towards a comprehensive understanding of vegetation, fire and climate changes over the past one million years. *Revue de Micropaléontologie*, 63:1–35.

Daniau, A. L., Harrison, S. P., and Bartlein, P. J. (2010). Fire regimes during the Last Glacial. *Quaternary Science Reviews*, 29(21-22):2918–2930.

Dansgaard, W. (1964). Stable isotopes in precipitation. *Tellus*, 16(4):436–468.

De Deckker, P. (2016). The Indo-Pacific Warm Pool: critical to world oceanography and world climate. *Geoscience Letters*, 3(1).

Deng, Z., chun Hung, H., Carson, M. T., Oktaviana, A. A., Hakim, B., and Simanjuntak, T. (2020). Validating earliest rice farming in the Indonesian Archipelago. *Scientific Reports*, 10(1):1–9.

Denniston, R. F., Wyrwoll, K.-H., Polyak, V. J., Brown, J. R., Asmerom, Y., Wanamaker, A. D., LaPointe, Z., Ellerbroek, R., Barthelmes, M., Cleary, D., Cugley, J., Woods, D., and Humphreys, W. F. (2013). A Stalagmite record of Holocene Indonesian–Australian summer monsoon variability from the Australian tropics. *Quaternary Science Reviews*, 78:155–168.

Diefendorf, A. F. and Freimuth, E. J. (2017). Extracting the most from terrestrial plant-derived n-alkyl lipids and their carbon isotopes from the sedimentary record: A review. *Organic Geochemistry*, 103:1–21.

Diefendorf, A. F., Mueller, K. E., Wing, S. L., Koch, P. L., and Freeman, K. H. (2010). Global patterns in leaf 13C discrimination and implications for studies of past and future climate. *Proceedings of the National Academy of Sciences*, 107(13):5738–5743.

Dietze, E., Brykała, D., Schreuder, L. T., Jażdżewski, K., Blarquez, O., Brauer, A., Dietze, M., Obremska, M., Ott, F., Pieńczewska, A., Schouten, S., Hopmans, E. C., and Słowiński, M. (2019). Human-induced fire regime shifts during 19th century industrialization: A robust fire regime reconstruction using northern Polish lake sediments. *PLOS ONE*, 14(9):e0222011.

DiNezio, P. N., Timmermann, A., Tierney, J. E., Jin, F. F., Otto-Bliesner, B., Rosenbloom, N., Mapes, B., Neale, R., Ivanovic, R. F., and Montenegro, A. (2016). The climate response of the Indo-Pacific warm pool to glacial sea level. *Paleoceanography*, 31(6):866–894.

Dommain, R., Couwenberg, J., and Joosten, H. (2011). Development and carbon sequestration of tropical peat domes in south-east Asia: Links to post-glacial sea-level changes and Holocene climate variability. *Quaternary Science Reviews*, 30(7-8):999–1010.

Dotterweich, M. (2008). The history of soil erosion and fluvial deposits in small catchments of central Europe: Deciphering the long-term interaction between humans and the environment - A review. *Geomorphology*, 101(1-2):192–208.

Duan, Y. and He, J. (2011). Distribution and isotopic composition of *n*-alkanes from grass, reed and tree leaves along a latitudinal gradient in China. *GEOCHEMICAL JOURNAL*, 45(3):199–207.

Dubois, N. and Jacob, J. (2016). Molecular Biomarkers of Anthropic Impacts in Natural Archives: A Review. *Frontiers in Ecology and Evolution*, 4:92.

Dubois, N., Oppo, D. W., Galy, V. V., Mohtadi, M., Van Der Kaars, S., Tierney, J. E., Rosenthal, Y., Eglinton, T. I., Lückge, A., and Linsley, B. K. (2014). Indonesian vegetation response to changes in rainfall seasonality over the past 25,000 years. *Nature Geoscience*, 7(7):513–517.

Dubois, N., Saulnier-Talbot, É., Mills, K., Gell, P., Battarbee, R., Bennion, H., Chawchai, S., Dong, X., Francus, P., Flower, R., Gomes, D. F., Gregory-Eaves, I., Humane, S., Kattel, G., Jenny, J., Langdon, P., Massaferro, J., Mcgowan, S., Mikomägi, A., Thi, N., Ngoc, M., Ratnayake, A. S., Reid, M., Rose, N., Saros, J., Schillereff, D., Tolotti, M., and Valero-Garcés, B. (2018). First human impacts and responses of aquatic systems: A review of palaeolimnological records from around the world. *The Anthropocene Review*, 5(1):28–68.

Dupont, L. M. and Schefuß, E. (2018). The roles of fire in Holocene ecosystem changes of West Africa. *Earth and Planetary Science Letters*, 481:255–263.

Eglinton, G. and Hamilton, R. J. (1967). Leaf epicuticular waxes. *Science*, 156(3780):1322–1335.

Eglinton, T. I. and Eglinton, G. (2008). Molecular proxies for paleoclimatology. *Earth and Planetary Science Letters*, 275(1-2):1–16.

Ehleringer, J. R. (2005). The Influence of Atmospheric $CO_2$, Temperature, and Water on the Abundance of C3/C4 Taxa. In *A History of Atmospheric CO2 and Its Effects on Plants, Animals, and Ecosystems*, pages 214–231. Springer-Verlag, New York.

Ehleringer, J. R., Cerling, T. E., and Helliker, B. R. (1997). C4 photosynthesis, atmospheric $CO_2$, and climate. *Oecologia*, 112(3):285–299.

Ellis, E. C., Kaplan, J. O., Fuller, D. Q., Vavrus, S., Goldewijk, K. K., and Verburg, P. H. (2013). Used planet: A global history. *Proceedings of the National Academy of Sciences*, 110(20):7978–7985.

Feakins, S. J., Bentley, L. P., Salinas, N., Shenkin, A., Blonder, B., Goldsmith, G. R., Ponton, C., Arvin, L. J., Wu, M. S., Peters, T., West, A. J., Martin, R. E., Enquist, B. J., Asner, G. P., and Malhi, Y. (2016). Plant leaf wax biomarkers capture gradients in hydrogen isotopes of precipitation from the Andes and Amazon. *Geochimica et Cosmochimica Acta*, 182:155–172.

Field, R. D. and Shen, S. S. P. (2008). Predictability of carbon emissions from biomass burning in Indonesia from 1997 to 2006. *Journal of Geophysical Research: Biogeosciences*, 113(G4).

Field, R. D., Van Der Werf, G. R., and Shen, S. S. (2009). Human amplification of drought-induced biomass burning in Indonesia since 1960. *Nature Geoscience*, 2(3):185–188.

Fornace, K. L., Whitney, B. S., Galy, V., Hughen, K. A., and Mayle, F. E. (2016). Late Quaternary environmental change in the interior South American tropics: New insight from leaf wax stable isotopes. *Earth and Planetary Science Letters*, 438:75–85.

Garcin, Y., Schefuß, E., Schwab, V. F., Garreta, V., Gleixner, G., Vincens, A., Todou, G., Séné, O., Onana, J. M., Achoundong, G., and Sachse, D. (2014). Reconstructing C3 and C4 vegetation cover using *n*-alkane carbon isotope ratios in recent lake sediments from Cameroon, Western Central Africa. *Geochimica et Cosmochimica Acta*, 142:482–500.

Garcin, Y., Schwab, V. F., Gleixner, G., Kahmen, A., Todou, G., Séné, O., Onana, J.-M., Achoundong, G., and Sachse, D. (2012). Hydrogen isotope ratios of lacustrine sedimentary *n*-alkanes as proxies of tropical african hydrology: insights from a calibration transect across cameroon. *Geochimica et Cosmochimica Acta*, 79:106–126.

Gat, J. R. (1996). OXYGEN AND HYDROGEN ISOTOPES IN THE HYDROLOGIC CYCLE. *Annual Review of Earth and Planetary Sciences*, 24(1):225–262.

Giglio, L., Schroeder, W., and Justice, C. O. (2016). The collection 6 MODIS active fire detection algorithm and fire products. *Remote Sensing of Environment*, 178:31–41.

Gill, A. M. (1975). Fire and the Australian flora: a review. *Australian forestry*, 38(1):4–25.

Goldsmith, G. R., Matzke, N. J., and Dawson, T. E. (2013). The incidence and implications of clouds for cloud forest plant water relations. *Ecology Letters*, 16(3):307–314.

Gonfiantini, R., Roche, M.-A., Olivry, J.-C., Fontes, J.-C., and Zuppi, G. M. (2001). The altitude effect on the isotopic composition of tropical rains. *Chemical Geology*, 181(1-4):147–167.

Govender, N., Trollope, W. S., and Van Wilgen, B. W. (2006). The effect of fire season, fire frequency, rainfall and management on fire intensity in savanna vegetation in South Africa. *Journal of Applied Ecology*, 43(4):748–758.

Griffiths, M. L., Drysdale, R. N., Gagan, M. K., Zhao, J. X., Ayliffe, L. K., Hellstrom, J. C., Hantoro, W. S., Frisia, S., Feng, Y. X., Cartwright, I., Pierre,

E. S., Fischer, M. J., and Suwargadi, B. W. (2009). Increasing Australian-Indonesian monsoon rainfall linked to early Holocene sea-level rise. *Nature Geoscience*, 2(9):636–639.

Hameed, S. N., Jin, D., and Thilakan, V. (2018). A model for super El Niños. *Nature Communications*, 9(1):2528.

Hamilton, R., Stevenson, J., Li, B., and Bijaksana, S. (2019). A 16,000-year record of climate, vegetation and fire from Wallacean lowland tropical forests. *Quaternary Science Reviews*, 224:105929.

Han, Y., Peteet, D., Arimoto, R., Cao, J., An, Z., Sritrairat, S., and Yan, B. (2016). Climate and Fuel Controls on North American Paleofires: Smoldering to Flaming in the Late-glacial-Holocene Transition. *Scientific Reports*, 6(1):20719.

Hansen, M. C., Potapov, P. V., Moore, R., Hancher, M., Turubanova, S. A., Tyukavina, A., Thau, D., Stehman, S. V., Goetz, S. J., Loveland, T. R., Kommareddy, A., Egorov, A., Chini, L., Justice, C. O., and Townshend, J. R. (2013). High-resolution global maps of 21st-century forest cover change. *Science*, 342(6160):850–853.

Hantson, S., Scheffer, M., Pueyo, S., Xu, C., Lasslop, G., Van Nes, E. H., Holmgren, M., and Mendelsohn, J. (2017). Rare, Intense, Big fires dominate the global tropics under drier conditions. *Scientific Reports*, 7(1):7–11.

Hartnett, H. E., Keil, R. G., Hedges, J. I., and Devol, A. H. (1998). Influence of oxygen exposure time on organic carbon preservation in continental margin sediments. *Nature*, 391(6667):572–574.

Hebbeln, D. and cruise participants (2006). Report and preliminary results of RV Sonne Cruise SO-184, Pabesia, Durban (South Africa) - Cilacap (Indonesia) - Darwin (Australia), July 8th - September 13th, 2005.

Hedges, J. I., Eglinton, G., Hatcher, P. G., Kirchman, D. L., Arnosti, C., Derenne, S., Evershed, R. P., Kögel-Knabner, I., De Leeuw, J. W., Littke, R., Michaelis, W., and Rullkötter, J. (2000). The molecularly-uncharacterized component of nonliving organic matter in natural environments. *Organic Geochemistry*, 31(10):945–958.

Herrmann, N., Boom, A., Carr, A. S., Chase, B. M., West, A. G., Zabel, M., and Schefuß, E. (2017). Hydrogen isotope fractionation of leaf wax *n*-alkanes in southern african soils. *Organic Geochemistry*, 109:1–13.

Hirota, M., Holmgren, M., Van Nes, E. H., and Scheffer, M. (2011). Global resilience of tropical forest and savanna to critical transitions. *Science (New York, N.Y.)*, 334(6053):232–5.

Hoetzel, S., Dupont, L., Schefuß, E., Rommerskirchen, F., and Wefer, G. (2013). The role of fire in Miocene to Pliocene C 4 grassland and ecosystem evolution. *Nature Geoscience*.

Hoffmann, W. A., Geiger, E. L., Gotsch, S. G., Rossatto, D. R., Silva, L. C., Lau, O. L., Haridasan, M., and Franco, A. C. (2012a). Ecological thresholds at the savanna-forest boundary: How plant traits, resources and fire govern the distribution of tropical biomes. *Ecology Letters*, 15(7):759–768.

Hoffmann, W. A., Jaconis, S. Y., Mckinley, K. L., Geiger, E. L., Gotsch, S. G., and Franco, A. C. (2012b). Fuels or microclimate? Understanding the drivers of fire feedbacks at savanna-forest boundaries. *Austral Ecology*, 37(6):634–643.

Hsieh, Y.-P., Bugna, G., and Robertson, K. (2018). Thermochemical Properties of PM2.5 as Indicator of Combustion Phase of Fires. *Atmosphere*, 9(6):230.

Hunsinger, G. B., Mitra, S., Warrick, J. A., and Alexander, C. R. (2008). Oceanic loading of wildfire-derived organic compounds from a small mountainous river. *Journal of Geophysical Research: Biogeosciences*, 113(G2):n/a–n/a.

IPCC (2019). Climate Change and Land: an IPCC special report on climate change, desertification, land degradation, sustainable land management, food security, and greenhouse gas fluxes in terrestrial ecosystems [P.R. Shukla, J. Skea, E. Calvo Buendia, V. Masson-Delmotte, H.-O. Pörtner, D. C. Roberts, P. Zhai, R. Slade, S. Connors, R. van Diemen, M. Ferrat, E. Haughey, S. Luz, S. Neogi, M. Pathak, J. Petzold, J. Portugal Pereira, P. Vyas, E. Huntley, K. Kissick, M. Belkacemi, J. Malley, (eds.)]. In press. Technical report.

Jennerjahn, T. C., Ittekkot, V., Klöpper, S., Adi, S., Purwo Nugroho, S., Sudiana, N., Yusmal, A., Prihartanto, and Gaye-Haake, B. (2004). Biogeochemistry of a tropical river affected by human activities in its catchment: Brantas River estuary and coastal waters of Madura Strait, Java, Indonesia. *Estuarine, Coastal and Shelf Science*, 60(3):503–514.

Kalnay, E., Kanamitsu, M., Kistler, R., Collins, W., Deaven, D., Gandin, L., Iredell, M., Saha, S., White, G., Woollen, J., Zhu, Y., Leetmaa, A., Reynolds, R., Chelliah, M., Ebisuzaki, W., Higgins, W., Janowiak, J., Mo, K. C., Ropelewski, C., Wang, J., Jenne, R., Joseph, D., Kalnay, E., Kanamitsu, M., Kistler, R., Collins, W., Deaven, D., Gandin, L., Iredell, M., Saha, S., White, G., Woollen, J., Zhu, Y., Chelliah, M., Ebisuzaki, W., Higgins, W., Janowiak, J., Mo, K. C., Ropelewski, C., Wang, J., Leetmaa, A., Reynolds, R., Jenne, R., and Joseph, D. (1996). The NCEP/NCAR 40-Year Reanalysis Project. *Bulletin of the American Meteorological Society*, 77(3):437–471.

Keiluweit, M., Kleber, M., Sparrow, M. A., Simoneit, B. R. T., and Prahl, F. G. (2012). Solvent-Extractable Polycyclic Aromatic Hydrocarbons in Biochar: In fl uence of Pyrolysis Temperature and Feedstock. *Environmental Science & Technology*, 46:9333–9341.

Kershaw, A. P., van der Kaars, S., and Flenley, J. R. (2007). *The Quaternary history of far eastern rainforests*, pages 77–115. Springer Berlin Heidelberg, Berlin, Heidelberg.

Kolattukudy, P. (1967). Biosynthesis of paraffins in Brassica oleracea: Fatty acid elongation-decarboxylation as a plausible pathway. *Phytochemistry*, 6(7):963–975.

Konecky, B., Russell, J., and Bijaksana, S. (2016). Glacial aridity in central Indonesia coeval with intensified monsoon circulation. *Earth and Planetary Science Letters*, 437:15–24.

Konecky, B., Russell, J. M., Rodysill, J. R., Vuille, M., Bijaksana, S., and Huang, Y. (2013). Intensification of southwestern Indonesian rainfall over the past millennium. *Geophysical Research Letters*, 40(2):386–391.

Krull, E., Sachse, D., Mügler, I., Thiele, A., and Gleixner, G. (2006). Compound-specific $\delta^{13}$C and $\delta^{2}$H analyses of plant and soil organic matter: A preliminary assessment of the effects of vegetation change on ecosystem hydrology. *Soil Biology and Biochemistry*, 38(11):3211–3221.

Kuo, L.-J., Herbert, B. E., and Louchouarn, P. (2008). Can levoglucosan be used to characterize and quantify char/charcoal black carbon in environmental media? *Organic Geochemistry*, 39(10):1466–1478.

Kurita, N., Ichiyanagi, K., Matsumoto, J., Yamanaka, M. D., and Ohata, T. (2009). The relationship between the isotopic content of precipitation and the precipitation amount in tropical regions. *Journal of Geochemical Exploration*, 102(3):113–122.

Kwiatkowski, C., Prange, M., Varma, V., Steinke, S., Hebbeln, D., and Mohtadi, M. (2015). Holocene variations of thermocline conditions in the eastern tropical Indian Ocean. *Quaternary Science Reviews*, 114:33–42.

Labrière, N., Locatelli, B., Laumonier, Y., Freycon, V., and Bernoux, M. (2015). Soil erosion in the humid tropics: A systematic quantitative review. *Agriculture, Ecosystems & Environment*, 203:127–139.

Ladd, S. N. and Sachs, J. P. (2013). Positive correlation between salinity and *n*-alkane $\delta^{13}$C values in the mangrove Avicennia marina. *Organic Geochemistry*, 64:1–8.

Ladd, S. N. and Sachs, J. P. (2015). Influence of salinity on hydrogen isotope fractionation in Rhizophora mangroves from Micronesia. *Geochimica et Cosmochimica Acta*, 168:206–221.

Lehmann, C. E., Archibald, S. A., Hoffmann, W. A., and Bond, W. J. (2011). Deciphering the distribution of the savanna biome. *New Phytologist*, 191(1):197–209.

Lewis, S. C., Legrande, A. N., Kelley, M., and Schmidt, G. A. (2010). Water vapour source impacts on oxygen isotope variability in tropical precipitation during Heinrich events. *Climate of the Past*, 6(3):325–343.

Lima, A. L. C., Farrington, J. W., and Reddy, C. M. (2005). Combustion-derived polycyclic aromatic hydrocarbons in the environment - A review. *Environmental Forensics*, 6(2):109–131.

Liu, W. and Yang, H. (2008). Multiple controls for the variability of hydrogen isotopic compositions in higher plant *n*-alkanes from modern ecosystems. *Global Change Biology*, 14(9):2166–2177.

Locarnini, R. A., Mishonov, A. V., Antonov, J. I., Boyer, T. P., Garcia, H. E., Baranova, O. K., Zweng, M. M., Paver, C. R., Reagan, J. R., Johnson, D. R., et al. (2013). World ocean atlas 2013. volume 1, temperature.

Lohman, D. J., Bickford, D., and Sodhi, N. S. (2007). ENVIRONMENT: The Burning Issue. *Science*, 316(5823):376.

Lu, H., Zhu, L., and Zhu, N. (2009). Polycyclic aromatic hydrocarbon emission from straw burning and the influence of combustion parameters. *Atmospheric Environment*, 43(4):978–983.

Lüttge, U. (2004). Ecophysiology of Crassulacean Acid Metabolism (CAM). *Annals of Botany*, 93(6):629–652.

Maher, L. J. (1972). Nomograms for computing 0.95 confidence limits of pollen data. *Review of Palaeobotany and Palynology*, 13(2):85–93.

Mead, R., Xu, Y., Chong, J., and Jaffé, R. (2005). Sediment and soil organic matter source assessment as revealed by the molecular distribution and carbon isotopic composition of *n*-alkanes. *Organic Geochemistry*, 36(3):363–370.

Mertz, O., Padoch, C., Fox, J., Cramb, R. A., Leisz, S. J., Lam, N. T., and Vien, T. D. (2009). Swidden change in southeast asia: understanding causes and consequences. *Human Ecology*, 37(3):259–264.

Miller, D. R., Castañeda, I. S., Bradley, R. S., and MacDonald, D. (2017). Local and regional wildfire activity in central Maine (USA) during the past 900 years. *Journal of Paleolimnology*, 58(4):455–466.

Mohtadi, M., Oppo, D. W., Steinke, S., Stuut, J.-B. W., De Pol-Holz, R., Hebbeln, D., and Lückge, A. (2011). Glacial to Holocene swings of the Australian–Indonesian monsoon. *Nature Geoscience*, 4(8):540–544.

Mohtadi, M., Prange, M., Oppo, D. W., De Pol-Holz, R., Merkel, U., Zhang, X., Steinke, S., and Lückge, A. (2014). North Atlantic forcing of tropical Indian Ocean climate. *Nature*, 508(7498):76–80.

Mohtadi, M., Prange, M., Schefuß, E., and Jennerjahn, T. C. (2017). Late Holocene slowdown of the Indian Ocean Walker circulation. *Nature Communications*, 8(1):1–7.

Mohtadi, M., Prange, M., and Steinke, S. (2016). Palaeoclimatic insights into forcing and response of monsoon rainfall. *Nature*, 533(7602):191–199.

Monnin, E., Indermühle, A., Dällenbach, A., Flückiger, J., Stauffer, B., Stocker, T. F., Raynaud, D., and Barnola, J. M. (2001). Atmospheric $CO_2$ concentrations over the last glacial termination. *Science (New York, N.Y.)*, 291(5501):112–4.

Moorhouse, H. L., McGowan, S., Jones, M. D., Barker, P., Leavitt, P. R., Brayshaw, S. A., and Haworth, E. Y. (2014). Contrasting effects of nutrients and climate on algal communities in two lakes in the Windermere catchment since the late 19th century. *Freshwater Biology*, 59(12):2605–2620.

Mortazavi, B., Conte, M. H., Chanton, J. P., Weber, J. C., Martin, T. A., and Cropper, W. P. (2012). Variability in the carbon isotopic composition of foliage carbon pools (soluble carbohydrates, waxes) and respiration fluxes in southeastern U.S. pine forests. *J. Geophys. Res*, 117:2009.

Morwood, M., Sutikna, T., Saptomo, E., Westaway, K., Jatmiko, Awe Due, R., Moore, M., Yuniawati, D. Y., Hadi, P., Zhao, J.-x., Turney, C., Fifield, K., Allen, H., and Soejono, R. (2008). Climate, people and faunal succession on Java, Indonesia: evidence from Song Gupuh. *Journal of Archaeological Science*, 35(7):1776–1789.

Morwood, M. J., Soejono, R. P., Roberts, R. G., Sutikna, T., Turney, C. S., Westaway, K. E., Rink, W. J., Zhao, J. X., Van Den Bergh, G. D., Due, R. A., Hobbs, D. R., Moore, M. W., Bird, M. I., and Fifield, L. K. (2004). Archaeology and age of a new hominin from Flores in eastern Indonesia. *Nature*, 431(7012):1087–1091.

Moser, G., Schuldt, B., Hertel, D., Horna, V., Coners, H., Barus, H., and Leuschner, C. (2014). Replicated throughfall exclusion experiment in an Indonesian perhumid rainforest: Wood production, litter fall and fine root growth under simulated drought. *Global Change Biology*, 20(5):1481–1497.

Moy, C. M., Seltzer, G. O., Rodbell, D. T., and Anderson, D. M. (2002). Variability of El Niño/Southern Oscillation activity at millennial timescales during the Holocene epoch. *Nature*, 420(6912):162–165.

Murphy, B. P. and Bowman, D. M. (2012). What controls the distribution of tropical forest and savanna? *Ecology Letters*, 15(7):748–758.

Myers-Pigg, A. N., Louchouarn, P., and Teisserenc, R. (2017). Flux of dissolved and particulate low-temperature pyrogenic carbon from two high-latitude rivers across the spring freshet hydrograph. *Frontiers in Marine Science*, 4(FEB).

Niedermeyer, E. M., Forrest, M., Beckmann, B., Sessions, A. L., Mulch, A., and Schefuß, E. (2016). The stable hydrogen isotopic composition of sedimentary plant waxes as quantitative proxy for rainfall in the West African Sahel. *Geochimica et Cosmochimica Acta*, 184:55–70.

Niedermeyer, E. M., Sessions, A. L., Feakins, S. J., and Mohtadi, M. (2014). Hydroclimate of the western Indo-Pacific Warm Pool during the past 24,000 years. *Proceedings of the National Academy of Sciences*, 111(26):9402–9406.

O'Leary, M. H. (1988). Carbon Isotopes in Photosynthesis. *BioScience*, 38(5):328–336.

Ondei, S., Prior, L. D., Williamson, G. J., Vigilante, T., and Bowman, D. M. J. S. (2017). Water, land, fire, and forest: Multi-scale determinants of rainforests in the Australian monsoon tropics. *Ecology and Evolution*, 7(5):1592–1604.

Page, S. E., Siegert, F., Rieley, J. O., Boehm, H.-D. V., Jaya, A., and Limin, S. (2002). The amount of carbon released from peat and forest fires in indonesia during 1997. *Nature*, 420(6911):61–65.

Pascale, S., Lucarini, V., Feng, X., Porporato, A., and ul Hasson, S. (2016). Projected changes of rainfall seasonality and dry spells in a high greenhouse gas emissions scenario. *Climate Dynamics*, 46(3-4):1331–1350.

Peel, M. (2007). Guide to the Supplementary Material for Köppen-Geiger map colour scheme. pages 1–2.

Peterson, T. C. and Vose, R. S. (1997). An Overview of the Global Historical Climatology Network Temperature Database. *Bulletin of the American Meteorological Society*, 78(12):2837–2849.

Poliakova, A., Zonneveld, K. A., Kwiatkowski, C., Suryoko, M. A., and Behling, H. (2017). Marine environment, vegetation and land use changes during the late Holocene in South Kalimantan and East Java reconstructed based on pollen and organic-walled dinoflagellate cysts analysis. *Review of Palaeobotany and Palynology*, 238:105–121.

Power, M. J., Marlon, J., Ortiz, N., Bartlein, P. J., Harrison, S. P., Mayle, F. E., Ballouche, A., Bradshaw, R. H., Carcaillet, C., Cordova, C., Mooney, S., Moreno, P. I., Prentice, I. C., Thonicke, K., Tinner, W., Whitlock, C., Zhang, Y., Zhao, Y., Ali, A. A., Anderson, R. S., Beer, R., Behling, H., Briles, C., Brown, K. J., Brunelle, A., Bush, M., Camill, P., Chu, G. Q., Clark, J., Colombaroli, D., Connor, S., Daniau, A. L., Daniels, M., Dodson, J., Doughty, E., Edwards, M. E., Finsinger, W., Foster, D., Frechette, J., Gaillard, M. J., Gavin, D. G., Gobet, E., Haberle, S., Hallett, D. J., Higuera, P., Hope, G., Horn, S., Inoue, J., Kaltenrieder, P., Kennedy, L., Kong, Z. C., Larsen, C., Long, C. J., Lynch, J., Lynch, E. A., McGlone, M., Meeks, S., Mensing, S., Meyer, G., Minckley, T., Mohr, J., Nelson, D. M., New, J., Newnham, R., Noti, R., Oswald, W., Pierce, J., Richard, P. J., Rowe, C., Sanchez Goñi, M. F., Shuman, B. N., Takahara, H., Toney, J., Turney, C., Urrego-Sanchez, D. H., Umbanhowar, C., Vandergoes, M., Vanniere, B., Vescovi, E., Walsh, M., Wang, X., Williams, N., Wilmshurst, J., and Zhang, J. H. (2008). Changes in fire regimes since the last glacial maximum: An assessment based on a global synthesis and analysis of charcoal data. *Climate Dynamics*, 30(7-8):887–907.

Qian, J.-H. (2008). Why Precipitation Is Mostly Concentrated over Islands in the Maritime Continent. *Journal of the Atmospheric Sciences*, 65(4):1428–1441.

Qian, J.-H., Robertson, A. W., and Moron, V. (2010). Interactions among ENSO, the Monsoon, and Diurnal Cycle in Rainfall Variability over Java, Indonesia. *Journal of the Atmospheric Sciences*, 67(11):3509–3524.

Ramanathan, V., Crutzen, P. J., Kiehl, J. T., and Rosenfeld, D. (2001). Atmosphere: Aerosols, climate, and the hydrological cycle. *Science*, 294(5549):2119–2124.

Rasmusson, E. M. and Wallace, J. M. (1983). Meteorological aspects of the el nino/southern oscillation. *Science*, 222(4629):1195–1202.

Rauniyar, S. P. and Walsh, K. J. E. (2013). Influence of ENSO on the Diurnal Cycle of Rainfall over the Maritime Continent and Australia. *Journal of Climate*, 26(4):1304–1321.

Reid, J. S., Xian, P., Hyer, E. J., Flatau, M. K., Ramirez, E. M., Turk, F. J., Sampson, C. R., Zhang, C., Fukada, E. M., and Maloney, E. D. (2012). Multi-scale meteorological conceptual analysis of observed active fire hotspot activity and smoke optical depth in the Maritime Continent. *Atmospheric Chemistry and Physics*, 12(4):2117–2147.

Roderick, M. L., Noble, I. R., and Cridland, S. W. (1999). Estimating woody and herbaceous vegetation cover from time series satellite observations. GCTE/LUCC RESEARCH LETTER. *Global Ecology and Biogeography*, 8(6):501–508.

Rommerskirchen, F., Plader, A., Eglinton, G., Chikaraishi, Y., and Rullkötter, J. (2006). Chemotaxonomic significance of distribution and stable carbon isotopic composition of long-chain alkanes and alkan-1-ols in C4 grass waxes. *Organic Geochemistry*, 37(10):1303–1332.

Rowland, L., Malhi, Y., Silva-Espejo, J. E., Farfán-Amézquita, F., Halladay, K., Doughty, C. E., Meir, P., and Phillips, O. L. (2014). The sensitivity of wood production to seasonal and interannual variations in climate in a lowland Amazonian rainforest. *Oecologia*, 174(1):295–306.

Rozanski, K., Araguás-Araguás, L., and Gonfiantini, R. (2013). Isotopic Patterns in Modern Global Precipitation. Number January, pages 1–36.

Ruan, Y., Mohtadi, M., van der Kaars, S., Dupont, L. M., Hebbeln, D., and Schefuß, E. (2019). Differential hydro-climatic evolution of East Javanese ecosystems over the past 22,000 years. *Quaternary Science Reviews*, 218:49–60.

Russell, J. M., Vogel, H., Konecky, B. L., Bijaksana, S., Huang, Y., Melles, M., Wattrus, N., Costa, K., and King, J. W. (2014). Glacial forcing of central Indonesian hydroclimate since 60,000 y B.P. *Proceedings of the National Academy of Sciences*, 111(14):5100–5105.

Sachse, D., Billault, I., Bowen, G. J., Chikaraishi, Y., Dawson, T. E., Feakins, S. J., Freeman, K. H., Magill, C. R., McInerney, F. A., van der Meer, M. T., Polissar, P., Robins, R. J., Sachs, J. P., Schmidt, H.-L., Sessions, A. L., White, J. W., West, J. B., and Kahmen, A. (2012). Molecular Paleohydrology: Interpreting

the Hydrogen-Isotopic Composition of Lipid Biomarkers from Photosynthesizing Organisms. *Annual Review of Earth and Planetary Sciences*, 40(1):221–249.

Saji, N. and Yamagata, T. (2003). Possible impacts of Indian Ocean Dipole mode events on global climate. *Climate Research*, 25(2):151–169.

Saji, N. H., Goswami, B. N., Vinayachandran, P. N., and Yamagata, T. (1999). A dipole in the tropical Indian Ocean. *Nature*, 401(September):360–363.

Santín, C., Doerr, S. H., Kane, E. S., Masiello, C. A., Ohlson, M., de la Rosa, J. M., Preston, C. M., and Dittmar, T. (2016). Towards a global assessment of pyrogenic carbon from vegetation fires.

Schimmelmann, A., Sessions, A. L., and Mastalerz, M. (2006). Hydrogen Isotopic (D/H) Composition of Organic Matter During Diagenesis and Thermal Maturation. *Annual Review of Earth and Planetary Sciences*, 34(1):501–533.

Schkolnik, G. and Rudich, Y. (2006). Detection and quantification of levoglucosan in atmospheric aerosols: A review. *Analytical and Bioanalytical Chemistry*, 385(1):26–33.

Schreuder, L. T., Hopmans, E. C., Castañeda, I. S., Schefuß, E., Mulitza, S., Sinninghe Damsté, J. S., and Schouten, S. (2019). Late Quaternary Biomass Burning in Northwest Africa and Interactions With Climate, Vegetation, and Humans. *Paleoceanography and Paleoclimatology*, 34(2):153–163.

Schreuder, L. T., Hopmans, E. C., Stuut, J.-B. W., Sinninghe Damsté, J. S., and Schouten, S. (2018). Transport and deposition of the fire biomarker levoglucosan across the tropical North Atlantic Ocean. *Geochimica et Cosmochimica Acta*, 227:171–185.

Schüpbach, S., Kirchgeorg, T., Colombaroli, D., Beffa, G., Radaelli, M., Kehrwald, N. M., and Barbante, C. (2015). Combining charcoal sediment and molecular markers to infer a Holocene fire history in the Maya Lowlands of Pet en, Guatemala. *Quaternary Science Reviews*, 115:123–131.

Sémah, A.-M., Sémah, F., Moigne, A.-M., Ingicco, T., Purnomo, A., Simanjuntak, T., and Widianto, H. (2016). The palaeoenvironmental context of the Palaeolithic of Java: A brief review. *Quaternary International*, 416:38–45.

Shanahan, T. M., Hughen, K. A., McKay, N. P., Overpeck, J. T., Scholz, C. A., Gosling, W. D., Miller, C. S., Peck, J. A., King, J. W., and Heil, C. W. (2016). CO2 and fire influence tropical ecosystem stability in response to climate change. *Scientific Reports*, 6(1):29587.

Sikes, E. L., Medeiros, P. M., Augustinus, P., Wilmshurst, J. M., and Freeman, K. R. (2013). Seasonal variations in aridity and temperature characterize changing climate during the last deglaciation in New Zealand. *Quaternary Science Reviews*, 74:245–256.

Simanjuntak, T. and Asikin, I. N. (2004). [archaeology in island southeast asia and oceania] early holocene huyman settlement in eastern java. *Bulletin of the Indo-Pacific Prehistory Association*, 24:13.

Simoneit, B., Schauer, J., Nolte, C., Oros, D., Elias, V., Fraser, M., Rogge, W., and Cass, G. (1999). Levoglucosan, a tracer for cellulose in biomass burning and atmospheric particles. *Atmospheric Environment*, 33(2):173–182.

Slatkin, M. and Racimo, F. (2016). Ancient DNA and human history. *Proceedings of the National Academy of Sciences*, 113(23):6380–6387.

Snyman, H. and Fouché, H. (1993). Estimating seasonal herbage production of a semi-arid grassland based on veld condition, rainfall, and evapotranspiration. *African Journal of Range & Forage Science*, 10(1):21–24.

Staal, A., van Nes, E. H., Hantson, S., Holmgren, M., Dekker, S. C., Pueyo, S., Xu, C., and Scheffer, M. (2018). Resilience of tropical tree cover: The roles of climate, fire, and herbivory. *Global Change Biology*, 24(11):5096–5109.

Staver, A. C., Archibald, S., and Levin, S. A. (2011). The Global Extent and Determinants of Savanna and Forest as Alternative Biome States. *Science*, 334(6053):230–232.

Stein, A. F., Draxler, R. R., Rolph, G. D., Stunder, B. J. B., Cohen, M. D., Ngan, F., Stein, A. F., Draxler, R. R., Rolph, G. D., Stunder, B. J. B., Cohen, M. D., and Ngan, F. (2015). NOAA's HYSPLIT Atmospheric Transport and Dispersion Modeling System. *Bulletin of the American Meteorological Society*, 96(12):2059–2077.

Steinke, S., Prange, M., Feist, C., Groeneveld, J., and Mohtadi, M. (2014). Upwelling variability off southern Indonesia over the past two millennia. *Geophysical Research Letters*, 41(21):7684–7693.

Stephens, L., Fuller, D., Boivin, N., Rick, T., Gauthier, N., Kay, A., Marwick, B., Geralda, C., Armstrong, D., Barton, C. M., Denham, T., Douglass, K., Driver, J., Janz, L., Roberts, P., Rogers, J. D., Thakar, H., Altaweel, M., Johnson, A. L., Vattuone, M. M. S., Aldenderfer, M., Archila, S., Artioli, G., Bale, M. T., Beach, T., Borrell, F., Braje, T., Buckland, P. I., Jiménez Cano, N. G., Capriles, J. M., Castillo, A. D., Çilingiroglu, Ç., Cleary, M. N., Conolly, J., Coutros, P. R., Covey, R. A., Cremaschi, M., Crowther, A., Der, L., Di Lernia, S., Doershuk, J. F., Doolittle, W. E., Edwards, K. J., Erlandson, J. M., Evans, D., Fairbairn, A., Faulkner, P., Feinman, G., Fernandes, R., Fitzpatrick, S. M., Fyfe, R., Garcea, E., Goldstein, S., Goodman, R. C., Guedes, J. D., Herrmann, J., Hiscock, P., Hommel, P., Horsburgh, K. A., Hritz, C., Ives, J. W., Junno, A., Kahn, J. G., Kaufman, B., Kearns, C., Kidder, T. R., Lanoë, F., Lawrence, D., Lee, G. A., Levin, M. J., Lindskoug, H. B., López-Sáez, J. A., Macrae, S., Marchant, R., Marston, J. M., McClure, S., McCoy, M. D., Miller, A. V., Morrison, M., Matuzeviciute, G. M., Müller, J., Nayak, A., Noerwidi, S., Peres, T. M., Peterson, C. E., Proctor, L., Randall, A. R., Renette, S., Schug, G. R., Ryzewski, K., Saini, R., Scheinsohn,

V., Schmidt, P., Sebillaud, P., Seitsonen, O., Simpson, I. A., Soltysiak, A., Speakman, R. J., Spengler, R. N., Steffen, M. L., Storozum, M. J., Strickland, K. M., Thompson, J., Thurston, T. L., Ulm, S., Ustunkaya, M. C., Welker, M. H., West, C., Williams, P. R., Wright, D. K., Wright, N., Zahir, M., Zerboni, A., Beaudoin, E., Garcia, S. M., Powell, J., Thornton, A., Kaplan, J. O., Gaillard, M. J., Goldewijk, K. K., and Ellis, E. (2019). Archaeological assessment reveals Earth's early transformation through land use. *Science*, 365(6456).

Stibig, H.-J., Beuchle, R., and Janvier, P. (2002). *Forest Cover Map of Insular Southeast Asia at 1: 5 500 000 Derived from SPOT-VEGETATION Satellite Images*. Institute for Environment and Sustainability.

Storm, P., Wood, R., Stringer, C., Bartsiokas, A., de Vos, J., Aubert, M., Kinsley, L., and Grün, R. (2013). U-series and radiocarbon analyses of human and faunal remains from Wajak, Indonesia. *Journal of Human Evolution*, 64(5):356–365.

Stott, P. (2000). Progress in Physical Geography Combustion in tropical biomass fires : a critical review. *Progress in Physical Geography*.

Stuecker, M. F., Timmermann, A., Jin, F., Chikamoto, Y., Zhang, W., Wittenberg, A. T., Widiasih, E., and Zhao, S. (2017). Revisiting ENSO/Indian Ocean Dipole phase relationships. *Geophysical Research Letters*, 44(5):2481–2492.

Suciu, L. G., Masiello, C. A., and Griffin, R. J. (2019). Anhydrosugars as tracers in the Earth system. *Biogeochemistry*, 146(3):209–256.

Supari, Tangang, F., Salimun, E., Aldrian, E., Sopaheluwakan, A., and Juneng, L. (2018). ENSO modulation of seasonal rainfall and extremes in Indonesia. *Climate Dynamics*, 51(7-8):2559–2580.

Suwarman, R., Ichiyanagi, K., Tanoue, M., Yoshimura, K., Mori, S., Yamanaka, M. D., Kurita, N., and Syamsudin, F. (2013). The Variability of Stable Isotopes and Water Origin of Precipitation over the Maritime Continent. *Sola*, 9(0):74–78.

Thompson, D. M., Conroy, J. L., Collins, A., Hlohowskyj, S. R., Overpeck, J. T., Riedinger-Whitmore, M., Cole, J. E., Bush, M. B., Whitney, H., Corley, T. L., and Kannan, M. S. (2017). Tropical Pacific climate variability over the last 6000 years as recorded in Bainbridge Crater Lake, Galápagos. *Paleoceanography*, 32(8):903–922.

Tierney, J. E., Oppo, D. W., Legrande, A. N., Huang, Y., Rosenthal, Y., and Linsley, B. K. (2012). The influence of Indian Ocean atmospheric circulation on Warm Pool hydroclimate during the Holocene epoch. *Journal of Geophysical Research Atmospheres*, 117(19):1–9.

Timmermann, A., An, S.-I., Kug, J.-S., Jin, F.-F., Cai, W., Capotondi, A., Cobb, K. M., Lengaigne, M., McPhaden, M. J., Stuecker, M. F., Stein, K., Wittenberg, A. T., Yun, K.-S., Bayr, T., Chen, H.-C., Chikamoto, Y., Dewitte, B., Dommenget, D., Grothe, P., Guilyardi, E., Ham, Y.-G., Hayashi, M., Ineson, S., Kang, D., Kim, S., Kim, W., Lee, J.-Y., Li, T., Luo, J.-J., McGregor, S., Planton, Y.,

Power, S., Rashid, H., Ren, H.-L., Santoso, A., Takahashi, K., Todd, A., Wang, G., Wang, G., Xie, R., Yang, W.-H., Yeh, S.-W., Yoon, J., Zeller, E., and Zhang, X. (2018). El Niño–Southern Oscillation complexity. *Nature*, 559(7715):535–545.

Tobiszewski, M. and Namieśnik, J. (2012). PAH diagnostic ratios for the identification of pollution emission sources. *Environmental Pollution*, 162:110–119.

Turney, C. S., Kershaw, A. P., Lowe, J. J., van der Kaars, S., Johnston, R., Rule, S., Moss, P., Radke, L., Tibby, J., McGlone, M. S., Wilmshurst, J. M., Vandergoes, M. J., Fitzsimons, S. J., Bryant, C., James, S., Branch, N. P., Cowley, J., Kalin, R. M., Ogle, N., Jacobsen, G., and Fifield, L. K. (2006). Climatic variability in the southwest Pacific during the Last Termination (20-10 kyr BP). *Quaternary Science Reviews*, 25(9-10):886–903.

van der Kaars, S., Bassinot, F., De Deckker, P., and Guichard, F. (2010). Changes in monsoon and ocean circulation and the vegetation cover of southwest Sumatra through the last 83,000 years: The record from marine core BAR94-42. *Palaeogeography, Palaeoclimatology, Palaeoecology*, 296(1-2):52–78.

van der Kaars, S. and Dam, R. (1997). Vegetation and climate change in West-Java, Indonesia during the last 135,000 years. *Quaternary International*, 37(96):67–71.

van der Kaars, S. and De Deckker, P. (2003). Pollen distribution in marine surface sediments offshore Western Australia. *Review of Palaeobotany and Palynology*, 124(1-2):113–129.

van der Kaars, S., Penny, D., Tibby, J., Fluin, J., Dam, R. A., and Suparan, P. (2001). Late quaternary palaeoecology, palynology and palaeolimnology of a tropical lowland swamp: Rawa Danau, West-Java, Indonesia. *Palaeogeography, Palaeoclimatology, Palaeoecology*, 171(3-4):185–212.

van der Kaars, S. and van den Bergh, G. D. (2004). Anthropogenic changes in the landscape of west java (indonesia) during historic times, inferred from a sediment and pollen record from teluk banten. *Journal of Quaternary Science*, 19(3):229–239.

van der Kaars, W. A. and Dam, M. A. (1995). A 135,000-year record of vegetational and climatic change from the Bandung area, West-Java, Indonesia. *Palaeogeography, Palaeoclimatology, Palaeoecology*, 117(1-2):55–72.

van der Werf, G. R., Randerson, J. T., Giglio, L., Gobron, N., and Dolman, A. J. (2008). Climate controls on the variability of fires in the tropics and subtropics. *Global Biogeochemical Cycles*, 22(3):1–13.

van Noordwijk, M., Tanika, L., and Lusiana, B. (2017). Flood risk reduction and flow buffering as ecosystem services – Part 2: Land use and rainfall intensity effects in Southeast Asia. *Hydrology and Earth System Sciences*, 21(5):2341–2360.

Veenendaal, E. M., Torello-Raventos, M., Miranda, H. S., Sato, N. M., Oliveras, I., van Langevelde, F., Asner, G. P., and Lloyd, J. (2018). On the relationship

between fire regime and vegetation structure in the tropics. *New Phytologist*, 218(1):153–166.

Visser, K., Thunell, R., and Goñi, M. A. (2004). Glacial-interglacial organic carbon record from the Makassar Strait, Indonesia: Implications for regional changes in continental vegetation. *Quaternary Science Reviews*, 23(1-2):17–27.

Vogts, A., Badewien, T., Rullkötter, J., and Schefuß, E. (2016). Near-constant apparent hydrogen isotope fractionation between leaf wax *n*-alkanes and precipitation in tropical regions: Evidence from a marine sediment transect off SW Africa. *Organic Geochemistry*, 96:18–27.

Vogts, A., Moossen, H., Rommerskirchen, F., and Rullkötter, J. (2009). Distribution patterns and stable carbon isotopic composition of alkanes and alkan-1-ols from plant waxes of African rain forest and savanna C3 species. *Organic Geochemistry*, 40(10):1037–1054.

Wakeham, S. G., Schaffner, C., and Giger, W. (1980). Polycyclic aromatic hydrocarbons in Recent lake sediments—I. Compounds having anthropogenic origins. *Geochimica et Cosmochimica Acta*, 44(3):403–413.

Wang, J., Ge, C., Yang, Z., Hyer, E. J., Reid, J. S., Chew, B. N., Mahmud, M., Zhang, Y., and Zhang, M. (2013). Mesoscale modeling of smoke transport over the Southeast Asian Maritime Continent: Interplay of sea breeze, trade wind, typhoon, and topography. *Atmospheric Research*, 122(December):486–503.

Wang, W., Meng, B., Lu, X., Liu, Y., and Tao, S. (2007). Extraction of polycyclic aromatic hydrocarbons and organochlorine pesticides from soils: A comparison between Soxhlet extraction, microwave-assisted extraction and accelerated solvent extraction techniques. *Analytica Chimica Acta*, 602(2):211–222.

Wang, X., Thai, P. K., Mallet, M., Desservettaz, M., Hawker, D. W., Keywood, M., Miljevic, B., Paton-Walsh, C., Gallen, M., and Mueller, J. F. (2017). Emissions of Selected Semivolatile Organic Chemicals from Forest and Savannah Fires. *Environmental Science & Technology*, 51(3):1293–1302.

Webster, P. J., Magaña, V. O., Palmer, T. N., Shukla, J., Tomas, R. A., Yanai, M., and Yasunari, T. (1998). Monsoons: Processes, predictability, and the prospects for prediction. *Journal of Geophysical Research: Oceans*, 103(C7):14451–14510.

Whitlock, C., Higuera, P. E., McWethy, D. B., and Briles, C. E. (2010). Paleoecological perspectives on fire ecology: revisiting the fire-regime concept. *The Open Ecology Journal*, 3(1).

Whitlock, C. and Larsen, C. (2001). *Charcoal as a Fire Proxy*, pages 75–97. Springer Netherlands, Dordrecht.

Whitten, T., Soeriaatmadja, R. E., and Afiff, S. A. (1996). *The ecology of Java and Bali*. Periplus Editions (HK) Limited.

Wicaksono, S. A., Russell, J. M., and Bijaksana, S. (2015). Compound-specific carbon isotope records of vegetation and hydrologic change in central Sulawesi, Indonesia, since 53,000 yr BP. *Palaeogeography, Palaeoclimatology, Palaeoecology*, 430:47–56.

Wicaksono, S. A., Russell, J. M., Holbourn, A., and Kuhnt, W. (2017). Hydrological and vegetation shifts in the Wallacean region of central Indonesia since the Last Glacial Maximum. *Quaternary Science Reviews*, 157:152–163.

Wiegand, T., Snyman, H. A., Kellner, K., and Paruelo, J. M. (2004). Do Grasslands Have a Memory: Modeling Phytomass Production of a Semiarid South African Grassland. *Ecosystems*, 7(3).

Wu, M. S., Feakins, S. J., Martin, R. E., Shenkin, A., Bentley, L. P., Blonder, B., Salinas, N., Asner, G. P., and Malhi, Y. (2017). Altitude effect on leaf wax carbon isotopic composition in humid tropical forests. *Geochimica et Cosmochimica Acta*, 206:1–17.

Wurster, C. M., Rifai, H., Zhou, B., Haig, J., and Bird, M. I. (2019). Savanna in equatorial Borneo during the late Pleistocene. *Scientific Reports*, 9(1):1–7.

Xie, P., Arkin, P. A., Xie, P., and Arkin, P. A. (1997). Global Precipitation: A 17-Year Monthly Analysis Based on Gauge Observations, Satellite Estimates, and Numerical Model Outputs. *Bulletin of the American Meteorological Society*, 78(11):2539–2558.

Yan, M., Wang, B., Liu, J., Zhu, A., Ning, L., and Cao, J. (2018). Understanding the Australian Monsoon change during the Last Glacial Maximum with a multi-model ensemble. *Climate of the Past*, 14(12):2037–2052.

Yang, S., Zhang, T., Li, Z., and Dong, S. (2019). Climate variability over the maritime continent and its role in global climate variation: A review. *Journal of Meteorological Research*, 33(6):993–1015.

Yunker, M. B., Macdonald, R. W., Vingarzan, R., Mitchell, R. H., Goyette, D., and Sylvestre, S. (2002). PAHs in the Fraser River basin: A critical appraisal of PAH ratios as indicators of PAH source and composition. *Organic Geochemistry*, 33(4):489–515.